ISBN 978-82-326-2370-9 (printed ver.)
ISBN 978-82-326-2371-6 (electronic ver.)
ISSN 1503-8181

Morten Engen

Doctoral thesis

Aspects of design of reinforced concrete structures using non-linear finite element analyses

Solution strategy, modelling uncertainty and material uncertainty

Doctoral theses at NTNU, 2017:149

Morten Engen

Aspects of design of reinforced concrete structures using non-linear finite element analyses

Solution strategy, modelling uncertainty and material uncertainty

Doctoral theses at NTNU, 2017:149

NTNU
Norwegian University of Science and Technology
Thesis for the Degree of
Philosophiae Doctor
Faculty of Engineering
Department of Structural Engineering

NTNU
Norwegian University of
Science and Technology

Doctoral theses at NTNU, 2017:149

NTNU

NTNU
Norwegian University of
Science and Technology

Morten Engen

Aspects of design of reinforced concrete structures using non-linear finite element analyses

Solution strategy, modelling uncertainty and material uncertainty

Thesis for the Degree of Philosophiae Doctor

Trondheim, October 2017

Norwegian University of Science and Technology
Faculty of Engineering
Department of Structural Engineering

NTNU
Norwegian University of
Science and Technology

NTNU
Norwegian University of Science and Technology

Thesis for the Degree of Philosophiae Doctor

Faculty of Engineering
Department of Structural Engineering

ISBN 978-82-326-2370-9 (printed ver.)
ISBN 978-82-326-2371-6 (electronic ver.)
ISSN 1503-8181

Doctoral theses at NTNU, 2017:149

Printed by NTNU Grafisk senter

Preface

This doctoral thesis is submitted in partial fulfilment of the degree of philosophiae doctor (PhD) at the Norwegian University of Science and Technology (NTNU). The research was carried out as an industrial PhD project at the Department of Structural Engineering, Faculty of Engineering at NTNU in Trondheim and at Multiconsult ASA in Oslo. The main supervisor was Professor Max A. N. Hendriks from NTNU and Delft University of Technology in the Netherlands. The co-supervisors were Professor Jan Arve Øverli from NTNU and PhD Erik Åldstedt from Multiconsult ASA.

The PhD project was funded by Multiconsult ASA and The Research Council of Norway under grant number NFR 231829/O30. The project started in August 2013 and the thesis was submitted in June 2017.

The thesis consists of two parts: i) one part describing the context of the work, summarizing the main contributions and drawing the main conclusions, and ii) one part containing two papers that are accepted and published, one paper that is accepted for publication and one paper that is under review, all in international scientific peer-reviewed journals.

The author, Morten Engen, declares that the work presented herein is his own and that it contains no material that has previously been submitted for a degree at this university or any other institution.

Oslo/Trondheim, September, 2017
Morten Engen

Acknowledgements

Many people have contributed to making this project possible.

My supervisor team, Professor Max A. N. Hendriks, Professor Jan Arve Øverli and PhD Erik Åldstedt, thank you for all your time and for sharing your knowledge and experience. Max and Jan, I am looking forward to see what we can accomplish in future collaborations, and Erik, I wish you all the best in the years to come as a retiree. I am also thankful for all contributions from Professor Jochen Köhler.

My closest leaders in Multiconsult in 2013, Mr. Per Horn and Mr. Brynjar Sandvik, had the courage to initiate the project, and their successors, Mr. Christian Nerland and PhD Egil Møen, followed it to the finish line. Your seemingly unlimited positive attitude and backing have encouraged me a lot, and I am sure that it has contributed to making the project relevant for the rest of our colleagues.

I would like to thank all my friends and colleagues from the Department of Structural Engineering at NTNU in Trondheim, and Multiconsult in Oslo, Mr. Finn-Idar Grøtta Giske and Mr. Reignard Tan, fellow PhD candidates at Multiconsult, Mr. Mattias Blomfors and Associate Professor Mario Plos from Chalmers University of Technology, PhD Gerd-Jan Schreppers and Mr. Wijtze Pieter Kikstra from DIANA FEA, PhD Ernst Mørtsell from NorBetong AS, Mr. Øyvind Sæter from Unicon AS, Mr. Roar Vigre from Ølen Betong AS, and all the students that did their master projects related to this project.

To my mom, dad, sister and the rest of my family, your support and inspiration are highly appreciated.

Dear Nina, I am forever thankful for your support through the last four years. You know that it has been a great challenge for me, and I know that it has been challenging for you too, but hey, we managed it together! Now I am looking forward to returning the favour!

Morten

Abstract

Non-linear finite element analyses (NLFEA) of reinforced concrete structures have gained much attention in the structural engineering community during the last decade, and the practising engineer is now equipped with an advanced tool that can be used in the design process. The three main objectives of the present work has been i) to develop a solution strategy for NLFEA applicable during design of large reinforced concrete structures, ii) to quantify the modelling uncertainty obtained with the solution strategy, and iii) to quantify the variability of the compressive strength of concrete. These are central ingredients in the semi-probabilistic safety formats for NLFEA introduced in the literature. A solution strategy comprises all the choices that need to be made in order to perform a NLFEA, and the modelling uncertainty indicates how well the analysis outcomes compare to the real physical behaviour.

A three dimensional material model for concrete was adapted and implemented in a finite element software. The material model required only one material parameter, the uniaxial compressive strength. The complete solution strategy is discussed in detail in the appended papers. A refinement of the solution strategy is only justified if the resulting modelling uncertainty is reduced, if necessary knowledge about the basic variables can be obtained, and if in the end it can be shown to produce results that provide a better basis for decision making.

The modelling uncertainty was quantified by comparing NLFEA predictions to experimental outcomes, resulting in a bias of 1.10 and a coefficient of variation of 0.11. All the uncertainties that are not explicitly considered in the NLFEA will implicitly contribute to the estimated modelling uncertainty, and a pure modelling uncertainty is thus not straightforward to obtain. This is unfortunate, since the modelling uncertainty will carry a large part of the uncertainties in the problem. However, it can be useful, since the analyst later does not need to consider the uncertainties that were not considered during quantification of the modelling uncertainty.

A hierarchical model for the variability of material properties was formulated for the study of the compressive strength of ready-mixed concrete. By combining Bayesian inference and maximum likelihood estimators, the contributions from the different hierarchical levels were quantified. The method was demonstrated on more than 14000 compressive strength recordings from the Norwegian market. The results indicate that the designer should specify strength classes that better utilize the strength potential of the durability class. A closer collaboration between the designer, contractor and the producer is expected to result in improved concrete specifications.

In addition to summarizing the main findings of the work, this thesis contains a part describing the background and the context of the work.

Keywords: non-linear finite element analyses, large reinforced concrete structures, practical applications, modelling uncertainty, structural design, ultimate limit state, hierarchical model for material variability, Bayesian inference, structural reliability.

Table of Contents

List of publications

Appended journal publications

Engen, M., Hendriks, M. A. N., Köhler, J., Øverli, J. A., Åldstedt, E., Mørtsell, E., Sæter, Ø. & Vigre, R.: Predictive strength of ready-mixed concrete: exemplified using data from the Norwegian market. Under review, 2017.

Engen, M., Hendriks, M. A. N., Øverli, J. A. & Åldstedt, E.: Solution strategy for non-linear finite element analyses of large reinforced concrete structures. Structural Concrete, 2015, 16(3), 389-397.

Engen, M., Hendriks, M. A. N., Øverli, J. A. & Åldstedt, E.: Non-linear finite element analyses applicable for the design of large reinforced concrete structures. Accepted for publication in European Journal of Environmental and Civil Engineering, 2017.

Engen, M., Hendriks, M. A. N., Köhler, J., Øverli, J. A. & Åldstedt, E.: A quantification of the modelling uncertainty of non-linear finite element analyses of large concrete structures. Structural Safety, 2017, 64(1), 1-8.

Other journal publications

Blomfors, M., Engen, M. & Plos, M.: Evaluation of safety formats for non-linear Finite Element Analyses of statically indeterminate concrete structures subjected to different load paths. Structural Concrete, 2016, 17(1), 44-51.

Aasheim, E. E., Lindemark, J., Lundberg, A. H. & Engen, M.: Dam Sarvsfossen. Cement, 2017, 69(3), 38-41.

Conference papers

Engen, M., Hendriks, M. A. N., Øverli, J. A. & Åldstedt, E.: Large scale non-linear finite element analyses of reinforced concrete structures. Proceedings of the 10th International PhD Symposium in Civil Engineering, July 21 to 23, 2014, Université Laval, Québec, Canada, 2014.

Engen, M., Hendriks, M. A. N., Øverli, J. A. & Åldstedt, E.: Application of NLFEA in the Design of Large Concrete Structures. Proceedings of the XXII Nordic Concrete Research Symposium, Reykjavik, Iceland, 2014.

Engen, M., Hendriks, M. A. N., Øverli, J. A. & Åldstedt, E.: Solution strategy for large scale non-linear finite element analyses of concrete structures. Concrete – Innovation and Design. fib Symposium Proceedings. 18 to 20 May 2015, Tivoli Congress Center, Copenhagen, Denmark, 2015.

Engen, M., Hendriks, M. A. N., Øverli, J. A. & Åldstedt, E.: Material model for non-linear finite element analyses of large concrete structures. Performance-based approaches for concrete

structures, *fib* Symposium 2016 Proceedings, Cape Town, South Africa, 21-23 November, 2016.

Engen, M., Hendriks, M. A. N., Øverli, J. A. & Åldstedt, E.: Reliability assessment of a large concrete structure making use of non-linear finite element analyses. The Second Concrete Innovation Conference, 6.-8. March, 2017, Tromsø, Norway.

Engen, M., Hendriks, M. A. N., Øverli, J. A. & Åldstedt, E.: Reliability assessments of large reinforced concrete structures using non-linear finite element analyses: challenges and solutions. High Tech Concrete: Where Technology and Engineering Meet. Proceedings of the 2017 fib Symposium, held in Maastricht, The Netherlands, June 12-14, 2017.

Technical lectures

Engen, M., Hendriks, M. A. N., Øverli, J. A. & Åldstedt, E.: A Comparative Study of Two Solution Strategies for NLFEA of Concrete Structures. DIANA User meeting, Parma, November 4th, 2014.

Engen, M., Hendriks, M. A. N., Øverli, J. A. & Åldstedt, E.: A material model suitable for NLFEA of large reinforced concrete structures. DIANA User meeting, Barcelona, October 29th, 2015.

Engen, M.: Modelling uncertainties in non-linear finite element analyses of new and existing concrete structures. 2nd Nordic mini-seminar on residual life and capacity of deteriorated concrete structures, Oslo, June 2nd, 2016.

Articles in popular science magazines

Engen, M.: Ikke-lineære elementanalyser av store betongkonstruksjoner (in Norwegian). Byggeindustrien, 2015, 7, 86.

Declaration of authorship

Morten Engen has planned and conducted the work, evaluated the results and written the appended papers and the rest of this thesis. The co-authors have contributed in planning the work, discussing the results and reviewing the manuscripts.

Part I – Background and summary

1. Introduction

1.1 Safe design in structural engineering

By expressing the nature as mathematical models, the structural engineer performs analyses, which help stakeholders make proper decisions (Benjamin & Cornell 1970). With regard to structural safety, the task can be to calculate the necessary structural dimensions and material strengths so that the structure is sufficiently safe when exposed to its expected loads (Thoft-Christensen & Baker 1982, Melchers 1999, Ditlevsen & Madsen 2005, Schneider 2006). For a new structure, the results from the analyses of the engineer can help the stakeholder to decide upon a structural concept, to select among different protective measures or to decide to realize the project or not. In case of an existing structure, the question can be whether the structure should be replaced or strengthened or not, or which repair strategy that should be selected. The findings of the engineer can therefore have significant economical and ecological impact, since more material use usually results in higher costs and larger environmental impact.

A simple example of structural design is to consider a reinforced concrete container for liquids which is open to air, such that the maximum amount of liquids stored in the container is limited to the size of the container. The engineer should design the container so that the load carrying capacity is sufficient for carrying the internal forces due to the contained liquids. In this case, the loads can be determined with a high level of confidence. However, the material strengths can be relatively uncertain. One solution could be to obtain strength measurements from the producers of the materials, and design the container with a capacity just sufficient for the minimum measured strengths. This would be a safe design only if the material variability was completely described by the measurements. A better solution would be to scale down the material strengths with factors taking into account the uncertainty, or the lack of knowledge about the material variability.

Consider the two-storey reinforced concrete frame in Fig. 1, which is subjected to a dominating horizontal load, E, due to wind. Since the loads and the material strengths are variable of nature and the calculation models are only simplifications of the nature, the structural engineer should consider these uncertainties when finding the necessary dimensions and material strengths. In the histograms in Fig. 1 the uncertain material strengths are illustrated by considering two production lines, one delivering batches of concrete with a cylinder strength f_c according to a recipe and one delivering reinforcement steel bars with a yield stress f_y. If two cylinders are cast from the same batch or from different batches of concrete, and the compressive strength is determined by testing, the results will vary between the tests. The variability of the concrete strength in a structure will in addition have variability due to casting, compaction and curing. Similarly for the reinforcement, the test results will vary between material tests. However, the variation of strength is smaller for the reinforcement steel than for the concrete. Due to the variation in material strength, the structural capacity, i.e. the maximum load $R = E$ that could be applied to the frame in an experiment, will vary between experiments if several equal frames were cast and loaded until failure. A part of the task of the engineer is to collect sufficient

knowledge about the uncertain parameters of the problem in order to make a safe prediction about the future.

Following the Eurocodes (CEN 2002, 2004), the usual way of taking into account the uncertainties in structural engineering analyses is to use the partial factor method. Here, the loads are multiplied by load factors and the material strengths are divided by material factors. The partial factors are larger than unity, and result in an increase of the loading and a decrease of the capacity. The partial material factor for concrete is larger than the factor for reinforcement steel due to the larger variation of concrete strength.

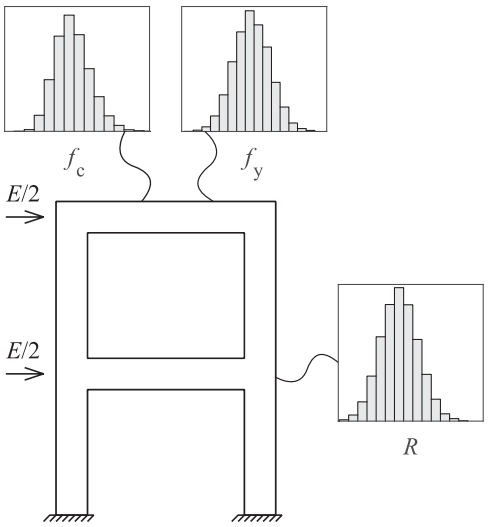

Fig. 1: Reinforced concrete frame subjected to the load E. The histograms indicate the variability of the compressive strength of concrete and the yield strength of the reinforcement, f_c and f_y, and the resulting variability in resistance R.

1.2 One- and two-step approaches for design of reinforced concrete structures

By considering the lower bound theorem of plasticity theory (see e.g. Nielsen 1984, Brekke et al. 1994, Cook & Young 1999, Melchers 1999, Lubliner 2008), a conservative estimate of the capacity of the frame in Fig. 1 is found by considering a set of internal forces which is i) in equilibrium with the external loads and ii) not exceeding the capacity locally in any section, and iii) by ensuring sufficient ductility by providing proper detailing of the reinforcement. If the frame is designed such that all critical sections are equally utilized, the lower bound solution would coincide with the formation of a mechanism, prohibiting any further loading and redistribution of internal forces. However, if the critical sections are not equally utilized, the loading could be further increased until the capacity is reached in enough sections to form a mechanism.

The internal force distribution of the frame in Fig. 1 can be calculated by hand, but due to the degree of statically indeterminacy, the engineer would most likely resort to computer-assisted methods. Today, linear finite element analyses (LFEA) are widely used in everyday practice. One of the main advantages of using LFEA is that the *principle of superposition* is valid. Hence, the engineer can perform separate analyses of each load case, and combine the results to form relevant load combinations afterwards. Based on the results from the LFEA, the structure is thus designed such that the capacity is not exceeded locally in any section. The detailing of the reinforcement is such that the full theoretical capacity of each cross-section can be mobilized by providing minimum reinforcement and sufficient anchorage lengths.

The method described above can be called a *two-step approach* (Schlune 2011, Schlune et al. 2012), since the response and the resistance are calculated in two steps using different assumptions regarding the material behaviour. The response of reinforced concrete is non-linear due to cracking of concrete even at low load levels. At higher load levels, the yield strength of the reinforcement can be exceeded, introducing additional non-linearities. For statically determinate structures, these stiffness reductions will not influence the distribution of internal forces. However, for statically indeterminate structures, the parts having the largest stiffness attract the larger portion of the internal forces. The non-linear response of reinforced concrete will thus result in a redistribution of the internal forces, which cannot be predicted by the LFEA.

In the LFEA, the estimated internal force distribution can be close to, but basically not equal to, the real distribution, because of the assumed linear elastic material behaviour, and the full capacity of the structure is not utilized since the redistribution of forces is not modelled. However, the two-step approach is effective due to the validity of the principle of superposition, and by definition conservative. Instead of using a LFEA, one could use a non-linear finite element analysis (NLFEA) for calculating a more realistic internal force distribution for a certain design load. However, this is still a two-step approach, since the sectional capacities are generally calculated using different material models, and raises the question about which values of the material parameters that should be input in the NLFEA. With reference to the material variation in Fig. 1, should the materials be represented by their *mean* or *most likely* values, their *nominal* or *characteristic* values, their low *design* values or something in between? The selected values for the material parameters influence the failure mode and stiffness of the frame, and thus the distribution of the internal forces, and should be selected with care.

Alternatively, since concrete and reinforcement steel are modelled with realistic material models, a NLFEA can be interpreted as a *virtual experiment*. Increasing the load until failure in this virtual experiment, would give an estimate of the load carrying capacity of the structure as a whole where all sections work together and contribute to the capacity. This represents a *one-step approach*, since the structural response and the structural resistance are calculated using the same assumptions regarding the material behaviour. Only those phenomena that are not explicitly modelled should be controlled separately, e.g. anchorage if the reinforcement is modelled as fully bonded and the transverse shear capacity if ordinary beam or shell elements

are used. Performing analyses with different values for the input parameters will give an indication of the variation of the load carrying capacity due to the material uncertainties, and semi-probabilistic methods can be used to estimate the design load carrying capacity based on this information. It should be noted that in NLFEA, the principle of superposition is no longer valid, and each relevant load combination should thus be analysed separately.

Any LFEA or NLFEA only represent simplifications of the reality, and the *modelling uncertainty* or *model uncertainty* indicates how well the analysis outcomes compare to the real physical behaviour (Ditlevsen 1982). The modelling uncertainty of NLFEA depends on how the analysis is performed and what kind of physical phenomenon that is modelled. There are several contributions in the literature devoted to the modelling uncertainty, both addressing one specific model (e.g. Engen et al. 2017a), and the effect of selecting different models (Schlune et al. 2012). It is emphasized that the modelling uncertainty does not imply that the outcomes of the NLFEA are random. If one NLFEA is repeated, the outcome will be the same, but it will be uncertain, since the model is only a simplification of the reality.

a) The Tresfjord Bridge (Statens Vegvesen) b) Dam Sarvsfossen (Bykle kommune)

Fig. 2: Typical large reinforced concrete structures.

The one-step approach has been elaborated on in the literature (CEB 1995, 1997, Henriques et al. 2002, Schlune et al. 2011, 2012, Cervenka 2013, Pimentel et al. 2014, Allaix et al. 2013, Blomfors et al. 2016), and with this method, the engineer is equipped with a tool that can be used to make realistic assessments of the load carrying capacity of structures. However, it is important to realize that the cost of performing NLFEA of reinforced concrete structures of realistic sizes, as illustrated in Fig. 2, can be significant. The use of NLFEA in everyday

engineering practice thus seems justified if significant cost savings can be expected. Hence, typical application areas are identified as

- structures with complex geometries,
- structures subjected to extreme loading,
- existing structures designed according to old design codes,
- existing structures subjected to new and increased loads, or
- existing structures exposed to deterioration mechanisms where the residual structural resistance is questioned.

In this work, emphasis has been put on developing a strategy for NLFEA within a one-step approach, applicable to analyses of *large reinforced concrete structures*, in order to facilitate the use by practicing engineers. Furthermore, the uncertainties related to material and modelling have been studied in order to contribute to ongoing discussions, and to be able to proceed towards a full one-step approach in future work.

1.3 Objectives and limitations

The objective of the present work is to develop the central parts to be used in the one-step approach for design of large reinforced concrete structures, and are summarized in the following three points:

1) Develop a solution strategy suitable for NLFEA of large reinforced concrete structures, where the purpose of the analysis is to estimate the ultimate limit capacity.
2) Validate the solution strategy and quantify the modelling uncertainty.
3) Quantify the variability of the compressive strength of concrete.

The work has been subject to the following limitations:

- No physical experiments or material tests have been performed.
- Only the ultimate limit load behaviour was considered.
- Only static loads were considered.

1.4 Structure of the thesis

This thesis consists of a Part I presenting the background for and summarizing the main contributions from the present work, and a Part II where the four papers containing the main contributions from the work are appended. The present work has been carried out in the crossing between two specialist topics:

- Non-linear finite element modelling.
- Structural reliability.

In order to put the work in the right context, the chapters thus have slightly different focus. Chs. 2 and 3 provide an introduction to uncertainties in engineering analyses, and structural reliability methods, written in the context of NLFEA. Ch. 4 introduces NLFEA in the context of structural reliability, and with special focus on modelling uncertainties and the application to structural engineering problems. The main contributions are summarized in Ch. 5, the main conclusions are drawn in Ch. 6 and suggestions for further research based on the present work are given in Ch. 7.

2. Uncertainties in engineering analyses

2.1 Engineering analyses

Design engineers use models to perform analyses and make predictions about a future outcome of a process, a problem which Cornell (1969) describes in the following way:

> *The design problem requires prediction through imperfect mathematical theories of the performance of structural systems constructed by fallible humans from material with variable properties when these systems are subjected to an unpredictable natural environment. All aspects of the problem are uncertain.*

Examples of engineering analyses and models can be prediction of the shear capacity of a reinforced concrete beam without shear reinforcement, representation of the yield stress of reinforcement steel as a normally distributed random variable, prediction of the 100-year snow load in the municipality of Gran in Norway, or NLFEA predictions of the load carrying capacities of large reinforced concrete structures. A mechanical model relates the value of a derived variable to the values of a set of basic variables. The derived variable can typically only be observed in specially designed laboratory or field experiments, while the basic variables are typically readily observable in standard material tests.

Two examples of mechanical models are the deflection Δ at mid-span of a lightly reinforced concrete beam subjected to a distributed load q assuming an un-cracked cross-section

$$\Delta = r\frac{qL^4}{E_{\mathrm{c}}I_{\mathrm{c}}} \quad , \tag{1}$$

and an equation deriving the Young's modulus E_{c} from the cylinder strength f_{c}, both measured in MPa (CEN 2004),

$$E_{\mathrm{c}} = 22\left(\frac{f_{\mathrm{c}}}{10}\right)^{0.3} \quad . \tag{2}$$

In Eq. (1), L is the length of the beam, I_c is the second moment of inertia of the area and r is an uncertain parameter of the model taking into account the effect of the boundary conditions. If the beam is assumed simply supported, the parameter can be assumed $r = 5/384$. In Eq. (2) the numbers 22, 10 and 0.3 are values assigned to the uncertain parameters of the model. The outcome of the models deviate from what is observed in experiments because the values of the basic variables are uncertain, and because the models are only approximations to the reality. Note that computer models, like NLFEA, are implicit models, meaning that the models give results for given input using a number of combined sub-models that are known to the analyst, but not directly visible as closed form expressions. The basic variables of a NLFEA are the variables that need to be input in order to get a solution.

Likewise, probability theory is used to construct rational models to describe observable uncertainties in the models and the variables. As an example, it is common to assume that the yield strength of reinforcement steel can be represented as a normally distributed random variable according to

$$f_{\mathrm{y}} \sim \mathrm{N}\left(f_{\mathrm{y}}|\mu_{f_c}, \sigma_{f_{\mathrm{y}}}^2\right) = \frac{1}{\sqrt{2\pi}\sigma_{f_{\mathrm{y}}}} \exp\left(-\frac{1}{2}\frac{\left[f_{\mathrm{y}} - \mu_{f_{\mathrm{y}}}\right]^2}{\sigma_{f_{\mathrm{y}}}^2}\right) \quad , \tag{3}$$

where $\mu_{f_{\mathrm{y}}}$ and $\sigma_{f_{\mathrm{y}}}^2$ are the mean and variance of the yield strength. $\mu_{f_{\mathrm{y}}}$ and $\sigma_{f_{\mathrm{y}}}^2$ can generally be said to be uncertain parameters of the probabilistic model. The measure of the spread of the variable can also be given in terms of the coefficient of variation, $V_{f_{\mathrm{y}}} = \sigma_{f_{\mathrm{y}}}/\mu_{f_{\mathrm{y}}}$.

The uncertainties can be categorized according to their nature as either *aleatory* or *epistemic*, or according to their source as either *physical uncertainties* or *modelling uncertainties*. Note that the estimates of both physical uncertainties and modelling uncertainties are themselves uncertain since the estimates are usually based on a limited data set. Such additional uncertainties are denoted *statistical uncertainties*. This categorization will be elaborated on in the following.

2.2 Aleatory and epistemic uncertainties: randomness and uncertainty

In order to discuss the uncertainties in a structured manner, it is useful to introduce the terms *aleatory* and *epistemic* uncertainties (Der Kiureghian 1989, Faber 2005, Der Kiureghian & Ditlevsen 2009). According to the *Oxford English Dictionary*, aleatory describes something that depends on chance, like the throw of a dice. Aleatory uncertainties are thus uncertainties due to the inherent randomness of a phenomenon, e.g. the outcome of a coin toss or the compressive strength obtained in a future batch of concrete produced according to a given recipe. Epistemic, on the other hand, derives from epistemology, which is the branch of philosophy that deals with knowledge. Epistemic uncertainty is thus the uncertainty due to a lack of knowledge, e.g. the uncertain weight of a bag of potatoes or the uncertain compressive strength of concrete in an existing structure.

The uncertainty in the outcome of most phenomena has contributions from both aleatory and epistemic uncertainty, however it is only the epistemic contribution that can be reduced by observations or by increasing the knowledge about the phenomenon, statistical uncertainties are thus purely epistemic. Aleatory and epistemic uncertainties can alternatively be referred to as *randomness* and *uncertainty* (Igusa et al. 2002).

2.3 Physical uncertainties

Physical uncertainty represents the uncertain values of the basic variables. The basic variables are typically material strengths and stiffnesses, load intensities and distributions, and variables describing the geometry. Examples are shown in Tab. 1.

Tab. 1: Examples of variables with physical uncertainties considered in assessments of reinforced concrete structures.

Material	• The compressive and tensile strengths of concrete. • The Young's modulus of concrete. • The yield strength of the reinforcement steel. • The uncertain relation between stresses and strains of the materials.
Geometry	• The cross-sectional thickness. • The cover to the reinforcement. • The cross-sectional area of the reinforcement bars. • Imperfections of the geometry.
Load	• Distribution and intensity of distributed loads. • Locations and intensities of point loads. • Ground motion intensity. • The mass densities of the materials.
Boundary conditions	• The stiffness and strength of surrounding structures and foundations. • Geometrical idealization of supports.

The values of the basic variables can be thought of as outcomes of random processes, and the categorization into aleatory or epistemic is best understood from an example. The concrete in a structure is produced according to a specified recipe, at the plant of a producer and supplied to the construction site (Rackwitz 1983, Engen et al. 2017c). At the construction site, the fresh concrete is placed in the formwork, properly compacted and left for curing, ensuring suitable curing conditions (Stewart 1995).

The actual strength at a spot in an existing structure can be determined by destructive or non-destructive testing. The estimate of the concrete strength thus depends on the accuracy of the measuring technique and the number of samples taken. Fig. 3 illustrates the effect of the number of samples on the estimated uncertainties. The measuring error can always be reduced by calibrating the measuring device or by using another technique, and the number of samples can always be increased, but due to the heterogeneous nature of concrete, a part of the uncertainties will always remain. The uncertainty is thus dominated by an epistemic part, but also has an aleatory contribution.

However, in a structure that has not yet been constructed, the strength at a spot in the structure is not yet realized from the random process described above. The outcome is uncertain, and it is uncertain due to the inherent randomness of the process of producing, casting and curing

concrete. If information about the specific producer, plant and recipe or about quality control measures are available, this information can be taken into account to reduce the uncertainties. Hence, in this case the uncertainty is a combination of aleatory and epistemic.

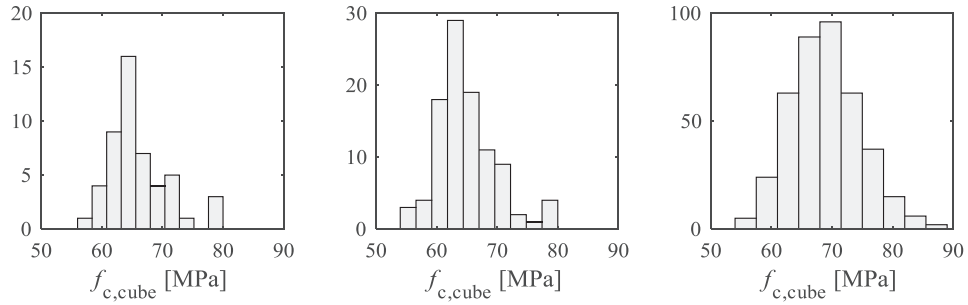

a) 50 observations. b) 100 observations. c) 400 observations.

Fig. 3: Compressive strength recordings from a Norwegian concrete plant with different numbers of observations.

Similar examples can be constructed for most material properties and structural dimensions. In other words, the uncertainties related to the properties of the structure changes from a combination of aleatory and epistemic to purely epistemic as the structure is being constructed (Faber 2005, Der Kiureghian & Ditlevsen 2009).

The uncertainties of the basic variables related to the loading are slightly different, and depend not only on whether the structure is constructed or not, but also on the nature of the load. The uncertainties of dead loads are comparable to the uncertainties in the properties of the structure. The basic variables related to variable loads, or live loads, on the other hand will always be outcomes of random processes. The random process can be bounded, for example by enforcing a limit for the height of vehicles that are allowed to drive over a bridge, and likely values of the loads can be derived from measurements. However, unlike the properties of the constructed structure, the values of a variable load can never be fully determined, and thus have a combination of aleatory and epistemic nature.

The physical uncertainties are described further in Papers I and IV (Engen et al. 2017c, 2017a).

2.4 Modelling uncertainties

Our mechanical models consist of mathematical expressions describing complex physical phenomena (Ditlevsen 1982, Der Kiureghian & Ditlevsen 2009). The mathematical expressions can be of variable degree of complexity and can depend on a limited number of variables, and the model can be selected from a range of different models describing the same physical phenomenon (Zhang & Mahadevan 2000, Beck & Yuen 2004, Droguett & Mosleh 2008). The degree of complexity and the number of variables is usually limited either by lack of knowledge or for practical reasons.

The modelling uncertainty thus arises due to the limited number of variables that are included in the model, the complexity of the mathematical model and the likelihood of the selected model being correct. In addition, if the model is empirically based, the parameters of the model are also uncertain since they are estimated from experimental observations using for example linear regression. The accuracy of the estimated values of the parameters depends on the number of observations that the estimate is based on, and can generally be improved if the number of observations is increased (Der Kiureghian & Ditlevsen 2009). The modelling uncertainty thus has an epistemic nature. It is emphasized that the fact that the models are uncertain does not mean that the outcomes of our models are random. In fact, if for instance a NLFEA prediction of the load-carrying capacity of the dam in Fig. 2b is repeated, the outcome will always be the same, however, the outcome is uncertain, since the model is only a simplification of the reality.

A model can have a set of variables that need to be treated as basic variables. If some of the variables are not directly available or directly observable in standard material tests, and there exist models expressing any of the variables as function of other variables, these models can be used as sub-models. Continuing the examples from above, the model for Young's modulus in Eq. (2) can be used as a sub-model in the model for the deflection in Eq. (1), and the model for the deflection becomes a function of f_{c} instead of E_{c}. This is common in NLFEA of concrete structures, where material models for concrete usually take many basic variables, for example compressive strength, tensile strength, Young's modulus, Poisson's ratio, fracture energy in tension and compression and measures of ultimate strains.

It is important to note that as soon as a sub-model is used for estimating the value of one of the variables, the sub-model becomes a part of the model, and the modelling uncertainty of the sub-model contributes to the modelling uncertainty of the whole model. The variable that is estimated changes from a variable that is explicitly modelled as a basic variable to a variable that is implicitly taken care of by the model. In other words, what is not explicitly considered in the model, implicitly contributes to the modelling uncertainty (Ditlevsen 1982, Engen et al. 2017a).

In the context of NLFEA, the modelling uncertainty, θ, is usually defined as

$$\theta = \frac{R_{\mathrm{exp}}}{R_{\mathrm{NLFEA}}} \quad , \tag{4}$$

where R_{exp} is the measured outcome from an experiment, and R_{NLFEA} is the predicted outcome of the experiment using NLFEA (*fib* 2013, JCSS 2001). R_{exp} has the same nature as the concrete in a structure, i.e. it can be interpreted as an outcome of a random process. Hence, due to the relation in Eq. (4), the *estimated* modelling uncertainty also depends on the uncertainty in the outcome and measurement of R_{exp} (Holický et al. 2016, Engen et al. 2017a). Quantification of

the modelling uncertainty of NLFEA, and implications of model refinements are discussed in Paper IV (Engen et al. 2017a) and will be discussed further in Sec. 4.4.

Note that there are also modelling uncertainties related to the probabilistic models for the same reasons as above, i.e. the probabilistic model describing some physical variation is only an approximation of the real physical variation. Examples of models being approximations of real behaviour are shown in Fig. 4.

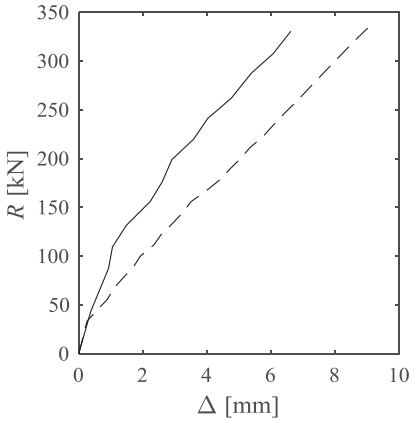

a) NLFEA prediction (dashed) of a benchmark experiment (solid).

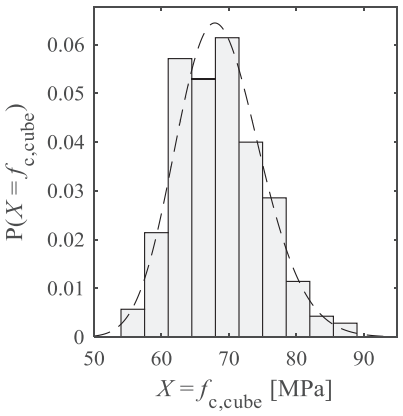

b) Probabilistic model (dashed) fitted to observed material variability (histogram).

Fig. 4: Examples of models that approximate real behaviour.

3. Structural reliability methods

3.1 Performance-based design

According to EN 1990 (CEN 2002) a structure should be designed and constructed in such a way that it has sufficient structural capacity, serviceability and durability within its complete service life with a sufficient degree of reliability. Reliability is the ability of the structure or structural component to fulfil the criteria for which it is designed, within its intended service life, and is normally given in terms of a probabilistic measure. Furthermore, the design criteria are formulated quantitatively as limit states, separating the performance of the structure into a safe and an unsafe region. The exceedance of a limit state is denoted as *failure*, and typical ultimate limit states and serviceability limit states are shown in Tab. 2. The structure will *fail* when an extreme load is encountered, or when a certain load combination results in an extreme load effect such that the structure enters a *failure state*. The design problem thus consists of two parts: 1) predict a reasonable magnitude for the extreme load or load effect, and 2) predict a reasonable value for the strength of the structure from the information available (Thoft-Christensen & Baker 1982).

Tab. 2: Typical ultimate limit states and serviceability limit states.

Ultimate limit state	• The local bending moment in a section exceeding the bending moment capacity of the section. • The external load exceeding the load bearing capacity of the structure.
Serviceability limit state	• The deflections are exceeding the maximum allowable deflections limited due to safe operation of machinery. • The crack widths exceeding a maximum allowable crack width limited for durability or aesthetical reasons.

In the literature, design principles based on limit states, service life and probabilistic measures are typically referred to as probability- or reliability-based (Cornell 1969, Hasofer & Lind 1974, Vrouwenvelder 2013) and performance-based (Ellingwood 2008, Bigaj-van Vliet & Vrouwenvelder 2013).

The purpose of this chapter is to introduce structural reliability methods, demonstrate the background for the codified *semi-probabilistic safety formats* for NLFEA that have been introduced in the literature (e.g. *fib* 2013) and to indicate a framework for more detailed analysis methods that can be used in cases where the simple semi-probabilistic safety formats are insufficient.

3.2 Interpretation of probability

The term *probability* can be given the *classical*, *frequentist* or *Bayesian* interpretation (see Apostolakis 1990, Faber 2005, Schneider 2006, Gelman et al. 2014). In the *classical interpretation*, probability is a fraction or concentration, for example the probability of picking

a green ball from a basket with a known number of green and yellow balls. In the *frequentist interpretation*, probability is a measure of the number of outcomes if a trial is repeated a large number of times. If one continued to pick balls from the basket with green and yellow balls, and put the ball back into the basket after each trial, the number of outcomes with a green ball divided by the total number of trials will eventually converge to the classical interpretation of probability. This interpretation is the common starting point in most courses in statistics, and the calculus of frequentist probability is widely developed.

The expected lifetime of for example small electronical components can be understood with the frequentist interpretation of probability, since such components are usually manufactured in large numbers. However, since most buildings and infrastructure are one-of-a-kind, the frequentist interpretation is not readily applicable to structural reliability. One can imagine constructing a large number of the dam in Fig. 2b, counting all the dams that would fail, divide this number by the number of constructed dams and say that this is the probability of failure, however, it is not realistic. Hence, structural engineers do not easily appreciate the frequentist interpretation of probability.

Instead, the *Bayesian interpretation* of probability is more relevant in structural engineering. This interpretation is of a conditional probability that is subjective, and often denoted *subjectivist*. Probability can be interpreted as the *degree of belief* given the state of knowledge and the method for estimating the probability. Hence, the probability of failure found from a reliability assessment is not a property of the structure under consideration, but a property of the analysis based on engineering judgement given the state of knowledge. Furthermore, with this interpretation it is equally meaningful to discuss "the probability of good skiing conditions in your winter holiday", "the probability of picking a green ball from a basket of green and yellow balls" and "the probability that the capacity of a dam being exceeded during heavy rain or snow smelting during its lifetime of 100 years". Note that even though the interpretation of structural reliability is *Bayesian* or *subjectivist*, the *frequentist* calculus is applied, and available probability distributions are used to represent uncertainties.

3.3 The basic reliability problem

The ultimate limit state is usually expressed in terms of the resistance R and the load E as

$$R = E \quad , \tag{5}$$

or in terms of the limit state function g as

$$g = R - E = 0 \quad , \tag{6}$$

where $g > 0$ is the safe region and $g \leq 0$ is the unsafe region (Thoft-Christensen & Baker 1982, Schneider 2006). In most structural engineering problems, the load and resistance are not independent. For example, the cross-sectional height of a slab will influence both the capacity

and the dead weight, and the cross-sectional dimensions of axially loaded slender columns will influence both the capacity and the lateral deformations due to eccentricities and hence the additional bending moments due to second order effects. Eq. (6) can thus alternatively be written in terms of the basic variables of the problem, collected in the vector $\boldsymbol{x}$, as

$$g(\boldsymbol{x}) = 0 \quad . \tag{7}$$

The vector of the n basic variables, $\boldsymbol{x}$, can be interpreted as a vector in an n-dimensional space, and the limit state function, $g(\boldsymbol{x}) = 0$, can be visualized as a plane separating the safe region from the unsafe region. The basic reliability problem seeks an answer to one of the two alternative questions:

1) Given our state of knowledge, what is the probability of E exceeding R, $p_\mathrm{f} = \mathrm{P}(R \leq E)$?
2) Given our state of knowledge, what is the probability of having an unsafe combination of the values for the basic variables, $p_\mathrm{f} = \mathrm{P}(g(\boldsymbol{x}) \leq 0)$?

The difference between the resistance and the load in Eq. (5) is often denoted the safety margin, and the purpose of the design process is thus to ensure that the structure has a sufficient safety margin. The safety margin is considered sufficient if the estimated probability of failure, p_f, expressed as the reliability index, β, is larger than the target reliability index, β_target. The reliability index is defined as

$$\beta = -\Phi^{-1}(p_\mathrm{f}) \quad , \tag{8}$$

where Φ^{-1} is the inverse of the cumulative standard normal distribution. Examples of values for the β_target from EN 1990 (CEN 2002) are shown in Tab. 3.

Tab. 3: Typical target reliability indices, β_target, according to EN 1990 for the ultimate and the serviceability limit state with reference periods one and 50 years (CEN 2002). The numbers in parentheses indicate the associated probability of failure, $p_\mathrm{f} = \Phi(-\beta_\mathrm{target})$.

Limit state	β_target	
	One year	**50 years**
Ultimate limit state	4.7 ($1.3 \cdot 10^{-6}$)	3.8 ($0.7 \cdot 10^{-4}$)
Irreversible serviceability limit state	2.9 ($1.9 \cdot 10^{-3}$)	1.5 ($0.7 \cdot 10^{-1}$)

Based on the reasoning in the previous sections, p_f should be interpreted as the degree of belief in the structure not fulfilling the quantitative design criteria. It is noted that the target reliability index not only is a function of probability, but also is calibrated to previous practice (Cornell 1969, Ellingwood & Galambos 1982, Ellingwood 2008) or can be the result of an optimization process taking into account for example the cost of increasing the reliability and the willingness

of the society to invest in safety (Rackwitz 2000). In the case of an existing structure, the target reliability index will generally be accepted to be lower than in the case of a new structure, since the cost of increasing the reliability of an existing structure is larger than for a new structure which is still on the drawing table (*fib* 2017).

3.4 Estimate of the probability of failure

The methods for estimating the probability of failure are usually grouped according to their *level of sophistication* from Level 1 to 3 (Thoft-Christensen & Baker 1982, Schneider 2006). Examples of the methods and the corresponding levels of sophistication are shown in Tab. 4, and the methods are demonstrated in Fig. 5 using a known limit state function $g(\boldsymbol{x}) = 0$.

The probability of failure is generally calculated by the integral

$$p_\mathrm{f} = \int_{g(\boldsymbol{x})\leq 0} f(\boldsymbol{x})\mathrm{d}\boldsymbol{x} \quad , \tag{9}$$

where a known joint probability distribution of the basic variables, $f(\boldsymbol{x})$, is integrated over the unsafe region, $g(\boldsymbol{x}) \leq 0$. An exact solution of Eq. (9) can only be found analytically in a very few cases, e.g. where $f(\boldsymbol{x})$ is the normal or the rectangular distribution and the limit state function $g(\boldsymbol{x}) = 0$ is linear. In other cases, the integral is solved either by numerical integration or by simulation. These methods pertain to the Level 3 methods described in Tab. 4.

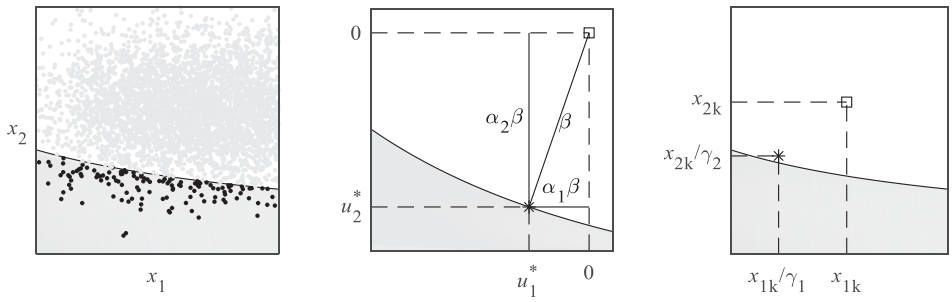

a) Level 3 method: p_f is found by dividing the number of outcomes in the unsafe region by the total number of outcomes.

b) Level 2 method: a nominal reliability index, β, is found by locating the point on $g(\boldsymbol{u}) = 0$ closest to the origin in the standard normal space.

c) Level 1 method: the nominal values for the basic variables, $x_{i\mathrm{k}}$, are scaled with partial factors, γ_i, in order to impose an intended safety level.

Fig. 5: Demonstration of the three levels of sophistication. The solid curved line is the limit state function, $g(\boldsymbol{x}) = 0$, and the shaded area is the unsafe region, $g(\boldsymbol{x}) \leq 0$.

Tab. 4: The levels of sophistication in reliability assessment methods (adapted from Thoft-Christensen & Baker 1982 and Schneider 2006).

	Description	**Representation of basic variables**	**Examples of methods**
Level 3	Methods where the true probability of failure is obtained by considering the full joint probability density function of the basic variables, and considering the true shape of the failure domain.	Probability density functions.	Monte Carlo, importance sampling, Latin hypercube sampling.
Level 2	Methods applying approximated probability distributions and approximations for the limit state function. Only nominal estimates of the probability of failure are obtained, that should only be used for comparison purposes.	Two values, e.g. mean and coefficient of variation.	First order reliability methods (FORM) and second order reliability methods (SORM) and their inverse formulations.
Level 1	Methods currently available in design codes where an intended level of safety on component level is attained by use of partial factors for load and resistance variables. Statements about the probability of failure cannot be made.	One single value, e.g. characteristic or nominal.	Partial factor method.

The Level 3 methods will give exact estimates of the probability of failure if the analyst has full knowledge of the problem at hand (Der Kiureghian 1989). One Level 3 method is the *Monte Carlo* method. Here, random realizations are generated for each of the basic variables as shown in Fig. 5a, taking into account the respective distributions and possible correlation between the basic variables. The limit state function is furthermore evaluated for each of the sets of random realizations and the probability of failure is the number of limit state evaluations giving $g(\boldsymbol{x}) \leq 0$ divided by the total number of evaluations. Further improvements to this method aiming at reducing the necessary number of limit state function evaluations include for example importance sampling (Melchers 1999) and Latin hypercube sampling (McKay et al. 1979, Olsson et al. 2003). Two important drawbacks make the Level 3 methods unsuitable for structural engineering applications:

- Full knowledge about the statistical distributions of the basic variables is in general not possible to obtain.
- Since a large number of samples is necessary to obtain the necessary accuracy in the estimate of p_f, and the limit state function is often complex or time consuming to evaluate, the method will be costly or impossible to use.

Using available exact or approximated transformation rules, the vector of basic variables, $\boldsymbol{x}$, can be transformed to a vector of uncorrelated standard normally distributed variables, $\boldsymbol{u}$, with means equal to zero and unit-variances (Hasofer & Lind 1974). After the transformation, the vector $\boldsymbol{u}$ and the limit state function, $g(\boldsymbol{u}) = 0$, will be located in the so-called *standard normal space* or *u-space*, with the origin corresponding to the mean value of the variables $\boldsymbol{x}$, shown in Fig. 5b. In Level 2 methods, $g(\boldsymbol{u}) = 0$ is approximated by a first- or second-order polynomial, and an approximated value for β is the minimum distance from $g(\boldsymbol{u}) = 0$ to the origin. The point on $g(\boldsymbol{u}) = 0$ closest to the origin, $\boldsymbol{u}^*$, is the point at the boundary between the safe and the unsafe region with the highest probability of occurring, and is often denoted as the *design point*. If $g(\boldsymbol{u}) = 0$ is far from the origin, the safety margin is large, giving a large β and a corresponding small p_f.

The design point can be found in an iterative manner, and several procedures are available in the literature (Hasofer & Lind 1974, Rackwitz & Fiessler 1978, Shinozuka 1983, Liu & Der Kiureghian 1991). If the limit state function is approximated by a linear polynomial, the method is denoted First Order Reliability Method (FORM), and an example of a FORM solution is shown in Fig. 5b. Also shown in the figure are the sensitivity factors, α_i, that indicate the contribution from the variation of each of the basic variables to the probability of failure. The FORM solution is exact if the limit state is linear and the basic variables can be transformed to standard normally distributed variables by a one-to-one transformation. For large β, i.e. low p_f, FORM is a good approximation in other cases as well. The FORM solution can be improved by including second-order terms in the approximated limit state function, and this class of improved methods is denoted Second Order Reliability Methods (SORM) (Hohenbichler et al. 1987).

Assuming that the compressive strength of concrete, f_c, and the yield strength of the reinforcement, f_y, are the only basic variables for the resistance of reinforced concrete, the corresponding sensitivity factors α_{f_c} and α_{f_y} can be estimated by a FORM analysis. In an over-reinforced cross-section, the bending moment capacity will be governed by failure of the compressive zone before the yield strength of the reinforcement is reached. In this case, α_{f_c} would be significantly larger than α_{f_y}, since the concrete governs the failure mode. For an under-reinforced cross-section, where the failure mode is governed by yielding of the reinforcement steel, the opposite would be the case, i.e. $\alpha_{f_y} \gg \alpha_{f_c}$. This illustrates the added value of the results from analyses with the Level 2 methods.

In the Level 1 methods, the design point is estimated directly by scaling characteristic or nominal values for the basic variables by partial factors. Design code developers calibrate the values of the partial factors in order to reach a target reliability level on the structural component level. By applying partial factors it is assumed that the values of the basic variables lie in the safe region, $g(\boldsymbol{x}) > 0$, see Fig. 5c. Implicit in the partial factors in the Eurocodes (CEN 2002) are assumptions of a linear limit state function following Eq. (6) and constant sensitivity factors for the resistance, $\alpha_{\mathrm{R}} = 0.8$, and load, $\alpha_{\mathrm{E}} = -0.7$, respectively. Further assuming that the load and resistance can be treated independently, the target reliability index for the resistance becomes $\alpha_{\mathrm{R}}\beta_{\mathrm{target}}$.

From this short summary of structural reliability methods it should be noted that the Level 2 methods are approximations of the Level 3 methods and that the Level 1 methods are calibrated to solutions obtained with the Level 2 methods. Since the Level 1 methods are based on probabilistic measures, allowing the engineer to directly incorporate a target reliability and the variability of the basic variables, but only a design point is obtained, the method is often denoted as *semi-probabilistic* (Cornell 1969, Ellingwood & Galambos 1982, Ellingwood 2008).

3.5 Response surfaces and Bayesian regression

In the methods introduced in the previous section, it was assumed that the limit state function was known and available as an analytical expression on closed form. This is necessary since the different methods usually require calculation of the gradients of the limit state function. However, if the structural response is evaluated using NLFEA, such analytical expressions will not be available. In that case it can be useful to fit a *response surface* to the results from the NLFEA (Faravelli 1989). A response surface is a polynomial of a user-specified degree with unknown coefficients on the form

$$R_{\mathrm{NLFEA}}(\boldsymbol{x}) \approx \boldsymbol{y}(\boldsymbol{x})\boldsymbol{b} + e \quad , \tag{10}$$

where $R_{\mathrm{NLFEA}}(\boldsymbol{x})$ is the NLFEA prediction using the values of the basic variables $\boldsymbol{x}$, the row vector $\boldsymbol{y}(\boldsymbol{x})$ contains powers of the basic variables and the column vector $\boldsymbol{b}$ contains the k unknown coefficients of the response surface. $R_{\mathrm{NLFEA}}(\boldsymbol{x})$ can be the load carrying capacity of a structure or the deflection or crack width at a certain point for a given set of loads. The modelling uncertainty is usually included by multiplying Eqs. (4) and (10), i.e.

$$R = \theta R_{\mathrm{NLFEA}}(\boldsymbol{x}) \approx \theta\ (\boldsymbol{y}(\boldsymbol{x})\boldsymbol{b} + e) \quad , \tag{11}$$

such that the modelling uncertainty θ is treated as a basic variable in addition to $\boldsymbol{x}$. The error term, e, is due to approximating the NLFEA prediction with a polynomial, and is usually assumed normally distributed with a mean equal to zero and an unknown variance, i.e. $e \sim \mathrm{N}(e|0, \sigma_{\mathrm{e}}^2)$. Often, a second-order polynomial without cross-terms is used (Bucher &

Bourgund 1990), giving $\boldsymbol{y}(\boldsymbol{x}) = \{1, x_1, x_2, x_1^2, x_2^2\}$ and $\boldsymbol{b} = \{b_0, b_1, b_2, b_{11}, b_{22}\}^T$ in a situation with two basic variables, such that the response surface is given by

$$R_{\mathrm{NLFEA}}(\boldsymbol{x}) \approx b_0 + b_1 x_1 + b_2 x_2 + b_{11} x_1^2 + b_{22} x_2^2 + e \quad . \tag{12}$$

The k unknown coefficients can be estimated by performing NLFEA at a set of l points $\boldsymbol{x}_j$. These points can be denoted as *sampling points*, *experimental points* or *training points* for the response surface, and are usually arranged around a centre in a pattern with a specified spacing (Faravelli 1989). In order to determine the coefficients, there must be at least as many sampling points as unknown coefficients, i.e. $l \geq k$. The m NLFEA predictions are collected in the column vector $\boldsymbol{c} = \left\{R_{\mathrm{NLFEA},1}, \dots, R_{\mathrm{NLFEA},l}\right\}^T$, the powers of the sampling points are collected in the matrix $\boldsymbol{A} = [\boldsymbol{y}(\boldsymbol{x}_1), \dots, \boldsymbol{y}(\boldsymbol{x}_l)]^T$ and the error terms associated with each sampling point are collected in the column vector $\boldsymbol{e} = \{e_1, \dots, e_l\}^T$, giving the following linear system of equations

$$\boldsymbol{c} = \boldsymbol{A}\boldsymbol{b} + \boldsymbol{e} \quad . \tag{13}$$

By solving for the unknown coefficients, $\boldsymbol{b}$, the following conditional expressions are obtained for the expected value

$$\mathrm{E}[\boldsymbol{b}|R, \boldsymbol{x}] = (\boldsymbol{A}^T\boldsymbol{A})^{-1}\boldsymbol{A}^T\boldsymbol{c} = \widehat{\boldsymbol{b}} \tag{14}$$

and the variance

$$\mathrm{VAR}[\boldsymbol{b}|R, \boldsymbol{x}] = (\boldsymbol{A}^T\boldsymbol{A})^{-1}\sigma_{\mathrm{e}}^2 = \boldsymbol{V}_{\mathrm{b}}\sigma_{\mathrm{e}}^2 \tag{15}$$

of the coefficients, respectively, by taking into account the assumptions regarding the probability distribution for the error term. In the classical response surface method (Faravelli 1989, Bucher & Bourgund 1990), the coefficients are treated in a deterministic manner, i.e. neglecting the uncertainty introduced by the response surface and the correlation between the coefficients as induced by Eq. (15). By treating the coefficients as uncertain variables, a probability distribution for the coefficients can be predicted by using *Bayesian regression* (Gelman et al. 2014). As a first step, the variance of the error term, σ_{e}^2, can be estimated with the following unbiased estimator

$$\mathrm{s}_{\mathrm{e}}^2 = \frac{1}{l-k}\left(\boldsymbol{A}\widehat{\boldsymbol{b}} - \boldsymbol{c}\right)^T\left(\boldsymbol{A}\widehat{\boldsymbol{b}} - \boldsymbol{c}\right) \quad , \tag{16}$$

which is defined for $l > k$. Treating also the coefficients as uncertain variables our problem now has the following $n + k + 1$ random variables that can be incorporated in a FORM analysis: i) n basic variables $\boldsymbol{x}$, ii) k uncertain parameters of the response surface, and iii) the modelling uncertainty θ.

The response surface method is often combined with FORM according to the following approach:

1) Fit the response surface to a set of sampling points. The first set of sampling points are often centred on the mean values of the basic variables.
2) Find the location of the design point.
3) Find a new centre for the sampling points based on the design point and the old centre.
4) Check for convergence and repeat from 1) if necessary.

In the literature, much focus has been put on step 3) from the approach above (Bucher & Bourgund 1990, Rajashekar & Ellingwood 1993, Allaix & Carbone 2011, Zhao & Qiu 2013) in order to reduce the necessary number of updates of the response surface, and hence reduce the necessary number of NLFEA predictions.

3.6 Inverse reliability methods and semi-probabilistic safety formats for NLFEA

The Level 2 and 3 reliability methods discussed in Sec. 3.4 can be used to estimate the reliability of a structure for a given level of knowledge. However, in many structural engineering cases the inverse can in fact be more useful, i.e. an estimate of the value of the limit state function for a given β_{target}. Using the methods inverse FORM or SORM and treating the load and resistance as independent variables, the resistance for a given $\alpha_{\text{R}}\beta_{\text{target}}$ can be estimated based on knowledge about the basic variables of the resistance (Li & Foschi 1998, Giske et al. 2017).

Simpler inverse methods can be derived by considering a *Taylor series expansion* without higher order terms of the predicted resistance as function of the basic variables of the resistance, $R_{\text{NLFEA}}(\boldsymbol{x})$, around a point $\boldsymbol{x}_0$, i.e.

$$R_{\text{NLFEA}}(\boldsymbol{x}) \approx R_{\text{NLFEA}}(\boldsymbol{x}_0) + \sum_{i=1}^{n}\left[\left(x_i - x_{0,i}\right)\frac{\partial R_{\text{NLFEA}}}{\partial x_i}\right] \quad , \tag{17}$$

where $\partial R_{\text{NLFEA}}/\partial x_i$ is the partial derivative of the resistance with respect to basic variable x_i. Eq. (17) can be interpreted as a linear combination of the n basic variables $\boldsymbol{x}$, and the expected value and variance can be found from

$$\text{E}[R_{\text{NLFEA}}(\boldsymbol{x})] \approx R_{\text{NLFEA}}(\boldsymbol{x}_0) + \sum_{i=1}^{n}\left[\left(\mu_{x_i} - x_{0,i}\right)\frac{\partial R_{\text{NLFEA}}}{\partial x_i}\right] \quad , \tag{18}$$

and

$$\mathrm{VAR}[R_{\mathrm{NLFEA}}(\boldsymbol{x})] \approx \sum_{i=1}^{n}\left[\sigma_{x_i}^2\left(\frac{\partial R_{\mathrm{NLFEA}}}{\partial x_i}\right)^2\right] \quad , \tag{19}$$

respectively, assuming uncorrelated basic variables. Eq. (19) can easily be extended to also take into account correlation. Assuming that the Taylor series expansion can be taken around the point represented by the mean values of the basic variables, $\boldsymbol{x}_{\mathrm{m}} = \{\mu_{x_1}, \dots, \mu_{x_n}\}^T$, and that the partial derivative can be approximated by

$$\frac{\partial R_{\mathrm{NLFEA}}}{\partial x_i} \approx \frac{\Delta R_{\mathrm{NLFEA},i}}{\Delta x_i} = \frac{R_{\mathrm{NLFEA}}(\boldsymbol{x}_i) - R_{\mathrm{NLFEA}}(\boldsymbol{x}_{\mathrm{m}})}{\Delta x_i} \quad , \tag{20}$$

where $\boldsymbol{x}_i = \{\mu_{x_1}, \dots, \mu_{x_i} - \Delta x_i, \dots, \mu_{x_n}\}^T$ is a point where all basic variables are represented by the mean value except variable x_i which is reduced by the value Δx_i, Eqs. (18) and (19) simplify to Eqs. (21) and (22) respectively and the coefficient of variation of the NLFEA prediction is given by Eq. (23) (Schlune et al. 2011, 2012).

$$\mathrm{E}[R_{\mathrm{NLFEA}}(\boldsymbol{x})] \approx R_{\mathrm{NLFEA}}(\boldsymbol{x}_{\mathrm{m}}) = R_{\mathrm{NLFEA,m}} \tag{21}$$

$$\mathrm{VAR}[R_{\mathrm{NLFEA}}(\boldsymbol{x})] \approx \sum_{i=1}^{n}\left[\sigma_{x_i}^2\left(\frac{R_{\mathrm{NLFEA}}(\boldsymbol{x}_i) - R_{\mathrm{NLFEA}}(\boldsymbol{x}_{\mathrm{m}})}{\Delta x_i}\right)^2\right] \tag{22}$$

$$V_{R_{\mathrm{NLFEA}}} = \frac{\sqrt{\mathrm{VAR}[R_{\mathrm{NLFEA}}(\boldsymbol{x})]}}{\mathrm{E}[R_{\mathrm{NLFEA}}(\boldsymbol{x})]} \tag{23}$$

By assuming normal or log-normal distributions for the basic variables, the increment Δx_i can be calculated as a function of a step factor f times the standard deviation or the coefficient of variation of the variable, see the work by Schlune et al. (2011, 2012) for further details. Furthermore, if a log-normal distribution is assumed for the resistance, the resistance can be expressed as

$$R = \theta\, G\, R_{\mathrm{NLFEA}}(\boldsymbol{x}) \quad , \tag{24}$$

if only the basic variables related to the materials, and not the geometry, are included in $\boldsymbol{x}$. θ is the modelling uncertainty assumed represented by a log-normally distributed variable with mean μ_θ and coefficient of variation V_θ. G is a random variable taking into account the effect of the uncertainties of the geometry on the resistance, assumed to be represented by a log-normally distributed variable with unit-mean and coefficient of variation V_{G}. The resistance corresponding to the target reliability of the resistance, $\alpha_{\mathrm{R}}\beta_{\mathrm{target}}$, can then be estimated from

$$R_{\mathrm{d}} = R_{\mathrm{NLFEA,m}}\mu_{\theta}\exp[-\alpha_{\mathrm{R}}\beta_{\mathrm{target}}V_{\mathrm{R}}] = \frac{R_{\mathrm{NLFEA,m}}}{\gamma_{\mathrm{R}}} \quad , \tag{25}$$

where the sensitivity factor of the resistance α_{R} was discussed in Sec. 3.4 and the coefficient of variation of the resistance can be estimated as

$$V_{\mathrm{R}} = \sqrt{V_{\theta}^2 + V_{\mathrm{G}}^2 + V_{R_{\mathrm{NLFEA}}}^2} \quad . \tag{26}$$

Note that V_{G} and $V_{R_{\mathrm{NLFEA}}}$ represent the uncertainty of the resistance due to the uncertainty of the basic variables, i.e. how the uncertainties of the basic variables propagate through the resistance. γ_{R} is usually denoted the *global resistance factor* and can be compared to the partial factors currently used in most design codes. However, where the partial factors incorporate the uncertainties on material level, the global resistance factor incorporates the uncertainties on global level, thus allowing the engineer to assess the resistance of the structure as a whole and the effects of the uncertainties, by realistic estimates of the load-bearing capacity.

A further simplification is obtained by only considering the constant term in Eq. (17). Assuming that the NLFEA prediction using the lower 5%-fractile values of the basic variables yield the lower 5%-fractile value of the resistance, i.e. the NLFEA prediction using characteristic values $\boldsymbol{x}_{\mathrm{k}}$ gives the characteristic value of the resistance $R_{\mathrm{NLFEA,k}}$, the following relation can be derived based on the assumption of a log-normal distribution for the resistance

$$R_{\mathrm{NLFEA,k}} = R_{\mathrm{NLFEA,m}}\exp[-1.645V_{\mathrm{R_{NLFEA}}}] \quad . \tag{27}$$

By inverting Eq. (27), the coefficient of variation of the NLFEA prediction due to the uncertainties of the basic variables can be estimated from

$$V_{R_{\mathrm{NLFEA}}} = \frac{1}{1.645}\ln\left[\frac{R_{\mathrm{NLFEA,m}}}{R_{\mathrm{NLFEA,k}}}\right] \quad , \tag{28}$$

which can be input to Eqs. (26) and (25). The method involving the last simplification is called the *method of estimation of coefficient of variation of resistance* (ECOV) (Cervenka 2013) and is included in the fib *Model Code for Concrete Structures 2010* (*fib* 2013). The application of the ECOV method and the method suggested by Schlune et al. have been demonstrated in the literature (Schlune et al. 2011, 2012, Belletti et al. 2011, 2013, 2014, 2015, Cervenka 2013, Allaix et al. 2013, Pimentel et al. 2014, Blomfors et al. 2016, Engen et al. 2017d).

4. Non-linear finite element analyses of reinforced concrete structures

4.1 NLFEA in structural engineering

So far, NLFEA of reinforced concrete structures have been introduced as analyses where concrete and reinforcement are modelled with realistic material models. In addition to material non-linearities, NLFEA can also include non-linearities due to geometry and contact. In analyses of arch dams, for example, the interface between the reinforced concrete arch and the bedrock should be free to separate and slide so that no tensile forces are introduced in the structure due to artificial restraining (Aasheim et al. 2017). However, in this work, the main emphasize has been put on the material non-linearities. Although there are several application areas for NLFEA (Vecchio 2001, *fib* 2008), as shown in Tab. 5, attention will be paid to the application of NLFEA during design or reassessment of structures in the ultimate limit state, and more specifically to the one-step approach discussed in Chs. 1 and 3.

Tab. 5: Typical application areas for NLFEA of reinforced concrete structures.

Design of new structures or reassessment of existing structures	• Capacity prediction of existing deteriorated structures, existing structures subjected to new or increased loads and/or existing structures designed according to superseded design codes. • Study of structural effects due to intentional or unintentional undesirable events, e.g. explosions or ship impacts, and development of adequate protective measures. • One- and two-step approaches for structural design.
Research and development	• Simulations of experiments to develop a deeper understanding of governing phenomena. • Development of material models for NLFEA based on comparison with experimental results.
Forensic engineering	• Investigation of the causes of structural collapse.
Development of design codes	• Calibration of Level 1 or simplified Level 2 reliability methods based on more sophisticated Level 2 or Level 3 methods.

In everyday structural engineering, LFEA are used to calculate the internal force distribution due to external loads. Due to the assumed linear behaviour of the structure, the solution is found by solving a linear set of equations. For plate and shell structures, the results are usually presented as diagrams or contour plots showing the distribution of internal bending moments, transverse shear forces, and axial forces or in-plane forces allowing for efficient design calculations either by hand or using specialized design software (Brekke et al. 1994).

In NLFEA, however the problem is solved using an incremental-iterative method. Incremental, since the external loads are applied in several load steps or load increments. Iterative, since in

each load step, the solution is found by consecutively, or iteratively, updating the response in order to take into account the effects of non-linearities and to approach equilibrium between external loads and internal forces. At each load step, the equilibrium iterations are continued until a user-prescribed convergence criterion is satisfied or a predefined maximum number of iterations is reached. Several challenges are thus encountered, for example:

How many load steps should be used?

What is the adequate degree of equilibrium that can be accepted?

and if a one-step approach is used, and since there is usually no clear-cut definition of structural failure in NLFEA:

What is the actual structural capacity predicted by the NLFEA?

The results from the NLFEA will usually not include a statement saying whether the capacity is still ok or not in a given load step, but basically just indicate if the solution was converged or not, or if the analysis was aborted due to divergence. The results from NLFEA also comprise more than just a set of internal forces. Information about for example cracking of concrete and yielding of the reinforcement will be available in every integration point of the concrete and reinforcement elements for every load step, and should be reviewed by the analyst in order to justify the adequacy of the outcome.

In Sec. 2.4 the modelling uncertainty was introduced, and it was noted that the modelling uncertainty depends on which mathematical models that are selected to represent the physical problem at hand. The modelling uncertainty thus depends on our selected strategy for obtaining a solution from the NLFEA, and the term *solution strategy* is used throughout this chapter to describe the set of choices that need to be made in a NLFEA. In this chapter, special emphasis will be put on how NLFEA *could* be performed in everyday structural engineering by selecting or developing a proper solution strategy, the effect of different degrees of refinement in our models and finally, aspects related to quantification of the modelling uncertainty. A thorough introduction to the theory behind NLFEA is beyond the scope of this thesis, and the reader should consult standard textbooks (Zienkiewicz & Taylor 1994, Bathe 2006, Belytschko et al. 2014).

4.2 The process of developing a solution strategy

A solution strategy for NLFEA comprises choices regarding kinematic compatibility, material models and equilibrium, as illustrated in Tab. 6. Most analysis software include several possibilities for combining different material models, for using a variety of different element types and for solving the equilibrium equations with different iterative methods. A broad suite of methods or models should be available for the user, since most models will be more suited to some applications than others. However, the user should select the solution strategy with care

and be aware of the consequences of the choices that are made (Vecchio 2001, *fib* 2008, Hendriks et al. 2017a). For example, the boundary conditions can play a significant role, either by introducing artificial tensile forces, leading to premature cracking, or by restraining longitudinal elongation, leading to an overestimation of the benefit from the compressive membrane effect in slabs and beams. In shell structures like the dam shown in Fig. 2, shell elements can seem to be the most natural choice of element type, however the inherent assumption of plane sections is most likely violated by cross-sectional thicknesses of several meters, leaving solid elements as the only viable option. Also, the application of loads, such as distributed pressures, will generally become more accurate for solid elements than for shell elements.

Tab. 6: Examples of the content of a solution strategy for NLFEA.

Kinematic compatibility	• Finite element types for concrete and reinforcement, including order of numerical integration. • Finite element sizes. • Idealization of geometry. • Idealization of boundary conditions.
Material models	• Material models for concrete and reinforcement. • Material models for possible interfaces and boundary conditions.
Equilibrium	• Iterative methods for the solution of the non-linear equilibrium equations. • Convergence criteria and suitable tolerances. • Method for determining if the capacity was reached or not.

The engineer is left with two general approaches for selecting a solution strategy, either develop his or her own solution strategy for a specific purpose, or select a solution strategy based on a set of guidelines developed for safe use of NLFEA (Hendriks et al. 2017a, 2017b). The process of developing a solution strategy consists of the four main activities 1) definition, 2) verification, 3) validation and 4) demonstration of applicability, as illustrated in Tab. 7.

In the *definition* activity, the engineer would usually explore the available options in available software or review relevant literature. The results obtained from analyses with different solution strategies might be compared in order to find the most suitable for the purpose. The engineer can define the solution strategy following two different categories or philosophies, either

i) use sub-models with a range of free parameters that can be fitted to experimental observations, or
ii) select sub-models that are only functions of readily observable basic variables.

An example of the first category can be if Eq. (2) was used as a sub-model for the Young's modulus without fixing the parameters of the model to the values predefined by the design code. An example of the second category could be the solution strategy developed in the present work, where the compressive cylinder strength of concrete is the only required input to the material model for concrete. Note that which category that is selected by the engineer is a matter of taste and depends on whether experimental results are available for calibration or not. Many free parameters most likely leads to overfitting of the model (Beck & Yuen 2004), giving good predictions for the cases that were used in the calibration process, but most likely leading to worse predictions elsewhere. However, in a design situation or when an existing structure is being assessed, calibration is less applicable since no observations are usually available describing the true behaviour of the structure.

Tab. 7: The activities in the process of developing a solution strategy for NLFEA.

Definition	Select suitable material models, element types, iteration methods, etc.
Verification	Apply fundamental checks to assess if the model works as expected and assess the sensitivity to variations of the solution strategy, e.g. mesh size sensitivity and load step size sensitivity.
Validation	Assess how well the NLFEA predictions compare to the real structural behaviour, i.e. quantifying the modelling uncertainty by comparing NLFEA predictions to experimentally obtained results.
Demonstration of applicability	Prove that the solution strategy is suitable for the intended purpose.

During *verification* and *validation*, the engineer would seek answers to the questions *Are we solving the equations right?* and *Are we solving the right equations?* (Roache 1998, Engen et al. 2017a). In the NLFEA context, verification thus comprises sensitivity studies of for example the element sizes, the element types, the load step sizes, the convergence tolerances and the iteration methods. Verification also comprise typical single element tests that are performed in order to check if the material models behave as expected. Validation on the other hand, is related to the idealization of the structural geometry, boundary conditions and material behaviour and thus involves quantification of the modelling uncertainty for the selected solution strategy. If a solution strategy was defined following category i) above, these activities would also include estimating the values for the free parameters of the sub-models. Based on the findings in the verification and validation activities, the engineer might take a step back to the definition activity and make changes to the solution strategy.

The last step involves a *demonstration of applicability* by testing the solution strategy on realistic cases similar to the practical design problem it is intended for. The purpose of the final activity is to reveal if the expected important phenomena can be captured and the level of detail in the results is sufficient to be used as a basis for decisions. Note that the process has a subjective nature, leaving to the engineer to decide what is *good enough* or *detailed enough*.

The process of developing a solution strategy is further discussed in Paper II and III (Engen et al. 2015, 2017b) appended to the thesis.

4.3 The degree of refinement of the solution strategy

A solution strategy for NLFEA for structural engineering purposes should produce results that agree as close as possible with the observed behaviour from experiments, but apart from that, be as simple as possible (Beck & Yuen 2004). The refinement of the solution strategy should be limited to a level reflecting the significance of the decisions that are made based on the analysis outcomes (Der Kiureghian & Ditlevsen 2009), and the engineer's level of knowledge about the problem at hand. That is, a refinement of the solution strategy is only justified if the values of the possible additional basic variables can be found with a reasonable degree of belief, and if the uncertainty in the outcome of the NLFEA is reduced to such an extent that the confidence of the decision maker is improved. This can be obtained by selecting a solution strategy with a limited number of basic variables, where the basic variables are of a nature that are observable in experiments, thus giving the engineer the possibility to reduce the epistemic uncertainties by testing.

Selecting a complex solution strategy with many basic variables and free parameters results in a problem with a large contribution from epistemic uncertainties of the basic variables, since there are many variables with uncertain values. Such solution strategies can also have a limited range of validity since the free parameters can be fitted to a limited range of experimental observations. On the other hand, a simpler solution strategy will have a higher modelling uncertainty since the effects that are not explicitly modelled are implicitly contributing to the modelling uncertainty (Ditlevsen 1982, Engen et al. 2017a). The simpler models can have the benefit of being more widely applicable, or equally applicable in a wide range of problems, but the more complex solution strategies will have the benefit that the uncertainties can be reduced by reducing the epistemic uncertainties of the basic variables (Faber 2005). Note that if values of any of the basic variables are not available, the values are usually estimated using additional sub-models, and as noted in Sec. 2.4 the modelling uncertainty of the additional sub-models contribute to the modelling uncertainty of the solution strategy.

With reference to Secs. 3.5 and 3.6 the degree of refinement of the solution strategy has direct impact on assessments using the one-step approach, for example based on the method suggested by Schlune et al. (2011, 2012), or Level 2 analyses based on the response surface method. If more basic variables are included in the model, more analyses are needed in order to estimate the coefficient of variation of the resistance or the unknown coefficients of the response surface, and the scope of the assessment increases.

When being introduced to the topic of NLFEA of reinforced concrete structures, one can be confronted with statements like

Program A gives much better results than Program B.

or

With NLFEA, you can obtain exactly the result you want.

Although these can be true in some cases, such statements should not reflect the attitude of the expert. Statements of the first type reflect more the commercial part than the academic or engineering part of the topic of NLFEA. Different analysis software have different libraries of sub-models, however since each user in any case and with any software would do the utmost effort in making predictions with a modelling uncertainty as low as possible, a clear-cut distinction between, or ranking of, software seems not to be justified.

Statements of the second type can reflect the experience with using material models with many free parameters that need to be calibrated. If such solution strategies are applied outside the range they were calibrated, there will always be a risk of making inaccurate or unsafe predictions. Also, the second statement can reflect what we see as the outcome of blind prediction competitions (e.g. Jaeger & Marti 2009a, 2009b) where experts do their best in predicting an unknown outcome of an experiment. The results from such competitions usually have significant variation, and can give valuable insight in the effects of selecting different solution strategies and of not knowing the result of the experiment on beforehand.

4.4 Quantification of the modelling uncertainty

The models used in engineering analyses are only approximations of the reality. The question that must be asked is whether the model is suitable for the particular application where it is to be used. This can be assessed by quantifying the modelling uncertainty. The modelling uncertainty of a solution strategy for NLFEA, θ as defined in Eq. (4), is usually assumed represented by a log-normally distributed variable. The probability distribution for the modelling uncertainty can be given in terms of the mean, μ_θ, and the coefficient of variation, V_θ, that are generally unknown parameters and should be estimated by performing benchmark analyses, i.e. comparing NLFEA predictions to known experimental outcomes.

The mean can be denoted the *bias* and indicates the average fit to experimental results. Note that if a model with free parameters is calibrated to experimental outcomes using some form of regression similar to what was discussed in Sec. 3.5, i.e. a category i) model as introduced in Sec. 4.2, the bias will be $\mu_\theta = 1.0$ for the set of experiments it was calibrated to, due to the assumptions regarding the properties of the error term. However, if a category ii) model is used, $\mu_\theta \neq 1.0$. The coefficient of variation is a measure of the *spread* of the NLFEA predictions. For example, if no NLFEA prediction is found to be equal to the experimental outcome, the predictions can still on average be close to the experimental outcomes, however having a coefficient of variation that depends on the respective deviations from the average. In Paper IV

appended to this thesis (Engen et al. 2017a) a method based on Bayesian inference is suggested for quantifying the modelling uncertainty.

In the literature, one can encounter one of the following three limiting cases when NLFEA predictions are compared to experimental outcomes:

1) One experimental outcome is compared to NLFEA predictions using different solution strategies.
2) The outcomes of a number of nominally equal experiments are compared to one NLFEA prediction of the experiment using one solution strategy.
3) One experimental outcome from each of a range of different experiments are compared to corresponding NLFEA predictions using one solution strategy.

If the modelling uncertainty is estimated in each of the cases, the estimate will describe three different effects. In the first case, the estimator for the modelling uncertainty, θ_1, becomes

$$\theta_{1,i} = \frac{R_{\text{exp}}}{R_{\text{NLFEA},i}} \quad , \tag{29}$$

where $R_{\text{NLFEA},i}$ is NLFEA prediction i. By taking the expected value of Eq. (29) it can be shown that the bias will be the ratio between the experimental outcome and the average NLFEA prediction and can have a contribution from the variation of the predictions. By finding the coefficient of variation of Eq. (29), it can be shown that this only depends on the variation of the NLFEA predictions. θ_1 is thus a measure of the inherent randomness in the population of models, or *between-model* uncertainty, and describes the obtained uncertainty in the prediction if a model was selected randomly to predict the experimental outcome. Interesting to note is that if R_{exp} was an average of the outcomes from a number of nominally equal experiments instead of only the outcome from one of the experiments, this would only influence the bias and not the coefficient of variation of θ_1.

Case 1 is the typical outcome from blind prediction competitions described above. Tab. 8 shows outcomes from a selection of blind prediction competitions, complementing the overview published by Schlune et al. (2012). The entries to the competitions include a broad variety of analysis methods, not only NLFEA. It can be seen that the largest spread and the most un-conservative bias was obtained in the estimate of the first failure load of the large beam tested by Collins et al. (2015). In the ten first cases in Tab. 8, the failure mode in the experiment was governed by the concrete. In the rest of the cases, the reinforcement contributed to crack control, and hence improved the ductility. The biases in the two sets of cases are similar, but the spread is larger in the first set, indicating that failure modes governed by the concrete are more challenging to predict accurately. It is interesting to note that the seemingly simple problem of slender columns (Strauss et al. 2015) has on average slightly un-conservative predictions, however with a low spread.

Tab. 8: Outcomes of blind prediction competitions. The between-model uncertainty is presented with the expected value and the coefficient of variation in parentheses.

Reference	Type of structural element	Number of participants	Between-model uncertainty
Collins et al. (1985)	Panel A loaded in plane stress	27	0.90 (0.19)
	Panel B loaded in plane stress	27	1.22 (0.44)
	Panel C loaded in plane stress	27	1.02 (0.24)
	Panel D loaded in plane stress	27	0.87 (0.46)
Collins et al. (2015)	Large beam, first failure	66	0.81 (0.60)
	Large beam, second failure	43	1.18 (0.35)
Jaeger & Marti (2009a, 2009b)	Slab, A1	8	0.90 (0.36)
	Slab, B1	8	1.14 (0.35)
	Slab, C1	8	0.85 (0.42)
	Slab, D1	8	1.09 (0.35)
	Slab, A2	8	0.92 (0.13)
	Slab, B2	8	1.06 (0.08)
	Slab, C2	8	0.91 (0.13)
	Slab, D2	8	1.13 (0.05)
van Mier & Ulfkjær (2000)	Small over-reinforced beam	8	1.09 (0.14)
	Large over-reinforced beam	8	1.08 (0.15)
Strauss et al. (2015)	Slender columns	8	0.88 (0.07)

In the second case, the estimator for the modelling uncertainty, θ_2, becomes

$$\theta_{2,i} = \frac{R_{\mathrm{exp},i}}{R_{\mathrm{NLFEA}}} \quad , \tag{30}$$

where $R_{\mathrm{exp},i}$ is the outcome of experiment i. Since R_{NLFEA} is a constant, θ_2 only describes the average and the variation of the experimental outcomes, scaled by the constant NLFEA prediction. Eq. (30) thus describes the physical variation of the experiment.

In the third case, the estimator becomes

$$\theta_{3,i} = \left(\frac{R_{\mathrm{exp}}}{R_{\mathrm{NLFEA}}}\right)_i \quad , \tag{31}$$

and θ_3 describes the uncertainty in the prediction obtained with the selected solution strategy. Opposed to θ_1 which describes between-model uncertainty, θ_3 describes *within-model* uncertainty. It is emphasized that if Eq. (31) is to give reasonable results, the engineer must

have available the experimental outcome $R_{\exp}$ and the corresponding values of the basic variables that are needed for input to the NLFEA prediction (Ditlevsen 1982, Der Kiureghian & Ditlevsen 2009). In addition, if values of some of the basic variables need to be estimated using available sub-models, the sub-models must be applied consistently from case to case. Otherwise, θ_3 will not describe the modelling uncertainty of the specific solution strategy. Interesting to note here is that if $R_{\exp}$ in Eq. (31) was replaced by the average of the outcomes from a number of nominally equal experiments instead of only one outcome, both the estimated bias and the coefficient of variation of the modelling uncertainty would be influenced. This indicates that the estimated modelling uncertainty also gets contributions from the uncertainty of the measurement of the experimental outcome, and from the physical uncertainties related to the experimental outcome. A pure modelling uncertainty without additional contributions from measuring uncertainties and physical uncertainties is thus not trivial to obtain. This is elaborated on in Paper IV appended to the thesis (Engen et al. 2017a).

Tab. 9 shows examples of modelling uncertainties obtained using different solution strategies developed for structural engineering purposes reported in the literature. In all the cases in Tab. 9, the solution strategies were developed following the procedure outlined in Sec. 4.2, i.e. first selecting a set of sub-models with a limited number of basic variables before validating the solution strategy by performing benchmark analyses.

Tab. 9: Modelling uncertainties estimated by comparing experimental outcomes with predictions using one specified solution strategy. The within-model uncertainty is presented with the expected value and the coefficient of variation in parentheses.

Reference	**Number of benchmark analyses**	**Within-model uncertainty**
Hendriks et al. (2017b)	13	1.11 (0.22)
Selby & Vecchio (1993)	18	1.05 (0.17)
Kotsovos et al., compiled in Engen et al. (2014)	69	1.02 (0.14)
Engen et al. (2017a)	38	1.10 (0.11)

Often, the modelling uncertainty for a defined range of values of the basic variables, or for specific failure modes, is sought. In that case, only a sample of experimental outcomes could be selected, reflecting the defined range. If however, the relevant subset of values for the basic variables and the failure mode is unknown, the sample of benchmark experiments should cover a larger range. This would be relevant in a design situation, where the failure mode is not known on beforehand, it can be different for different values of the basic variables and the failure mode might be due to interaction between different sectional forces. If a range of values for the basic variables is used, the correlation between the modelling uncertainty and the other basic variables could also be assessed. Several studies where the modelling uncertainty has been quantified using Eq. (31), can be found in the literature (Allaix et al. 2015, Holický et al. 2016, Engen et al. 2015, 2017a).

5. Summary of main contributions

5.1 Paper I

Predictive strength of ready-mixed concrete: exemplified using data from the Norwegian market

The variability of the compressive strength of ready-mixed concrete was studied by devising a method based on Bayesian inference and maximum likelihood estimators. A hierarchical model for the variability of material properties in concrete was formulated. The developed methods were demonstrated on more than 14000 compressive strength recordings from Norwegian ready-mixed concrete plants from the period 2013-2017, and the contributions to the variability from the different levels of the hierarchy were quantified. The following contributions are highlighted:

- A systematic approach for quantifying the variability of the concrete strength was developed.
- A hierarchical model for the variability of concrete properties was suggested.
- A set of prior parameters for the compressive strength was derived, which can be updated with new measurements in order to predict the compressive strength in existing structures based on a limited number of core samples.
- A general probability distribution for the compressive strength was derived, addressing the contributions from different levels of the hierarchy.
- The results from the analysis of the large dataset can be combined with additional data, if made available, in order to improve the predictions or to quantify the variability on higher levels of the hierarchy.
- Since the durability class gives a required maximum water-binder ratio, and the strength of the concrete is governed by the water-binder ratio, the durability class introduces a strength potential if the concrete is subject to strict durability requirements and low strength requirements. The results indicate that the designer should specify a strength class which utilizes this strength potential.
- A closer collaboration between the designer, contractor and producer is expected to result in less variability and a more homogeneous population of concrete.

5.2 Paper II

Solution strategy for non-linear finite element analyses of large reinforced concrete structures

Results from benchmark analyses with two different solution strategies for NLFEA were compared in order to select one solution strategy for further development. The main difference between the two strategies were the material models for concrete, where one was based on a set of recently published guidelines for NLFEA (Hendriks et al. 2017a) and the other was based on the work by Kotsovos and co-workers (see e.g. Kotsovos & Pavlovic 1996). Note that the NLFEA predictions based on the guidelines were made by the author, and that the other results were collected from the literature. In order to simulate the conditions met when analysing large

concrete structures in a design situation, relatively large solid finite elements were used in all the benchmark analyses. The results indicated that no significant gain in accuracy with respect to the ultimate limit capacity was obtained by refining the modelling of the tensile and post-cracking behaviour of concrete when large finite elements were used. Note that in this paper, the modelling uncertainty was defined as the inverse of Eq. (4), i.e. in the form of a utilization ratio, however with no influence on the conclusions. The following contributions are highlighted:

- The modelling uncertainty was quantified for NLFEA using a set of guidelines in cases where large finite elements are used.
- The modelling uncertainty was also quantified using results of the same benchmark analyses published work by Kotsovos and co-workers.
- It was demonstrated that a detailed modelling of the tensile or post-cracking behaviour of concrete is of minor importance when predicting the ultimate limit capacity in NLFEA with relatively large finite elements.

5.3 Paper III

Non-linear finite element analyses applicable for the design of large reinforced concrete structures

Based on the findings from Paper II, the solution strategy based on the material model by Kotsovos and co-workers was further developed. The paper demonstrates the process of developing a solution strategy as discussed in Sec. 4.2. The three-dimensional material model was adapted to a smeared, non-orthogonal, fixed cracking framework in order to facilitate its implementation in a commercial finite element software. The material model for concrete required only one material parameter, the uniaxial compressive strength. Suitable element types for concrete and reinforcement were selected and elaborated on and recommendations were given for selecting an iterative solution method for the non-linear equilibrium equations. The complete solution strategy was verified by assessing the sensitivity to finite element size, load step size and iterative solution method. The solution strategy was validated by performing benchmark analyses. Finally, the applicability to NLFEA of large reinforced concrete structures was demonstrated on a specially designed shell structure. The following contributions are highlighted:

- The process of developing a solution strategy for NLFEA was outlined.
- The material model was thoroughly described highlighting the developments made by the author.
- Arguments for selecting adequate finite element types, iterative solution methods and convergence criteria were presented.
- The importance of having a consistent method for defining structural failure was emphasized.
- The version of the material model that was presented in this paper has been made available in the finite element software DIANA.

5.4 Paper IV

A quantification of the modelling uncertainty of non-linear finite element analyses of large concrete structures

The uncertainties in engineering analyses were discussed with special emphasis on the modelling uncertainties of NLFEA. In order to validate the solution strategy presented in Paper III, 38 benchmark analyses were performed. Based on the results from the benchmark analyses, and assuming that the modelling uncertainty could be represented by a log-normally distributed variable, the parameters of the probability distribution of the modelling uncertainty were estimated using Bayesian inference. The collection covered a range of failure modes and concrete strengths. In order to characterize the predicted failure modes in the NLFEA, a measure denoted *the ductility index* was developed. The ductility index was defined as the plastic dissipation in the reinforcement divided by the total plastic dissipation of the system. The ductility index attains a value of zero if all the internal stress redistribution is governed by the concrete, and increases to values closer to one when the redistribution is governed by plastic deformations in the reinforcement. Insignificant correlation between the modelling uncertainty and the basic variables was found. The following contributions are highlighted:

- The modelling uncertainty was quantified using Bayesian inference.
- The failure mode was characterized using the developed ductility index.
- The results demonstrated the influence of physical uncertainties on the modelling uncertainty as discussed in Sec. 4.4, and that a pure modelling uncertainty is not straight forward to obtain.
- The implications of this can be useful since, for example, if the unknown correlation between the compressive strength and Young's modulus or the spatial variability of the concrete strength was not explicitly taken into account during quantification of the modelling uncertainty, they should neither be taken into account at a later stage, since the effects are already included in the estimated modelling uncertainty.

5.5 The work seen in context

As noted in Sec. 1.4, the present work has been carried out in the crossing between two specialist topics. It can thus be useful to see Papers I to IV in the context of Chs. 2 to 4. Fig. 6 shows the context graphically, as a flow-chart for reliability-based structural design using NLFEA. The shaded areas indicate topics that are treated in the appended papers. The non-shaded boxes indicate topics that were *not* treated in the appended papers. These topics have been briefly touched upon in Chs. 2 to 4 and will be returned to in Ch. 7.

A structure can be idealized into a finite element model following the solution strategy discussed in Papers II and III. NLFEA i takes input values from the distributions for the material uncertainty, $\boldsymbol{x}_{\mathrm{m},i}$, and the geometrical uncertainty, $\boldsymbol{x}_{\mathrm{g},i}$, and the analysis is performed according to the solution strategy giving the result R_i. The material uncertainty of concrete is treated in Paper I. The outcome R_i is input to the structural reliability analysis, here denoted *Level 2*

method. *Level 2 method* here represents typical level 2 or simplified level 2 methods as described in Secs. 3.4 to 3.6. The modelling uncertainty discussed in Papers III and IV is a property of the selected solution strategy and is input to the structural reliability analysis, along with information on the distributions of the material uncertainties and the geometrical uncertainties and the target reliability.

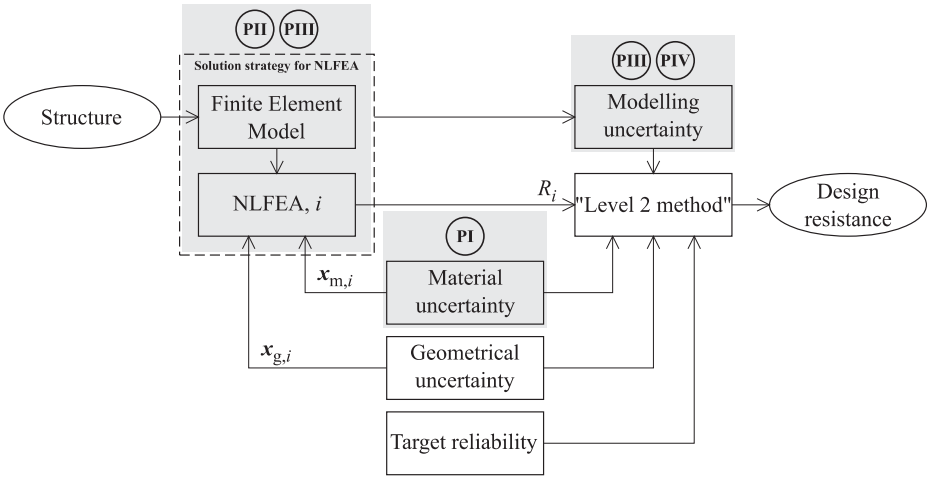

Fig. 6: The present work seen in the context of reliability-based structural design. The shaded areas indicate parts that are covered by the present work and PI to PIV represent Papers I to IV. $\boldsymbol{x}_{\mathrm{m},i}$ and $\boldsymbol{x}_{\mathrm{g},i}$ are the basic variables for material and geometry, respectively, R_i, is the outcome of analysis i and "Level 2 method" can be one of the Level 2 methods or semi-probabilistic safety formats discussed in Secs. 3.4 to 3.6.

From the structural reliability perspective, one wishes to differentiate the uncertainties as accurately as possible by including a number of basic variables. However from the NLFEA perspective this might not be feasible, since each new basic variable results in a larger number of analyses needed in order to assess the sensitivity of the response to the basic variables. Also, seeing the problem from the computational mechanics perspective, one could wish to incorporate as many variables as possible in the analysis model in order to get refined predictions of the structural behaviour. However, each basic variable should be introduced with suitable probability distribution functions. By increasing the complexity of the NLFEA, the computational cost increases, and by increasing the number of variables, the cost of the reliability assessment also increases.

6. Conclusions

The refinement of the solution strategy for NLFEA of reinforced concrete structures for structural engineering applications should reflect the level of knowledge that can be obtained about the problem at hand. A refinement of the solution strategy is only justified if the resulting modelling uncertainty is reduced, if necessary knowledge about the basic variables can be obtained and if in the end it can be demonstrated to yield less conservative estimates of the load carrying capacity.

With the present methods for quantifying the modelling uncertainty, the estimate will always have contributions from physical uncertainties. The phenomena that are not explicitly considered in the benchmark analyses from which the modelling uncertainty is estimated, are implicitly included in the modelling uncertainty. This can be unfortunate, since the modelling uncertainty will carry most of the uncertainties, and the engineer is left with few possibilities for reducing the epistemic uncertainties of the problem. However, it can also be useful, since all the uncertainties that could not be isolated in the benchmark analyses, are included in the modelling uncertainty, and should thus not be included in later analyses.

A systematic treatment of material variability by using a hierarchical model was found useful in the study of the compressive strength of ready-mixed concrete. The method is transparent and generic, and additional data from more plants, producers and regions are easily included. The results from the present work indicate that the designer should specify a strength class that utilizes the strength potential due to the constraints to the concrete recipe set by the durability requirements. A closer collaboration between designer, contractor and producer is expected to result in improved concrete specifications.

With the one-step approach for design of concrete structures, the engineer can focus on making realistic assessments of the load bearing capacity of the structure, and the effects of uncertainties, instead of being forced to always use conservative estimates of both the load effect and the resistance. By elaborating further on the reliability-based structural design methods shown in Fig. 6, with for example the one-step approach for design of concrete structures using NLFEA, the response surface method and inverse FORM, the engineer can be equipped with powerful design methods. Such methods promote innovation, since they consist of different sub-models where improvements in each sub-model can result in either a more realistic prediction of the structural resistance or a more realistic estimate of the effects of the uncertainties of the problem. This is important in order to reduce unnecessary conservatism in assessments of the structural capacity, increase the competitiveness of concrete in new structures and increase the reuse of existing concrete structures.

7. Suggestions for further research

Following the present work, it is suggested to work on the different parts shown in Fig. 6. Ideally, the different parts should be dealt with in parallel, since a refinement of only one of the parts is not justified before this results in an improved basis for the decision maker. The suggestions for further research are summarized in the following sections.

7.1 Solution strategy for NLFEA

Develop a criterion for structural failure in NLFEA. Such a criterion is useful to distinguish between load steps where failure happens and load steps that simply do not reach convergence. This was discussed in Paper III (Engen et al. 2017b), and one further step was recently described (Engen et al. 2017d).

Assess the applicability of the developed solution strategy for NLFEA to other types of loadings and limit states, for example crack width predictions in the serviceability limit state or ship impact or explosions in the accidental limit state. As a first step, the solution strategy was recently successfully applied to restrained deformations due to seasonal temperature variations (Lie et al. 2017).

7.2 Material variability

As a continuation of the collaboration with the concrete producers, it is suggested to study the material variability from the point of view of the producer, i.e. study the effects of the different constituents on the variability of properties like strength and stiffness. A hierarchical treatment of the variability can be applicable, and variabilities like within- and between aggregate type and cement type can be relevant.

The methodology suggested in Paper I can further be used to study for example the relation between the lab-strength and the strength obtained in the structure, the time development of strength and stiffness and the ratio of cylinder to cube strength, and eventually how these effects influence the structural reliability.

7.3 Modelling uncertainty

Future design codes could include brief guidance for how NLFEA should be used in the design process. The codes should be open to let the designers develop their own solution strategies, as described in Sec. 4.2, but should also provide values for the modelling uncertainty that could be used by the designer if this was not estimated in the validation phase. A suggestion is to study within- and between-model uncertainty, represented by θ_3 and θ_1 in Sec. 4.4, in order to estimate a reasonable upper bound suitable for a design code. A first step has been taken by Allaix et al. (2014) and Bertagnoli et al. (2015). A hierarchical treatment of uncertainties as suggested in Paper I might also be applicable for this purpose. The modelling uncertainty could be given either as a bias and a coefficient of variation, or as a global resistance factor.

The results in Tab. 9 indicate that models are usually on average on the safe side, since the bias is larger than unity. Although such results are conservative, and the bias can be compensated for if the modelling uncertainty is properly included, this also indicates that that the model is incomplete. Future studies of the modelling uncertainty should address this.

In Paper IV it was found that the physical uncertainties that are not explicitly considered in the NLFEA will contribute to the estimated modelling uncertainty. With the present definition of the modelling uncertainty, it is not straight forward to unravel the two sources of uncertainties. Using for example the knowledge from Paper I about the hierarchical treatment of material variability, further research could focus on estimating a pure modelling uncertainty.

7.4 Reliability-based design methods

The semi-probabilistic safety formats for NLFEA discussed in Sec. 3.6 have been demonstrated in the literature for relatively simple structural systems with clear failure modes. The applicability to structures with high degrees of statically indeterminacy and possibly competing failure modes should be addressed, in order to see if there are conditions under which the simple safety formats fail, and more elaborate methods are advisable.

One such method can be a combination of the response surface method and an inverse level 2 method. A topic which is yet to be elaborated on is the effect of correlation between the parameters of the response surface, and how the modelling uncertainty of the NLFEA influences the distributions of these parameters. A first step can be to consider Bayesian regression, as mentioned in Sec. 3.5.

Based on an extended study using a level 2 method, and if trends in the locations of the design points can be found, partial factors suitable for NLFEA can be calibrated. The results from such a study could also be used to advise the engineer in selecting proper values for the material parameters as input to NLFEA used in a two-step approach, as defined in Sec. 1.2.

References

Allaix, D. L. & Carbone, V. I.: An improvement of the response surface method. Structural Safety, 2011, 33(2), 165-172.

Allaix, D. L., Carbone, V. I. & Mancini, G.: Global safety format for non-linear analysis of reinforced concrete structures. Structural Concrete, 2013, 14(1), 29-42.

Allaix, D. L., Bertagnoli, G., Carbone, V. I. & Mancini, G.: A comparison of finite element solutions for 2D reinforced concrete structures. The fourth international fib congress, Mumbai, India, February 2014, 2014.

Allaix, D. L., Carbone, V. I. & Mancini, G.: Modelling uncertainties for the loadbearing capacity of corroded simply supported RC beams. Structural Concrete, 2015, 16(3), 333-341.

Apostolakis, G.: The Concept of Probability in Safety Assessments of Technological Systems. Science, 1990, 250(4986), 1359-1364.

Aasheim, E. E., Lindemark, J., Lundberg, A. H. & Engen, M.: Dam Sarvsfossen. Cement, 2017, 69(3), 38-41.

Bathe, K.-J.: Finite Element Procedures. Prentice Hall, 2006.

Beck, J. L. & Yuen, K.-V.: Model Selection Using Response Measurements: Bayesian Probabilistic Approach. Journal of Engineering Mechanics, 2004, 130(2), 192-203.

Belletti, B., Damoni, C. & Hendriks, M. A. N.: Development of guidelines for nonlinear finite element analyses of existing reinforced and pre-stressed beams. European Journal of Environmental and Civil Engineering, 2011, 15(9), 1361-1384.

Belletti, B., Damoni, C., den Uijl, J. A., Hendriks, M. A. N. & Walraven, J.: Shear resistance evaluation of prestressed concrete bridge beams: *fib* Model Code 2010 guidelines for level IV approximations. Structural Concrete, 2013, 14(3), 242-249.

Belletti, B., Damoni, C., Hendriks, M. A. N. & de Boer, A.: Analytical and numerical evaluation of the design shear resistance of reinforced concrete slabs. Structural Concrete, 2014, 15(3), 317-330.

Belletti, B., Pimentel, M., Scolari, M. & Walraven, J. C.: Safety assessment of punching shear failure according to the level of approximation approach. Structural Concrete, 2015, 16(3), 366-380.

Belytschko, T., Liu, W. K., Moran, B. & Elkhodary, K. I.: Nonlinear Finite Elements for Continua and Structures. John Wiley & Sons, 2014.

Benjamin, J. R. & Cornell, C. A.: Probability, Statistics and Decisions for Civil Engineers. McGraw-Hill Book Company, 1970.

Bertagnoli, G., La Mazza, D. & Mancini, G.: Effect of concrete tensile strength in non linear analyses of 2D structures - a comparison between three commercial finite element softwares. Third International Conference on Advances in Civil, Structural and Construction Engineering - CSCE, 2015.

Bigaj-van Vliet, A. & Vrouwenvelder, T.: Reliability in the performance-based concept of *fib* Model Code 2010. Structural Concrete, 2013, 14(4), 309-319.

Blomfors, M., Engen, M. & Plos, M.: Evaluation of safety formats for non-linear Finite Element Analyses of statically indeterminate concrete structures subjected to different load paths. Structural Concrete, 2016, 17(1), 44-51.

Brekke, D.-E., Åldstedt, E. & Grosch, H.: Design of Offshore Concrete Structures Based on Postprocessing of Results from Finite Element Analysis (FEA): Methods, Limitations and Accuracy. Proceedings of the Fourth (1994) International Offshore and Polar Engineering Conference, 1994.

Bucher, C. G. & Bourgund, U.: A fast and efficient response surface approach for structural reliability problems. Structural Safety, 1990, 7(1), 57-66.

CEB: Bulletin 229: New Developments in Non-linear Analysis Methods. Basic Papers from the Working Party. Comité Euro-International du Béton, 1995.

CEB: Bulletin 239: Non-linear analysis - Discussion Papers from the Working Party in Commission 1. Safety Evaluation and Monitoring - Discussion Papers from Task Group 1.4. Comité Euro-International du Béton, 1997.

CEN: EN 1990: Basis for structural design. 2002.

CEN: EN 1992-1-1. Eurocode 2: Design of concrete structures. Part 1-1: General rules and rules for buildings. 2004.

Cervenka, V.: Reliability-based non-linear analysis according to *fib* Model Code 2010 Structural Concrete, 2013, 14(1), 19-28.

Collins, M. P., Vecchio, F. J. & Melhorn, G.: An International Competition to Predict the Response of Reinforced Concrete Panels. Canadian Journal of Civil Engineering, 1985, 12(3), 624-644.

Collins, M. P., Bentz, E. C., Quach, P. T. & Proestos, G. T.: The Challenge of Predicting the Shear Strength of Very Thick Slabs. Concrete international, 2015, 37(11), 29-37.

Cook, R. D. & Young, W. C.: Advanced Mechanics of Materials. Prentice Hall, 1999.

Cornell, C. A.: A Probability-Based Structural Code. ACI Journal, 1969, 66(12), 974-985.

Der Kiureghian, A.: Measures of Structural Safety Under Imperfect States of Knowledge. Journal of Structural Engineering, 1989, 115(5), 1119-1140.

Der Kiureghian, A. & Ditlevsen, O.: Aleatory or epistemic? Does it matter? Structural Safety, 2009, 31(2), 105-112.

Ditlevsen, O.: Model uncertainty in structural reliability. Structural Safety, 1982, 1(1), 73-86.

Ditlevsen, O. & Madsen, H. O.: Structural Reliability Methods. Coastal, Maritime and Structural Engineering, Department for Mechanical Engineering, Technical University of Denmark, 2005.

Droguett, E. L. & Mosleh, A.: Bayesian Methodology for Model Uncertainty Using Model Performance Data. Risk Analysis, 2008, 28(5), 1457-1476.

Ellingwood, B. & Galambos, T. V.: Probability-based criteria for structural design. Structural Safety, 1982, 1(1), 15-26.

Ellingwood, B. R.: Structural reliability and performance-based engineering. Proceedings of the ICE - Structures and Buildings, 2008, 161(SB4), 199-207.

Engen, M., Hendriks, M. A. N., Øverli, J. A. & Åldstedt, E.: Application of NLFEA in the Design of Large Concrete Structures. Proceedings of the XXII Nordic Concrete Research Symposium, Reykjavik, Iceland, 2014.

Engen, M., Hendriks, M. A. N., Øverli, J. A. & Åldstedt, E.: Solution strategy for non-linear Finite Element Analyses of large reinforced concrete structures. Structural Concrete, 2015, 16(3), 389-397.

Engen, M., Hendriks, M. A. N., Köhler, J., Øverli, J. A. & Åldstedt, E.: A Quantification of the Modelling Uncertainty of Non-linear Finite Element Analyses of Large Concrete Structures. Structural Safety, 2017a, 64(1), 1-8.

Engen, M., Hendriks, M. A. N., Øverli, J. A. & Åldstedt, E.: Non-linear finite element analyses applicable for the design of large reinforced concrete structures. Accepted for publication in European Journal of Environmental and Civil Engineering, 2017b.

Engen M., Hendriks, M. A. N., Köhler, J., Øverli, J. A., Åldstedt, E., Mørtsell, E., Sæter, Ø. & Vigre, R.: Predictive strength of ready-mixed concrete: exemplified using data from the Norwegian market. Under review, 2017c.

Engen, M., Hendriks, M. A. N., Øverli, J. A. & Åldstedt, E.: Reliability assessments of large concrete structures making use of non-linear finite element analyses. The Second Concrete Innovation Conference, Tromsø 6th - 8th of March, 2017d.

Faber, M. H.: On the Treatment of Uncertainties and Probabilities in Engineering Decision Analysis. Journal of Offshore Mechanics, 2005, 127(3), 243-248.

Faravelli, L.: Response-Surface Approach for Reliability Analysis. Journal of Engineering Mechanics, 1989, 115(12), 2763-2781.

fib: Bulletin 45: Practitioner's guide to finite element modelling of reinforced concrete structures. International Federation for Structural Concrete (*fib*), 2008.

fib: *fib* Model Code for Concrete Structures 2010. Ernst & Sohn, 2013.

fib: Bulletin 80: Partial factor methods for existing concrete structures. International Federation for Structural Concrete (*fib*), 2017.

Gelman, A., Carlin, J. B., Stern, H. S., Dunson, D. B., Vehtari, A. & Rubin, D. B.: Bayesian Data Analysis. CRC Press, 2014.

Giske, F.-I. G., Leira, B. J. & Øiseth, O.: Long-term extreme response analysis of marine structures using inverse SORM. Proceedings of the ASME 2017 36th International Conference on Ocean, Offshore and Arctic Engineering, OMAE2017, June 25-30, Trondheim, Norway, 2017.

Hasofer, A. M. & Lind, N. C.: Exact and Invariant Second-Moment Code Format. Journal of the Engineering Mechanics Division, ASCE, 1974, 100(EM1), 111-121.

Hendriks, M. A. N., de Boer, A. & Belletti, B.: Guidelines for Nonlinear Finite Element Analysis of Concrete Structures. Rijkswaterstaat Centre for Infrastructure, Report RTD:1016-1:2017, 2017a.

Hendriks, M. A. N., de Boer, A. & Belletti, B.: Validation of the Guidelines for Nonlinear Finite Element Analysis of Concrete Structures - Part: Overview of results", Rijkswaterstaat Centre for Infrastructure, Report RTD:1016-2:2017, 2017b.

Henriques, A. A. R., Calheiros, F. & Figueiras, J. A.: Safety format for the design of concrete frames. Engineering Computations, 2002, 19(3/4), 346-363.

Hohenbichler, M., Gollwitzer, S., Kruse, W. & Rackwitz, R.: New light on first- and second-order reliability methods. Structural Safety, 1987, 4(4), 267-284.

Holický, M., Retief, J. & Sýkora, M.: Assessment of model uncertainties for structural resistance. Probabilistic Engineering Mechanics, 2016, 45, 188-197.

Igusa, T., Buonopane, S. G. & Ellingwood, B. R.: Bayesian analysis of uncertainty for structural engineering applications. Structural Safety, 2002, 24(2-4), 165-186.

Jaeger, T. & Marti, P.: Reinforced Concrete Slab Shear Prediction Competition: Experiments. ACI Structural Journal, 2009a, 106(3), 300-308.

Jaeger, T. & Marti, P.: Reinforced Concrete Slab Shear Prediction Competition: Entries and Discussion. ACI Structural Journal, 2009b, 106(3), 309-318.

JCSS: Probabilistic Model Code, 12th draft. Joint Committee on Structural Safety, 2001.

Kotsovos, M. D. & Pavlovic, M. N.: Structural Concrete: Finite-element analysis for limit-state design. Thomas Telford, 1995.

Li, H. & Foschi, R. O.: An inverse reliability method and its application. Structural Safety, 1998, 20(3), 257-270.

Lie, R., Aasheim, E. E. & Engen, M.: Thermal Cracking of a Concrete Arch Dam: FE analyses using a 3D non-linear material model for concrete. ICOLD Benchmark Workshop, 2017.

Liu, P.-L. & Der Kiureghian, A.: Optimization algorithms for structural reliability. Structural Safety, 1991, 9(3), 161-177.

Lubliner, J.: Plasticity Theory. Dover, 2008.

McKay, M. D., Beckman, R. J. and Conover, W. J.: A Comparison of Three Methods for Selecting Values of Input Variables in the Analysis of Output from a Computer Code. Technometrics, 1979, 21(2), 239-245.

Melchers, R. E.: Structural reliability analysis and prediction. John Wiley & Sons, 1999.

Nielsen, M. P.: Limit analysis and concrete plasticity. Prentice Hall, 1984.

Olsson, A. M., Sandberg, G. E. & Dahlbom, O.: On Latin hypercube sampling for structural reliability analysis. Structural Safety, 2003, 25(1), 47-68.

Pimentel, M., Brühwiler, E. & Figueiras, J. A.: Safety examination of existing concrete structures using the global resistance safety factor concept. Engineering Structures, 2014, 70, 130-143.

Rackwitz, R. & Fiessler, B.: Structural reliability under combined random load sequences. Computers & Structures, 1978, 9(5), 489-494.

Rackwitz, R.: Predictive distribution of strength under control. Materials and Structures, 1983, 16(4), 259-267.

Rackwitz, R.: Optimization - the basis of code-making and reliability verification. Structural Safety, 2000, 22(1), 27-60.

Rajashekar, M. R. & Ellingwood, B. R.: A new look at the response surface approach for reliability analysis. Structural Safety, 1993, 12(3), 205-220.

Roache, P. J.: Verification of Codes and Calculations. AIAA Journal, 1998, 36(5), 696-702.

Schneider, J.: Introduction to Safety and Reliability of Structures. IABSE, 2006.

Schlune, H.: Safety Evaluation of Concrete Structures with Nonlinear Analysis. PhD thesis, Chalmers University of Technology, 2011.

Schlune, H., Plos, M. & Gylltoft, K.: Safety formats for nonlinear analysis tested on concrete beams subjected to shear forces and bending moments. Engineering Structures, 2011, 33(8), 2350-2356.

Schlune, H., Plos, M. & Gylltoft, K.: Safety formats for non-linear analysis of concrete structures. Magazine of Concrete Research, 2012, 64(7), 563-574.

Selby, R. G. & Vecchio, F. J.: Three-Dimensional Constitutive Relations for Reinforced Concrete, Publication No. 93-02. University of Toronto - Department of Civil Engineering, University of Toronto - Department of Civil Engineering, 1993.

Shinozuka, M.: Basic Analysis of Structural Safety. Journal of Structural Engineering, 1983, 109(3), 721-740.

Stewart, M. G.: Workmanship and Its Influence on Probabilistic Models of Concrete Compressive Strength. ACI Materials Journal, 1995, 92(4), 361-372.

Strauss, A., Eschbacher, T., Kendický, P. & Benko, V.: Load capacity of slender compression members Part 1: Component tests and round robin test of the nonlinear numerical prediction of system behavior. Beton- und Stahlbetonbau, 2015, 110(12), 845-856.

Thoft-Christensen, P. & Baker, M. J.: Structural Reliability Theory and Its Application. Springer-Verlag Berlin Heidelberg New York, 1982.

van Mier, J. G. M. & Ulfkjær, J. P.: Round-Robin analysis of over-reinforced concrete beams - Comparison of results. Materials and Structures, 2000, 33(6), 381-390.

Vecchio, F. J.: Non-linear finite element analysis of reinforced concrete: at the crossroads? Structural Concrete, 2001, 2(4), 201-212.

Vrouwenvelder, A. C. W. M. T.: Reliability based structural design. Safety, Reliability and Risk Management, proceedings from the 22nd European Safety and Reliability annual conference in Amsterdam, 2013.

Zhang, R. & Mahadevan, S.: Model uncertainty and Bayesian updating in reliability-based inspection. Structural Safety, 2000, 22(2), 145-160.

Zhao, W. & Qiu, Z.: An efficient response surface method and its application to structural reliability and reliability-based optimization. Finite Elements in Analysis and Design, 2013, 67, 34-42.

Zienkiewicz, O. C. & Taylor, R. L.: The Finite Element Method: Volume 2 - Solid and Fluid Mechanics, Dynamics and Non-linearity. Mc-Graw-Hill Book Company, 1994.

Part II – Appended papers

Paper I

Predictive strength of ready-mixed concrete: exemplified using data from the Norwegian market

Engen, M., Hendriks, M. A. N., Köhler, J., Øverli, J. A., Åldstedt, E., Mørtsell, E., Sæter, Ø. & Vigre, R.

Under review, 2017.

Predictive strength of ready-mixed concrete: exemplified using data from the Norwegian market

Morten Engen[1,2], Max A. N. Hendriks[1,3], Jochen Köhler[1], Jan Arve Øverli[1], Erik Åldstedt[2], Ernst Mørtsell[1,4], Øyvind Sæter[5], Roar Vigre[6]

[1]NTNU, Norwegian University of Science and Technology, Department of Structural Engineering, Trondheim, Norway
[2]Multiconsult ASA, Oslo, Norway
[3]Delft University of Technology, Delft, the Netherlands
[4]NorBetong AS, Heimdal, Norway
[5]Unicon AS, Oslo, Norway
[6]Ølen Betong AS, Ølensvåg, Norway

ABSTRACT
A hierarchical model for the variability of material properties in ready-mixed concrete is formulated. The model distinguishes between variation on the batch, recipe, plant, producer, durability class, strength class and regional standard level. By considering Bayesian inference and maximum likelihood estimators, the contributions from the different hierarchical levels to the variability can be estimated. The methodology is demonstrated by considering more than 14000 compressive strength recordings from Norwegian ready-mixed concrete plants. The results suggest that the compressive cube strength of lab-cured specimens can be represented by a log-normally distributed variable with mean $1.28f_{\mathrm{ck,cube}}$ and coefficient of variation $V_{\mathrm{c,cube}} = 0.13$. Prior parameters for Bayesian updating are given for a range of strength and durability classes. The application of the results is demonstrated in two examples. Since the durability class gives a required maximum water-binder ratio, and the strength of the concrete is governed by the water-binder ratio, the durability class introduces a strength potential if the concrete is subject to strict durability requirements and low strength requirements. It is suggested that the designer should specify a strength class that utilizes this strength potential, and it is expected that a closer collaboration between the designer, contractor and producer will result in improved concrete specifications.

Keywords: Concrete compressive strength, hierarchical model for variability, Bayesian inference, informative prior distribution, maximum likelihood estimators, code calibration, structural reliability.

1. INTRODUCTION

Selecting the concrete type is an important decision in design of concrete structures. Following the Eurocodes [1-3] the concrete type is defined by requirements related to strength and durability. In Norway, this is implemented by assigning a strength and durability class, where the strength class is denoted by the letter B followed by the characteristic compressive strength of a lab-cured cylinder, see Tab. 1, and the durability class is denoted by the letter M or the letters MF followed by a number indicating the maximum effective water-binder ratio. The characteristic compressive strength is defined as the lower 5%-fractile of the strength. EN 206 gives the following durability classes for concrete in Norway: M90, M60, M45, MF45, M40 and MF40. In addition, The Norwegian Public Roads Administration introduces additional durability classes, e.g. SV30 and SV40, for infrastructure projects [4].

Table 1: *Relation between target cylinder strength, f_{ck}, and cube strength, $f_{ck,cube}$, for the strength classes given in Eurocode 2, EN 206 and* fib *Model Code 2010.*

	B10	**B20**	**B25**	**B30**	**B35**	**B45**	**B55**	**B65**	**B75**	**B85**	**B95**
f_{ck} [MPa]	10	20	25	30	35	45	55	65	75	85	95
$f_{\mathrm{ck,cube}}$ [MPa]	12	25	30	37	45	55	67	80	90	100	110

Based on the strength and durability class, workability requirements and other requirements related to e.g. appearance or carbon footprint, the producer designs a recipe. For a given strength and durability class produced at a specific plant, the main differences between different recipes are related to the maximum aggregate size, the fractions of the different aggregate sizes, the cement type, the amount of supplementary cementitious materials and the amount of entrained air. Conformity control is performed based on the strength at 28 days. Cubes with sides 100 mm are used for conformity control in Norway due to their easier handling, preparation and testing compared to cylinders.

Mirza et al. [5] presents an extensive literature review, and suggest that the main sources for variation of the compressive strength are the variation in properties and proportion of the constituents of the concrete mix, the variations in mixing, transporting, placing and curing methods, the variations in testing procedures and variations due to concrete being in a structure rather than in control specimens. Several other sources report similar findings [6-15], also addressing topics like size and shape of control specimen, casting direction, workmanship and type of structural component and location within the component.

Rackwitz [16] suggests methods for predicting the strength of concrete using Bayesian inference, and estimate prior data based on a collection of data from Southern Germany. The prior data were later reworked and included in the *JCSS Probabilistic Model Code* [17].

The effect of compliance criteria are studied taking into account autocorrelation [18], different types of criteria [19] and the concept of concrete families [20,21]. Later, the effect of compliance control and strength estimation [22] on structural reliability are addressed [23-25]. Foster et al. [26] report from a study on a collection of strength recordings from Australia, and it can be shown that the 28-day compressive strength of lab-cured cylinders can be represented by a normally distributed variable with mean $\mu_{\mathrm{c}} = 1.21 f_{\mathrm{ck}}$ and a coefficient of variation of $V_{\mathrm{c}} = 0.12$. Correlation with other material parameters for concrete can be found elsewhere [27-29], and the relation between cylinder and cube strength is discussed in several contributions [30-35].

In Eurocode 2 [2,36], and similarly in fib *Model Code for Concrete Structures 2010* [37], the concrete strength is assumed represented by a log-normally distributed variable. The variability of the concrete strength is reflected in the partial factor

$$\gamma_{\mathrm{c}} = 1.15 \exp\left(\alpha_{\mathrm{R}} \beta \sqrt{V_{\theta}^2 + V_{\mathrm{G}}^2 + V_{\mathrm{M}}^2} - 1.645 V_{\mathrm{M}}\right) \cong 1.50, \tag{1}$$

where $\alpha_{\mathrm{R}} = 0.8$ is the sensitivity factor for resistance, $\beta = 3.8$ is the target reliability index for a 50-year reference period, $V_{\theta} = 0.05$ is the modelling uncertainty, $V_{\mathrm{G}} = 0.05$ is the geometrical uncertainty, $V_{\mathrm{M}} = 0.15$ is the material uncertainty [36] including the contributions discussed by Mirza et al. [5], and the factor 1.15 reflects the ratio of the lab-strength to the strength obtained

in a structure. Eurocode 2 also suggests the relation $f_{\mathrm{cm}} = f_{\mathrm{ck}} + 8$ MPa between the mean and characteristic strength, assuming a standard deviation of approximately 5 MPa [38].

In the present work more than 14000 compressive strength recordings from Norwegian ready-mixed concrete plants were studied using a hierarchical model for the variability of material properties as suggested in the literature [16,17]. It is emphasized that the scope of the present work was to estimate the variation resulting from what the designer can control. The effects of the choices made by the contractor and the producer were thus not considered.

This work only provides statistical evidence for the lab-strength of cubes of ready-mixed concrete in Norway, such that the uncertain relation between the lab-strength of cubes and the strength obtained in a structure should be included if the present results are to be applied in e.g. a reliability assessment. For completeness, full details of the statistical analysis methods will be given along with a detailed summary of the results. This transparency is important for possible future extensions with additional data and to facilitate for correct application of the results.

2. HIERARCHICAL MODEL FOR THE VARIABILITY OF MATERIAL PROPERTIES IN CONCRETE

Fig. 1 shows how the hierarchical model for the variability of material properties in concrete was formulated in the present work. During concrete production, the producer controls for compliance using standardized test specimens. The variation between test specimens from one batch of concrete represents the *within-batch* variation. The variation *within* and *between* samples of observations on one level contributes to the variation *within* the next level, see Tab. 2. Hence, the variation within and between batches produced according to one *recipe* contribute to the *within-recipe* variation. Each batch is produced according to a given recipe, at a *concrete plant*, by a *concrete producer* in order to comply with a given *durability class* and *strength class*. The variation between plants and producers can be due to different availability and use of raw materials, but also due to cultural differences and the quality control regime at the respective plant. The concrete is produced within a region having a *supply controlled by a regional standard*, which is part of the *gross supply*. Since the designer specifies a strength and durability class, these levels are the entry points of information from the design process.

Table 2: *Description of the levels of the hierarchical model. The right column indicates that if a sample of observations at one level in the hierarchy is considered, one can make inference about the between-variation on that level and a contribution to the within-variation on the next higher level.*

Hierarchical level	**Inference from a sample of observations at the respective level**
Standard test specimens from one batch	Within batch
Batch	Within recipe / between batch
Recipe	Within plant / between recipe
Concrete plant	Within producer / between plant
Concrete producer	Within durability class / between producer
Durability class	Within strength class / between durability class
Strength class	Within region / between strength class
Supply controlled by regional standard	Within the gross supply / between region
The gross supply	-

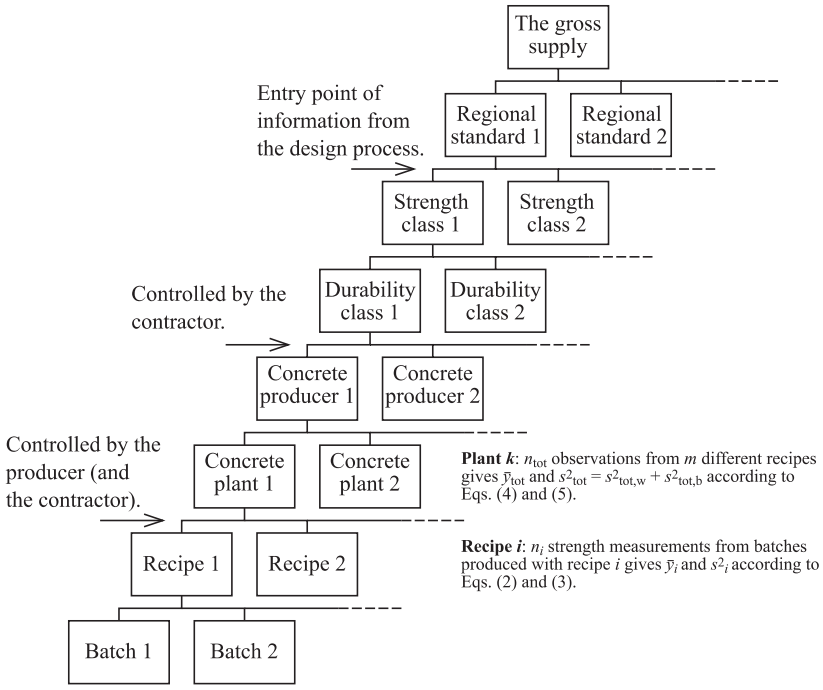

Figure 1: *Hierarchical model for the variability of material properties in concrete. The examples to the right in the figure indicates the application of the estimators in Sec. 3.1.*

3. METHODS FOR STATISTICAL ANALYSIS

3.1 Sample statistics for the hierarchical model

Assuming independent and interchangeable observations from a homogeneous population, unbiased estimators for the mean and variance of sample i with n_i observations are

$$\bar{y}_i = \frac{1}{n_i}\sum_{j=1}^{n_i} y_{i,j} \tag{2}$$

and

$$s_i^2 = \frac{1}{n_i - 1}\sum_{j=1}^{n_i}\left(y_{i,j} - \bar{y}_i\right)^2 \quad , \tag{3}$$

where $y_{i,j}$ is observation j in sample i. For example, i can refer to recipe i for obtaining a combination of strength and durability, and j can refer to a strength recording from batch j produced with that recipe. From this, one can derive the sample mean

$$\bar{y}_{\text{tot}} = \frac{1}{n_{\text{tot}}}\sum_{i=1}^{m} n_i \bar{y}_i \tag{4}$$

and variance

$$s_{\text{tot}}^2 = \frac{\sum_{i=1}^{m}([n_i - 1]s_i^2)}{n_{\text{tot}} - 1} + \frac{\sum_{i=1}^{m}(n_i \bar{y}_i^2) - n_{\text{tot}}\bar{y}_{\text{tot}}^2}{n_{\text{tot}} - 1} = s_{\text{tot,w}}^2 + s_{\text{tot,b}}^2 \tag{5}$$

of a group of m samples respectively, where $n_{\text{tot}} = \sum_{i=1}^{m} n_i$ is the total number of observations. Here, $\bar{y}_{\text{tot}}$, s_{tot}^2 and n_{tot} could include all the strength recordings for all recipes for a combination of strength and durability at a specific plant. For example the sample mean and variance for a combination of strength and durability class at a specific plant can thus be calculated directly by considering the sample mean, sample variance and number of observations for all the recipes obtaining the specified combination of strength and durability class at that plant, as indicated in Fig 1. Eq. (5) expresses the variance of the group of samples as the sum of the variance *within* and *between* the samples.

3.2 Bayesian inference

The derivations in this section are valid for normally distributed random variables, and are adapted from the literature [e.g. 16,39,40]. Following recommendations in the literature, the compressive cube strength of concrete, $f_{\text{c,cube}}$, is represented by a log-normally distributed variable [16,41], meaning that the natural logarithm of the cube strength is normally distributed. In the following, the variable y thus represents the natural logarithm of the cube strength, $y = \ln f_{\text{c,cube}}$.

Following *Bayes' theorem*, and assuming that y is normally distributed with mean μ and variance σ^2, the *joint posterior distribution* of the parameters μ and σ^2 given a set of n observations collected in the vector $\boldsymbol{y}$ is written as

$$f(\mu, \sigma^2|\boldsymbol{y}) = \frac{f(\mu, \sigma^2)L(\boldsymbol{y}|\mu, \sigma^2)}{\iint_{-\infty}^{\infty} f(\mu, \sigma^2)L(\boldsymbol{y}|\mu, \sigma^2)\mathrm{d}\mu\mathrm{d}\sigma^2} \quad , \tag{6}$$

where $f(\mu, \sigma^2)$ is the prior distribution of the parameters and $L(\boldsymbol{y}|\mu, \sigma^2)$ is the likelihood of the observations. The likelihood is established by considering the distribution of y:

$$L(\boldsymbol{y}|\mu, \sigma^2) = \prod_{i=1}^{n} \mathrm{N}(y_i|\mu, \sigma^2) = \left(\frac{1}{2\pi\sigma^2}\right)^{n/2} \exp\left(-\frac{1}{2\sigma^2}[(n-1)s^2 + n(\bar{y} - \mu)^2]\right) \quad , \tag{7}$$

where

$$\mathrm{N}(y_i|\mu, \sigma^2) = \sqrt{\frac{1}{2\pi\sigma^2}} \exp\left(-\frac{1}{2}\frac{[y_i - \mu]^2}{\sigma^2}\right) \tag{8}$$

is the normal distribution. If there exists no prior information about y, the proportionality

$$f(\mu, \sigma^2) \propto \frac{1}{\sigma^2} \tag{9}$$

can be used as a non-informative prior distribution for μ and σ^2. By combining Eqs. (7) and (9) with Eq. (6), the joint posterior distribution of μ and σ^2 is

$$f(\mu,\sigma^2|\boldsymbol{y}) = \mathrm{N}\left(\mu\middle|\bar{y},{}^{\sigma^2}\!/_{n}\right)\text{Inv-}\chi^2(\sigma^2|\nu s^2,\nu) \quad , \tag{10}$$

where

$$\text{Inv-}\chi^2(\sigma^2|\nu s^2,\nu) = \frac{1}{\Gamma(\nu/2)}\left(\frac{\nu s^2}{2}\right)^{\nu/2}\left(\frac{1}{\sigma^2}\right)^{(\nu/2+1)}\exp\left(-\frac{\nu s^2}{2\sigma^2}\right) \tag{11}$$

is the *scaled inverse-χ^2 distribution* with scale νs^2 and ν degrees of freedom. $\Gamma(\cdot)$ is the *Gamma-function* and $\nu = n-1$, assuming that the sample variance and mean are estimated from the same sample. From Eq. (10), the marginal posterior distribution of each parameter is found by integrating over the other, e.g. $f(\sigma^2|\boldsymbol{y}) = \int_{-\infty}^{\infty} f(\mu,\sigma^2|\boldsymbol{y})\mathrm{d}\mu$. The posterior predictive distribution of y is found from the total probability theorem

$$f(y|\boldsymbol{y}) = \iint_{-\infty}^{\infty}\mathrm{N}(y|\mu,\sigma^2)f(\mu,\sigma^2|\boldsymbol{y})\mathrm{d}\mu\mathrm{d}\sigma^2 \quad , \tag{12}$$

where the integral is over all possible values of μ and σ^2. The posterior distributions for μ, σ^2 and y, and the corresponding expected values and variances, are summarized in Tab. 3. The posterior distribution of y is given in Eq. (13), which is a *t-distribution* with location $\bar{y}$, scale $s\sqrt{\frac{\nu+2}{\nu+1}}$ and ν degrees of freedom. Eq. (14) can be used to estimate values of y with a non-exceedance probability α, where $t_{\alpha,\nu}$ is the upper α-fractile of the t-distribution with ν degrees of freedom.

Table 3: *Marginal posterior distributions, $f(\cdot\,|\boldsymbol{y})$, expected values, $E[\cdot]$, and variances, $VAR[\cdot]$, for μ, σ^2 and y, starting from a non-informative prior distribution.*

Variable	$f(\cdot\,\|\boldsymbol{y})$	$\mathrm{E}[\cdot]$	$\mathrm{VAR}[\cdot]$
μ	$t\left(\mu\middle\|\bar{y},s^2\frac{1}{\nu+1},\nu\right)$	$\bar{y}$	$\frac{\nu}{(\nu-2)(\nu+1)}s^2$
σ^2	$\text{Inv-}\chi^2(\sigma^2\|\nu s^2,\nu)$	$\frac{\nu}{\nu-2}s^2$	$\frac{2\nu^2}{(\nu-2)^2(\nu-4)}s^4$
y	$t\left(y\middle\|\bar{y},s^2\frac{\nu+2}{\nu+1},\nu\right)$	$\mathrm{E}[\mu]$	$\mathrm{VAR}[\mu]+\mathrm{E}[\sigma^2]$

$$f(y|\boldsymbol{y}) = t\left(y|\bar{y},s^2\tfrac{\nu+2}{\nu+1},\nu\right) = \frac{\Gamma\left(\frac{\nu+1}{2}\right)}{\Gamma\left(\frac{\nu}{2}\right)}\sqrt{\frac{1}{\nu\pi}}\sqrt{\frac{\nu+1}{s^2(\nu+2)}}\left(1+\frac{\nu+1}{\nu(\nu+2)}\left[\frac{y-\bar{y}}{s}\right]^2\right)^{-\frac{\nu+1}{2}} \tag{13}$$

$$\tilde{y} = \bar{y} + t_{\alpha,\nu}s\sqrt{\frac{\nu+2}{\nu+1}} \tag{14}$$

If prior information about y exist, a *conjugate informative prior distribution* with prior parameters $\bar{y}'$, n', s'^2 and ν' on the same form as Eq. (10) can be written as

$$f(\mu,\sigma^2) = \mathrm{N}\left(\mu\middle|\bar{y}', {\sigma^2}/{n'}\right)\text{Inv-}\chi^2\left(\sigma^2|\nu' s'^2,\nu'\right) \quad . \tag{15}$$

By combining Eqs. (7), (15) and (6) it can be shown that the joint posterior distribution of μ and σ^2 is given by Eq. (10) with *updated* parameters

$$n'' = n' + n \quad , \tag{16}$$

$$\bar{y}'' = \frac{1}{n''}(n\bar{y} + n'\bar{y}') \quad , \tag{17}$$

$$\nu'' = \nu' + \nu + 1 \quad , \tag{18}$$

and

$$\nu'' s''^2 = \nu s^2 + \nu' s'^2 + n\bar{y}^2 + n'\bar{y}'^2 - n''\bar{y}''^2 = \nu s^2 + \nu' s'^2 + \frac{nn'}{n+n'}(\bar{y} - \bar{y}')^2 \quad , \tag{19}$$

and the posterior distributions, expected values and variances of μ, σ^2 and y are given in Tab. 3, inserted for the updated parameters. Note that Eqs. (17) and (19) are parallel to Eqs. (4) and (5), and that in this case Bayesian updating involves inference on two samples of observations that are combined. The prior sample is often taken as a virtual sample where the sample size represents the information content in the sample.

If prior information exists only for the variance, the conjugate informative prior distribution would take the form

$$f(\mu,\sigma^2) = \text{Inv-}\chi^2\left(\sigma^2|\nu' s'^2,\nu'\right) \quad , \tag{20}$$

and following the same derivation as above gives the updated parameters

$$n'' = n \quad , \tag{21}$$

$$\bar{y}'' = \bar{y} \quad , \tag{22}$$

$$\nu'' = \nu' + \nu \quad , \tag{23}$$

and

$$\nu'' s''^2 = \nu s^2 + \nu' s'^2 \quad . \tag{24}$$

Since the inference is based on the log-normally distributed random variable $y = \ln f_{\mathrm{c,cube}}$, the results from the inference should be transformed in order to find the parameters of the distribution of $f_{\mathrm{c,cube}}$. By applying a coordinate transformation such that Eq. (8) is expressed as a function of $f_{\mathrm{c,cube}}$, and calculating the first two moments in a regular manner, it can be shown that the mean $\mu_{\mathrm{c,cube}}$ and coefficient of variation $V_{\mathrm{c,cube}} = \sigma_{\mathrm{c,cube}}/\mu_{\mathrm{c,cube}}$ can be calculated using

$$\mu_{\mathrm{c,cube}} = \exp\left(\mathrm{E}[y] + \frac{1}{2}\mathrm{VAR}[y]\right) \approx \exp(\mathrm{E}[y]) \tag{25}$$

and

$$V_{\mathrm{c,cube}} = \sqrt{\exp(\mathrm{VAR}[y]) - 1} \approx \sqrt{\mathrm{VAR}[y]} \quad , \tag{26}$$

where the errors of approximation in Eqs. (25) and (26) are less than 2% for $V_{\mathrm{c,cube}} < 0.2$.

3.3 Estimate of parameters for an informative prior distribution

Rackwitz [16] suggests *maximum likelihood estimators* (MLE) for estimating parameters for an informative prior distribution. By considering Eqs. (11) and (8) the likelihoods

$$L(\boldsymbol{y}_{\mathrm{tot}}|s^2_{\mathrm{MLE}}, \nu_{\mathrm{MLE}}) = \prod_{i=1}^{m} \text{Inv-}\chi^2(s_i^2[\boldsymbol{y}_i]|\nu_{\mathrm{MLE}} s^2_{\mathrm{MLE}}, \nu_{\mathrm{MLE}}) \tag{27}$$

and

$$L(\boldsymbol{y}_{\mathrm{tot}}|\bar{y}_{\mathrm{MLE}}, n_{\mathrm{MLE}}) = \prod_{i=1}^{m} \mathrm{N}(\bar{y}_i[\boldsymbol{y}_i]|\bar{y}_{\mathrm{MLE}}, s_i^2[\boldsymbol{y}_i]/n_{\mathrm{MLE}}) \tag{28}$$

are established based on m samples of observations from a concrete type, where $\boldsymbol{y}_{\mathrm{tot}}$ represents the collection of all the m samples $\boldsymbol{y}_i$, and $\bar{y}_i[\boldsymbol{y}_i]$ and $s_i^2[\boldsymbol{y}_i]$ are the sample mean and variance of sample $\boldsymbol{y}_i$. By maximizing the natural logarithms of the likelihoods, the following MLE are found, with parameters in Eq. (33).

$$s^2_{\mathrm{MLE}} = \frac{1}{A} \tag{29}$$

$$\nu_{\mathrm{MLE}} = \frac{1}{\ln A - B - \epsilon(\nu_{\mathrm{MLE}}^{-2})} \approx \frac{1}{\ln A - B} f\left(\frac{1}{\ln A - B}\right) \approx \frac{1}{\ln A - B} \tag{30}$$

$$\bar{y}_{\mathrm{MLE}} = \frac{C}{A} \tag{31}$$

$$n_{\mathrm{MLE}} = \frac{1}{D - \frac{C^2}{A}} \tag{32}$$

$$A = \frac{1}{m}\sum_{i=1}^{m}\frac{1}{s_i^2} \quad , \quad B = \frac{1}{m}\sum_{i=1}^{m}\ln\frac{1}{s_i^2} \quad , \quad C = \frac{1}{m}\sum_{i=1}^{m}\frac{\bar{y}_i}{s_i^2} \quad , \quad D = \frac{1}{m}\sum_{i=1}^{m}\frac{\bar{y}_i^2}{s_i^2} \tag{33}$$

The error term in Eq. (30), $\epsilon(\nu_{\mathrm{MLE}}^{-2})$, is due to truncation after the second term of $\partial \ln \Gamma(\nu/2)/\partial\nu$, and can be compensated for by multiplying with the factor $f\left(\frac{1}{\ln A - B}\right)$ given in Tab. 4. ν_{MLE} and n_{MLE} are measures of the information content in the estimated values of s^2_{MLE} and $\bar{y}_{\mathrm{MLE}}$,

often denoted the *degree of belief*. ν_{MLE} and n_{MLE} attain large values if the sample variances and means are similar.

Table 4: *Correction factor for Eq. (30) found by including higher order terms of* $\partial \ln \Gamma(\nu/2)/\partial\nu$ *in the numerical solution of Eq. (30).*

$\frac{1}{\ln A - B}$	0.5	1.0	1.5	2.0	3.0	5.0	10.0	20.0	40.0
$f\left(\frac{1}{\ln A - B}\right)$	2.42	1.44	1.20	1.14	1.10	1.06	1.03	1.02	1.01

If the concrete type is unknown, generalized prior parameters can be useful. Caspeele & Taerwe [42] suggest a method for obtaining approximated generalized prior parameters for the variance based on prior data from samples with unknown sample sizes m_j. In the present work, the sample sizes m_j are known, and generalized prior parameters $s^2_{\mathrm{MLE,gen}}$ to $n_{\mathrm{MLE,gen}}$ can be estimated by using the parameters A_{tot} to D_{tot} according to

$$m_{\mathrm{tot}} = \sum_{j=1}^{n} m_j \quad , \quad A_{\mathrm{tot}} = \frac{1}{m_{\mathrm{tot}}} \sum_{j=1}^{m} m_j A_j \quad , \ldots, \quad D_{\mathrm{tot}} = \frac{1}{m_{\mathrm{tot}}} \sum_{j=1}^{m} m_j D_j \tag{34}$$

where the subscript j refers to either strength class, durability class or combination of strength and durability class j. From this it is clear that $s^2_{\mathrm{MLE,gen}}$ and $\nu_{\mathrm{MLE,gen}}$ will be meaningful since the variances of the different classes are expected to be comparable. In contrast, $\bar{y}_{\mathrm{MLE},j}$ are not comparable due to the different target strengths. However, if $s^2_{\mathrm{MLE,gen}}$ is estimated with a reasonable degree of belief, $\delta_{\mathrm{MLE},j} = \bar{y}_{\mathrm{MLE,j}} - \ln f_{\mathrm{ck,cube},j}$ is expected to be comparable for different classes. δ should be interpreted as the natural logarithm of the ratio between the mean strength and the target cube strength, $f_{\mathrm{ck,cube}}$, from Tab. 1. Hence, $s^2_{\mathrm{MLE,gen}}$, $\nu_{\mathrm{MLE,gen}}$, $\delta_{\mathrm{MLE,gen}}$ and $n_{\mathrm{MLE,gen}}$ are estimated by replacing $\bar{y}_{\mathrm{MLE},j}$ with $\delta_{\mathrm{MLE},j}$ in the calculation of C_{tot} in Eq. (34), and inserting Eq. (34) in Eqs. (29) to (32). If $\delta_{\mathrm{MLE,gen}}$ is estimated with a reasonable degree of belief, its value can be used to estimate the location parameter of the prior distribution for a concrete with an arbitrary target strength.

3.4 Estimate of within-batch variation

Since the data acquired in the present work only included one strength measurement per batch, no direct inference could be made about the within-batch variation. However, it can be estimated. Assume that the natural logarithm of a strength recording from batch j, y_j, can be represented by a normally distributed variable expressed as $y = y_1 + y_2$ with $y_1 \sim \mathrm{N}\left(\mu_{\mathrm{y}}, \sigma^2/n\right)$ and $y_2 \sim \mathrm{N}(0, \sigma^2)$. Here, y_1 represents the uncertain mean of the batch and y_2 represents the random fluctuation due to an assumed known within-batch variance, σ^2. This is realistic in situations where more information is available about the variance compared to the mean. The variance of y is given by

$$\mathrm{VAR}[y] = \frac{\sigma^2}{n} + \sigma^2 = \sigma^2 \frac{n+1}{n} \quad , \tag{35}$$

with n being the number of batches that are considered. An estimate of $\mathrm{VAR}[y]$ is the sample variance s_i^2 of n_i observations for a given recipe i, and an estimator for the within-batch variation of recipe i thus becomes

$$s_{\mathrm{wb},i}^2 = s_i^2 \frac{n_i}{n_i + 1} \quad . \tag{36}$$

This indicates that the between-batch variance dominates the estimate if the number of observations is small, and that the within-batch variance dominates if the number increases. Based on Eq. (36), the MLE from Eqs. (29) and (30) can be used to estimate the within-batch variance.

4. RESULTS AND DISCUSSION

4.1 Compressive strength recordings from the Norwegian market

Three concrete producers provided more than 14000 compressive strength recordings covering most of the Norwegian supply in the period 2013-2017, shown in Tab. 5. The six strength classes B20-B55 were represented with 20 combinations of strength and durability classes. Only concretes with aggregates consisting of at least 50% coarse aggregates with size larger than 4 mm and a maximum aggregate size larger than 16 mm were considered.

Table 5: *Overview of the producers and plants that have contributed to the study.*

Producer	Plant	Observations
A	1	925
	2	751
	3	679
	4	419
	5	358
	6	258
B	1	612
	2	996
	3	543
	4	350
	5	479
	6	564
C	1	2065
	2	880
	3	841
	4	1698
	5	1789
Total		14207

4.2 Bayesian inference with non-informative prior

The sample mean and variance for each recipe were calculated using Eqs. (2) and (3). Eqs. (4) and (5) were further used to calculate the sample mean and variance on higher levels of the hierarchy, and the equations in Tab. 3 were used to calculate the expected value and variance of $y = \ln f_{\mathrm{c,cube}}$ on the respective level.

For brevity, detailed results from the plant level are left out of this presentation. At plant level for producer A and C the durability class was governing for the strength prediction, e.g.

B35M40, B35MF40 and B35SV40 were almost equally distributed as B45M40, B45MF40 and B45SV40, respectively. The within-recipe variation dominated, but the between-recipe variation was significant in most combinations of strength and durability classes. For the plants of producer C, a significant over-strength was observed in most instances of B35 concretes. The trend where the durability class was governing for the strength prediction was weaker for the plants of producer B, and the between-recipe variation was relatively large and dominated in eight combinations of strength and durability classes.

Tab. 6 shows the results on the producer level. The predicted characteristic strength should be compared to the target cube strength from Tab. 1. Due to statistical uncertainty, i.e. a small sample resulting in $\sqrt{\mathrm{VAR}[y]} \gg s$, a low value was predicted for the characteristic strength for B55M40 for producer A. For producer A, it can be seen that the between-plant variation was small and only dominant for B20M90. Due to large standard deviations, five strength predictions were lower than the target for producer B. For B25M90 and B30M60 this was due to within-plant variation, but for the higher strength classes the between-plant variation also influenced. Due to slightly low mean values, the predictions of B45MF40 and B45MF45 were lower than the target strengths for producer C. The contribution from between-plant variation was small in all cases. Since compliance control is based on samples where observations from different recipes are combined using the concrete family concept [20,21], the sometimes low predictions of the characteristic strength do not indicate that the producers deviate from the criteria in EN 206 [3].

Tab. 7 shows the results on the level of the combination of strength and durability class. Four predictions were lower than the target strength, either due to a large standard deviation due to within-producer variation, see e.g. B25M90, slightly low mean values, see B45MF40 and B45MF45, or due to statistical uncertainty, see B55M40. The contribution from between-producer variation was low in most cases, with the largest contribution for B35M40.

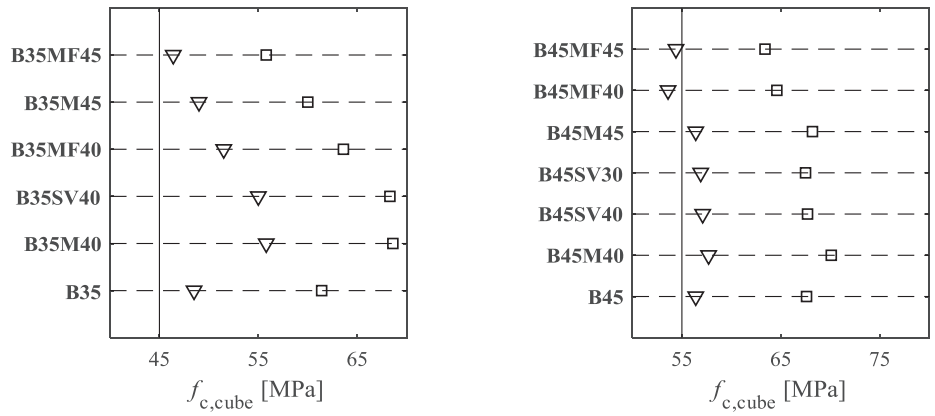

a) B35, note that B35M60 and B35SV30 were left out of the figure due to the low numbers of observations.

b) B45.

Figure 2: *Posterior predictions according to Tabs. 7 and 8 and Eq. (14) for the combinations of strength and durability classes. The solid lines indicate the target cube strength and the squares and the triangles indicate the median and the lower 5%-fractile of the posterior predictive distributions respectively.*

Finally, Tab. 8 shows the results from the level of the strength class. Only B25 did not reach the target strength. This was due to a slightly low mean strength and a large standard deviation with a significant contribution from between-durability class variation, where B25M60 was closer to a B30. B35 also got a significant contribution from between-durability class variation, as demonstrated in Fig. 2a, but the higher mean strengths of e.g. B35M40 resulted in a high mean strength for B35. The lower contribution from between-durability class variation for B45 is demonstrated in Fig. 2b.

In the bottom row of Tab. 8, the natural logarithm of the target strength is subtracted from the values of $\mathrm{E}[y]$, to get the variable δ as introduced in Sec. 3.3. It is interesting to note that $\mathrm{E}[\delta] = 0.25$ is approximately what could be estimated assuming $V_{\mathrm{c,cube}} = 0.15$, i.e. $\mathrm{E}[\delta] \approx 1.645 \cdot 0.15$. The results indicated that the cube strength could be represented by a log-normally distributed variable with mean

$$\mu_{\mathrm{c,cube}} \approx \exp\left(\ln f_{\mathrm{ck,cube}} + \mathrm{E}[\delta]\right) = 1.28 f_{\mathrm{ck,cube}} \tag{37}$$

and coefficient of variation

$$V_{\mathrm{c,cube}} \approx \sqrt{\mathrm{VAR}[y]} = 0.13 \quad . \tag{38}$$

The general coefficient of variation gets a dominant contribution from within-durability class variation, but also between-durability class variation, indicated by s_{w}^2/s^2 in Tab. 8, and between-strength class variation due to different $\mathrm{E}[\delta]$ for the different classes contribute.

Table 6: *Posterior inference per producer for different combinations of strength and durability classes, where $E[y]$ and $VAR[y]$ are the expected value and the variance of the posterior prediction of $y = ln\, f_{c,cube}$, s is the sample standard deviation, n is the sample size and $f_{c,cube,0.5}$ and $f_{c,cube,0.05}$ is the median and characteristic value of the posterior prediction in MPa. s_w^2/s^2 indicates the contribution from the within-plant variance to the total variance of the combination of strength and durability class at the respective producer.*

	$\mathrm{E}[y]$	$\sqrt{\mathrm{VAR}[y]}$	s	n	s_{w}^2/s^2	$f_{\mathrm{c,cube,0.5}}$	$f_{\mathrm{c,cube,0.05}}$
Producer A							
B20M90	3.52	0.13	0.13	33	0.40	33.7	26.8
B25M60	3.78	0.10	0.10	20	0.59	43.6	36.3
B25M90	3.59	0.10	0.09	33	0.90	36.4	30.8
B30M60	3.86	0.12	0.12	1076	0.81	47.4	39.2
B35M40	4.22	0.10	0.10	179	0.94	67.9	57.1
B35M45	4.05	0.12	0.12	409	0.95	57.5	47.5
B35M60	3.94	0.06	0.05	8	1.00	51.2	45.5
B35MF40	4.17	0.11	0.11	183	0.79	64.8	54.4
B35MF45	4.03	0.11	0.11	308	0.98	56.5	47.0
B35SV40	4.21	0.11	0.11	162	0.86	67.7	56.0
B45M40	4.21	0.10	0.10	235	0.89	67.3	56.7
B45MF40	4.20	0.10	0.10	212	0.97	66.7	56.6
B45SV30	4.19	0.10	0.10	68	1.00	65.9	55.5
B45SV40	4.24	0.11	0.11	458	0.77	69.4	58.2
B55M40	4.30	0.09	0.07	6	1.00	74.0	60.5

Producer B							
B20M90	3.55	0.12	0.11	16	0.69	34.9	28.0
B25M90	3.61	0.18	0.17	54	0.98	37.1	27.5
B30M60	3.81	0.12	0.12	956	0.78	45.0	36.8
B30MF45	3.98	0.11	0.07	5	1.00	53.6	41.8
B35M40	4.09	0.14	0.13	120	0.36	60.0	47.9
B35M45	4.03	0.13	0.13	466	0.58	56.3	45.5
B35MF40	4.09	0.19	0.18	59	0.34	59.5	43.3
B35MF45	4.01	0.12	0.12	276	0.66	55.2	45.4
B35SV30	4.10	0.08	0.04	4	1.00	60.2	48.4
B35SV40	4.14	0.11	0.11	62	0.47	62.7	51.7
B45M40	4.21	0.13	0.13	161	0.44	67.3	54.3
B45MF40	4.15	0.12	0.12	332	0.68	63.3	52.0
B45SV30	4.24	0.10	0.09	49	0.38	69.7	59.1
B45SV40	4.18	0.10	0.10	824	0.73	65.6	55.8
B55SV40	4.38	0.10	0.10	160	0.96	80.0	68.2
Producer C							
B20M90	3.59	0.11	0.11	131	0.72	36.3	30.1
B30M60	3.83	0.10	0.10	2363	0.91	45.9	38.8
B35M40	4.27	0.10	0.10	458	0.91	71.4	60.2
B35M45	4.13	0.10	0.10	1138	0.79	62.5	52.6
B35MF40	4.16	0.12	0.12	120	0.66	64.0	52.7
B35MF45	4.02	0.11	0.11	464	0.86	55.6	46.5
B35SV40	4.25	0.14	0.14	280	0.71	69.9	55.8
B45M40	4.30	0.10	0.10	343	0.91	73.4	61.7
B45M45	4.22	0.11	0.11	52	0.82	68.2	56.4
B45MF40	4.17	0.11	0.11	161	0.88	64.8	53.9
B45MF45	4.15	0.09	0.08	34	0.92	63.4	54.4
B45SV40	4.22	0.10	0.10	1729	0.88	68.4	57.7

Table 7: *Posterior inference per combination of strength and durability classes, where the variables are defined in Tab. 6.* s_w^2/s^2 *indicates the contribution from the within-producer variance to the total variance of the combination of strength and durability class.*

	$\mathrm{E}[y]$	$\sqrt{\mathrm{VAR}[y]}$	s	n	s_w^2/s^2	$f_{\mathrm{c,cube,0.5}}$	$f_{\mathrm{c,cube,0.05}}$
B20M90	3.57	0.12	0.12	180	0.94	35.7	29.3
B25M60	3.78	0.10	0.10	20	1.00	43.6	36.3
B25M90	3.61	0.15	0.15	87	1.00	36.8	28.7
B30M60	3.83	0.11	0.11	4395	0.97	46.1	38.3
B30MF45	3.98	0.11	0.07	5	1.00	53.6	41.8
B35M40	4.23	0.13	0.12	757	0.75	68.6	55.8
B35M45	4.09	0.12	0.12	2013	0.85	60.0	49.0
B35M60	3.94	0.06	0.05	8	1.00	51.2	45.5
B35MF40	4.15	0.13	0.13	362	0.94	63.6	51.5
B35MF45	4.02	0.11	0.11	1048	0.99	55.8	46.4
B35SV30	4.10	0.08	0.04	4	1.00	60.2	48.4
B35SV40	4.22	0.13	0.13	504	0.93	68.3	55.0
B45M40	4.25	0.12	0.12	739	0.87	70.1	57.7
B45M45	4.22	0.11	0.11	52	1.00	68.2	56.4
B45MF40	4.17	0.11	0.11	705	0.96	64.6	53.6
B45MF45	4.15	0.09	0.08	34	1.00	63.4	54.4
B45SV30	4.21	0.10	0.10	117	0.96	67.5	56.9
B45SV40	4.22	0.10	0.10	3011	0.96	67.7	57.1
B55M40	4.30	0.09	0.07	6	1.00	74.0	60.5
B55SV40	4.38	0.10	0.10	160	1.00	80.0	68.2

Table 8: *Posterior inference per strength class, where the variables are defined in Tab. 6.* s_w^2/s^2 *indicates the contribution from the within-durability class variance to the total variance of the strength class. The general posterior predictive inference is for the variable* $\delta = y - ln\, f_{ck,cube}$.

	$\mathrm{E}[y]$	$\sqrt{\mathrm{VAR}[y]}$	s	n	s_w^2/s^2	$f_{\mathrm{c,cube,0.5}}$	$f_{\mathrm{c,cube,0.05}}$
B20	3.57	0.12	0.12	180	1.00	35.7	29.3
B25	3.64	0.16	0.15	107	0.81	38.0	29.3
B30	3.83	0.11	0.11	4400	1.00	46.1	38.3
B35	4.12	0.14	0.14	4696	0.72	61.4	48.5
B45	4.21	0.11	0.11	4658	0.96	67.6	56.4
B55	4.38	0.10	0.10	166	0.98	79.8	68.0
General	0.25	0.13	-	-	-	-	-

4.3 Parameters for an informative prior distribution

Informative prior parameters were estimated with the MLE on the strength and durability class level, based on groups of samples at the plant level. The results can be used in Eqs. (16) to (19), or Eqs. (21) to (24), assuming that the observations in the sample $\boldsymbol{y}$ originate from one producer and plant, and replacing $\bar{y}'$, s', n' and ν' with $\bar{y}_{\mathrm{MLE}}$, s_{MLE}, n_{MLE} and ν_{MLE}, respectively. Note that ν_{MLE} was estimated by solving Eq. (30) numerically.

Tab. 9 shows the results of the MLE per combination of strength and durability class. $\bar{y}_i$ and s_i^2 input to Eq. (33) were the sample mean and variance of a sample containing all the observations from the recipes obtaining a specified combination of strength and durability class at plant i. m could range from 2 to 17, excluding combinations represented at only one plant. Generally the

results showed higher degrees of belief, in terms of n and ν, and lower standard deviations compared to the results by Rackwitz [16] shown in Tab. 10.

Table 9: *MLE for different combinations of strength and durability class.*

	$\bar{y}_{\mathrm{MLE}}$	n_{MLE}	s_{MLE}	ν_{MLE}	m
B20M90	3.54	1.4	0.09	6.7	12
B25M60	3.77	1.8	0.07	6.5	2
B25M90	3.65	5.2	0.05	1.3	5
B30M60	3.83	3.8	0.10	21.4	17
B35M40	4.18	0.8	0.08	6.5	14
B35M45	4.06	1.6	0.09	7.2	17
B35MF40	4.14	0.8	0.09	7.0	14
B35MF45	4.01	2.8	0.09	8.7	15
B35SV40	4.21	1.0	0.08	4.7	12
B45M40	4.21	1.0	0.08	5.7	17
B45M45	4.19	5.7	0.07	2.9	4
B45MF40	4.17	2.5	0.09	11.6	15
B45MF45	4.14	8.1	0.09	33.8	2
B45SV30	4.24	0.9	0.06	11.0	5
B45SV40	4.21	3.4	0.08	9.5	16
B55SV40	4.36	9.8	0.06	3.8	3
General	0.26	0.6	0.08	5.0	170

Table 10: *Prior data for the cube strength of ready-mixed concrete as suggested by Rackwitz [16] assuming a log-normal distribution. $\bar{y}'$ and s' represent the prior knowledge about the mean and standard deviation, and n' and ν' are the degree of belief in $\bar{y}'$ and s' respectively.*

	$\bar{y}'$	n'	s'	ν'
C15	3.40	1.5	0.14	6.0
C25	3.65	1.5	0.12	6.0
C35	3.85	1.5	0.09	6.0
C45	3.98	1.5	0.07	6.0

For B25M90, the variances at the plants of producer B dominated in Sec. 4.2, but were dominated by the lower variances at the plants of producer A in the MLE. This explains the low values for s_{MLE} and ν_{MLE}. The contrasting high value of n_{MLE} was recognized in the low contribution from between-plant and -producer variation shown in Tabs. 6 and 7. ν_{MLE} of B30M60 was associated with the small variation of the variances between the plants and producers. The low values for n_{MLE} for B35M40 and B35MF40 reflected that the durability class was governing for the strength prediction for producers A and C, but less governing for producer B. The low variation in the variance between plants and the relatively low contribution from between-plant and -producer variance for B45MF40 and B45SV40, resulted in high values for ν_{MLE} and n_{MLE} respectively. The low n_{MLE} for B45SV30 was reflected in the large contribution from between-plant variance for producer B.

Tab. 11 shows the MLE per durability class, where $\bar{y}_i$ and s_i^2 are the sample mean and variance of the group of samples with the same durability class at plant i, and the estimated variances would thus include a contribution from between-strength class variance. Interesting to note from the results were the high values for the degree of belief, both with respect to the mean and the standard deviation. These results were not surprising, since the durability class gives a required

maximum water-binder ratio, and the strength of the concrete is governed by the water-binder ratio.

Table 11: *MLE for different durability classes.*

	$\bar{y}_{\mathrm{MLE}}$	n_{MLE}	s_{MLE}	ν_{MLE}	m
M40	4.19	1.1	0.08	10.4	17
M45	4.06	1.6	0.09	7.4	17
M60	3.83	4.1	0.10	21.9	17
M90	3.57	2.4	0.10	6.8	13
MF40	4.17	2.2	0.09	10.7	16
MF45	4.01	2.8	0.09	8.3	15
SV30	4.24	0.8	0.06	11.2	5
SV40	4.21	3.2	0.09	8.0	16
General	-	-	0.09	7.7	116

Tab. 12 shows the MLE per strength class, where $\bar{y}_i$ and s_i^2 are the sample mean and variance of the group of samples with the same strength class at plant i, and the estimated standard deviations would thus include a contribution from between-durability class variance.

Table 12: *MLE for different strength classes.*

	$\bar{y}_{\mathrm{MLE}}$	n_{MLE}	s_{MLE}	ν_{MLE}	m
B20	3.54	1.4	0.09	6.7	12
B25	3.67	1.2	0.06	1.4	7
B30	3.83	3.9	0.10	21.3	17
B35	4.07	2.2	0.11	22.8	17
B45	4.19	2.2	0.09	20.4	17
B55	4.35	4.9	0.06	5.0	4
General	0.24	1.1	0.09	4.1	74

Taking the values of the general MLE with the highest degree of belief, Tabs. 12 and 11 indicate that if the strength and durability class is unknown, and the producer and plant is known, the mean and coefficient of variation of the cube strength respectively, can be estimated with a reasonable degree of belief according to

$$\mu_{\mathrm{c,cube}} \approx \exp\left(\ln f_{\mathrm{ck,cube}} + \delta_{\mathrm{MLE}}\right) = 1.27 f_{\mathrm{ck,cube}} \tag{39}$$

and

$$V_{\mathrm{c,cube}} \approx s_{\mathrm{MLE}} = 0.09 \quad . \tag{40}$$

Since samples with low sample standard deviations tend to dominate, and the between-plant and -producer variance is not taken into account, the general MLE of the variance was smaller than the general estimate in Sec. 4.2.

4.4 Within-batch variation

For estimating the within-batch variation, the samples of observations for each recipe were treated separately, i.e. without combining samples from different recipes as in Sec. 4.3. The sample variance and the sample size of recipe i were input to Eq. (36) to obtain the estimator for the within-batch variation of recipe i, $s_{\mathrm{wb},i}^2$. Furthermore, the value of $s_{\mathrm{wb},i}^2$ for each recipe

obtaining a specified strength class or combination of strength and durability class was input to Eqs. (33), (29) and (30). Tabs. 13 and 14 show the results per combination of strength and durability class and per strength class respectively. Note that Tab. 13 indicates for example that at the 17 plants considered in the present work, there were $m = 69$ recipes for obtaining a B45M40. The estimates of the standard deviation of the within-batch variation ranged from 0.03 for B45SV30 to 0.07 for B20M90, and from 0.05 for B25-B55 to 0.07 for B20. The general estimate of the within-batch variation was comparable to results from the literature [5,11,12].

Table 13: *MLE of the within-batch variation for different combinations of strength and durability class.*

	$s_{\mathrm{wb,MLE}}$	$\nu_{\mathrm{wb,MLE}}$	m
B20M90	0.07	3.8	26
B25M60	0.04	3.2	3
B25M90	0.05	1.4	16
B30M60	0.05	1.6	129
B35M40	0.05	1.9	59
B35M45	0.04	1.4	105
B35MF40	0.05	1.6	49
B35MF45	0.06	2.6	72
B35SV40	0.05	2.1	40
B45M40	0.05	2.0	69
B45M45	0.05	2.1	8
B45MF40	0.05	1.7	56
B45MF45	0.06	11.4	5
B45SV30	0.03	1.4	11
B45SV40	0.04	1.6	91
B55SV40	0.05	3.9	6
General	0.05	1.6	745

Table 14: *MLE of the within-batch variation for different strength classes.*

	$s_{\mathrm{wb,MLE}}$	$\nu_{\mathrm{wb,MLE}}$	m
B20	0.07	3.8	26
B25	0.05	1.5	19
B30	0.05	1.6	130
B35	0.05	1.6	327
B45	0.05	1.6	240
B55	0.05	4.2	7
General	0.05	1.6	749

4.5 General probability distribution

Based on the preceding sections, a general probability distribution was established, as summarized in Tab. 15. Considering Tabs. 8 and 12, the mean compressive cube strength was taken as

$$\mu_{\mathrm{c,cube}} \approx \exp\left(\ln f_{\mathrm{ck,cube}} + \mathrm{E}[\delta]\right) = f_{\mathrm{ck,cube}} \exp(0.25) \approx 1.28 f_{\mathrm{ck,cube}} \quad , \tag{41}$$

where $f_{\mathrm{ck,cube}}$ is the target cube strength from Tab. 1.

According to Tab. 8, the coefficient of variation of the cube strength at the highest level of the hierarchy can be taken as

$$V_{\mathrm{c,cube}} \approx \sqrt{\mathrm{VAR}[y]} = 0.13 \quad , \tag{42}$$

and assuming that Tabs. 11 and 14 represent the within-plant and within-batch variation respectively, the respective coefficients of variation can be taken as $V_{\mathrm{wp}} \approx s_{\mathrm{MLE,gen}} = 0.09$ and $V_{\mathrm{wb}} \approx s_{\mathrm{wb,MLE,gen}} = 0.05$. The total coefficient of variation can be given as

$$V_{\mathrm{c,cube}} = \sqrt{V_{\mathrm{wb}}^2 + V_{\mathrm{bbr}}^2 + V_{\mathrm{bpp}}^2} = 0.13 \quad , \tag{43}$$

where $V_{\mathrm{bbr}} = \sqrt{V_{\mathrm{wp}}^2 - V_{\mathrm{wb}}^2} \approx 0.08$ is the between-batch and -recipe variation and $V_{\mathrm{bpp}} = \sqrt{V_{\mathrm{c,cube}}^2 - V_{\mathrm{wp}}^2} \approx 0.09$ is the between-plant and -producer variation.

Table 15: *Parameters for the general probability distribution for the compressive cube strength. $f_{ck,cube}$ is the target cube strength.*

Mean	$\mu_{\mathrm{c,cube}} = 1.28 f_{\mathrm{ck,cube}}$
Total variation	$V_{\mathrm{c,cube}} = \sqrt{V_{\mathrm{wb}}^2 + V_{\mathrm{bbr}}^2 + V_{\mathrm{bpp}}^2} = 0.13$
Within-batch variation	$V_{\mathrm{wb}} = 0.05$
Between-batch and -recipe variation	$V_{\mathrm{bbr}} = 0.08$
Between-plant and -producer variation	$V_{\mathrm{bpp}} = 0.09$

5. APPLICATION EXAMPLES

5.1 General remarks

Two examples are introduced to demonstrate the application of the results: one existing and one new structure. Stewart [10] suggests that the compressive strength in a structure can be calculated based on the lab-strength of cylinders according to

$$f_{\mathrm{c}} = k_{\mathrm{cp}} k_{\mathrm{cr}} f_{\mathrm{c,lab}} \quad , \tag{44}$$

where k_{cp} and k_{cr} are factors considering the effects of compaction and curing respectively. It was assumed that the concrete was placed with fair performance of the compaction and exposed to fair curing conditions for at least seven days, resulting in mean values $\mu_{\mathrm{cp}} = 0.87$ and $\mu_{\mathrm{cr}} = 1.00$, and coefficients of variation $V_{\mathrm{cp}} = 0.06$ and $V_{\mathrm{cr}} = 0.05$. With a poor level of compaction and poor curing conditions, the mean values and the coefficients of variation of the factors decrease and increase, respectively. A nominal ratio between the cylinder and cube strength of 0.85 was used, and the coefficient of variation of the lab-strength of cylinders was assumed to be properly described by the one estimated for cubes, justified by evidence in the literature reviewed in the introduction. The compressive strength in the structure was thus represented by a log-normally distributed variable with mean

$$\mu_{\mathrm{c}} = 0.85 \cdot 0.87 \cdot 1.00 \cdot \mu_{\mathrm{c,cube}} \approx 0.74 \exp(\mathrm{E}[y]) \tag{45}$$

and coefficient of variation

$$V_{\mathrm{c}} = \sqrt{0.06^2 + 0.05^2 + V_{\mathrm{c,cube}}^2} \approx \sqrt{0.006 + \mathrm{VAR}[y]} \quad , \tag{46}$$

assuming that Eqs. (25) and (26) are valid approximations. It should be noted that the ratio between the cylinder and cube strength also has a significant coefficient of variation [30-35] which should be taken into account in Eq. (46) if a detailed strength prediction is necessary. However, for the present application examples, the nominal ratio was assumed sufficient.

5.2 Example 1: Existing structure

The sample of six cores drilled from an existing structure presented by Steenbergen & Vervuurt [43] was considered. The sample mean and standard deviation of the natural logarithm of the core strengths were $\bar{y} = 4.40$ and $s = 0.12$, and with six observations, $\nu = 5$. Assuming a non-informative prior, Eq. (14) can be used to estimate the lower 5%-fractile of the cylinder strength as

$$f_{\mathrm{c},0.05} = \exp\left(\bar{y} - t_{0.05,5} s \sqrt{\frac{7}{6}}\right) = 62.7 \text{ MPa} \quad . \tag{47}$$

Assuming that the generalized prior data for the variance given in Tab. 12 is valid for the population of concrete from which the six cores originate, Eqs. (23) and (24) update the prior data for the variance, added the contributions from compaction and curing, according to

$$\nu'' = \nu_{\mathrm{MLE,gen}} + \nu = 9.1 \tag{48}$$

and

$$s'' = \sqrt{\frac{\nu_{\mathrm{MLE,gen}}\left(s_{\mathrm{MLE,gen}}^2 + V_{\mathrm{cp}}^2 + V_{\mathrm{cr}}^2\right) + \nu s^2}{\nu''}} = 0.12 \quad . \tag{49}$$

Eq. (49) is derived from Eq. (24), assuming that the prior value of the variance can be given by $s'^2 = s_{\mathrm{MLE,gen}}^2 + V_{\mathrm{cp}}^2 + V_{\mathrm{cr}}^2$. The estimated lower 5%-fractile of the cylinder strength becomes

$$f_{\mathrm{c},0.05} = \exp\left(\bar{y} - t_{0.05,9.1} s'' \sqrt{\frac{11.1}{10.1}}\right) = 64.8 \text{ MPa} \quad . \tag{50}$$

The influence of the prior data on the updated standard deviation was small since the values of the sample standard deviation and the prior were similar. However, the prior data increased the *information content* in the posterior prediction, shown in Fig. 3, resulting in a 3% increase of the estimated lower 5%-fractile of the cylinder strength.

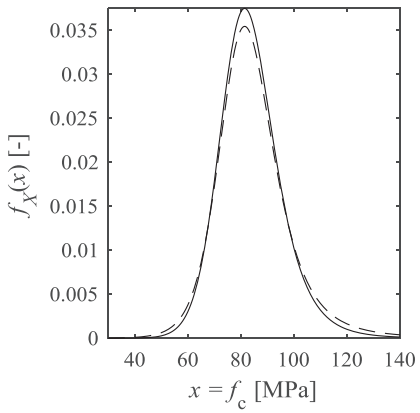

Figure 3: *Posterior predictive distributions based on non-informative (dashed) and informative (solid) prior distributions for the cylinder strength in Example 1.*

5.3 Example 2: New structure

A structure was assumed to be designed with a concrete B45M40. At an early stage in the design process, it is reasonable to consider the whole population of B45 when estimating the design compressive strength, i.e. the strength class level in the hierarchical model in Fig. 1. Considering Tab. 8 and the assumptions above, the mean compressive strength becomes

$$\mu_{\mathrm{c}} = 0.74 \exp(\mathrm{E}[y]) = 49.8 \text{ MPa} \quad , \tag{51}$$

the total coefficient of variation becomes

$$V_{\mathrm{tot,c}} = \sqrt{V_\theta^2 + V_{\mathrm{G}}^2 + V_{\mathrm{c}}^2} = \sqrt{0.05^2 + 0.05^2 + (0.006 + \mathrm{VAR}[y])} = 0.15 \quad , \tag{52}$$

and the design compressive strength becomes

$$f_{\mathrm{c,des}} = \mu_{\mathrm{c}} \exp\left(-\alpha_{\mathrm{R}} \beta V_{\mathrm{tot,c}}\right) = 31.4 \text{ MPa} \quad , \tag{53}$$

assuming that V_θ, V_{G} and $\alpha_{\mathrm{R}}\beta$, attain the values from Eq. (1). Comparing the design strength with the target cylinder strength from Tab. 1, f_{ck}, gives an effective partial material factor

$$\gamma_{\mathrm{c,eff.}} = \frac{f_{\mathrm{ck}}}{f_{\mathrm{c,des}}} = 1.44 \quad , \tag{54}$$

which could be compared with $\gamma_{\mathrm{c}} = 1.5$ from Eq. (1). By including more information by moving downwards in the hierarchical model, and considering Tabs. 7 and 6, the results in Tab. 16 are obtained. The different estimates of $\gamma_{\mathrm{c,eff.}}$ are results of considering different subpopulations of B45 and B45M40, having different mean values and coefficients of variation. If a sufficient amount of information is made available, it could be possible to move further downwards in the hierarchy, and possibly exclude both between-plant and between-recipe variation.

Table 16: *Results from Example 2, demonstrating the effect of including more information in the estimate of the design compressive strength. μ_c is the mean strength in the structure, $V_{tot,c}$ is the total coefficient of variation, $f_{c,des}$ is the design compressive strength and $\gamma_{c,eff.}$ is the effective partial material factor according to Eqs. (51) to (54).*

Knowledge	μ_c [MPa]	$V_{tot,c}$ [-]	$f_{c,des}$ [MPa]	$\gamma_{c,eff.}$ [-]
B45	49.8	0.15	31.4	1.44
B45M40	51.8	0.16	31.9	1.41
B45M40, Prod. A	49.8	0.15	32.0	1.40
B45M40, Prod. B	49.8	0.17	30.0	1.50
B45M40, Prod. C	54.5	0.15	35.1	1.28

6. CONCLUSION

By studying strength recordings from Norwegian ready-mixed concrete plants, the variability of the compressive cube strength has been quantified on different hierarchical levels. The highest studied level of the hierarchy was the strength class, which represents the entry point of information in the design process. During design of a new structure, the designer specifies a certain strength and durability class, and the fact that the producer, plant, recipe and batch is unknown is reflected in the coefficient of variation at the highest level of the hierarchy. The presented results are easily combined with additional data, e.g. from the European market, or from a supply controlled by a different regional standard.

It has been demonstrated how the level of knowledge of the designer influences the uncertainty that must be taken into account, and thus the estimated design compressive strength in the structure. With today's diversity in assessment methods both with regard to structural behaviour and uncertainty differentiation, and the strong focus on reassessments of existing structures, data on a form similar to what has been presented herein could be considered included in future design codes. This could stimulate to a safe use of advanced assessment methods, with an aim to reduce unnecessary conservatism and increase the competitiveness of concrete.

The scope of the present work was to estimate the variation resulting from what the designer can control. The results indicate that the designer should specify a strength class that utilizes the strength potential of the durability class, and avoid combinations like e.g. B35M40 and B25M60, where a resulting over-strength could introduce a safety margin, but also unintended variation in the population. A closer collaboration between the designer, contractor and producer is expected to result in improved concrete specifications. A natural continuation of this work could be to address the influence of the different constituents on the estimated variation, i.e. study the variation from a producer's point of view with the possible aim of reducing unintended variation, and obtaining a more homogenous population of concrete.

ACKNOWLEDGEMENTS

The work presented in this paper is part of an industrial PhD funded by Multiconsult ASA and the Research Council of Norway.

REFERENCES

1. CEN: EN 1990: Basis for structural design. 2002.
2. CEN: EN 1992-1-1. Eurocode 2: Design of concrete structures. Part 1-1: General rules and rules for buildings. 2004.
3. CEN: EN 206: Concrete. Specification, performance, production and conformity. 2013.

4. *Vegdirektoratet*: Håndbok R762 Prosesskode 2: Standard beskrivelsestekster for bruer og kaier (in Norwegian). Statens Vegvesen, 2014.
5. *Mirza, S. A., Hatzinikolas, M. & MacGregor, J. G.*: Statistical Description of Strength of Concrete. Journal of the Structural Division, ASCE, 1979, 105(ST6), 1021-1037.
6. *Campbell, R. H. & Tobin, R. E.*: Core and Cylinder Strengths of Natural and Lightweight Concrete. ACI Journal, 1967, 64(4), 190-195.
7. *Bloem, D. L.*: Concrete Strength in Structures. ACI Journal, 1968, 65(3), 176-187.
8. *Drysdale, R. G.*: Variation of concrete strength in existing buildings. Magazine of Concrete Research, 1973, 25(85), 201-207.
9. *Yip, W. K. & Tam, C. T.*: Concrete strength evaluation through the use of small diameter cores. Magazine of Concrete Research, 1988, 40(143), 99-105.
10. *Stewart, M. G.*: Workmanship and Its Influence on Probabilistic Models of Concrete Compressive Strength. ACI Materials Journal, 1995, 92(4), 361-372.
11. *Bartlett, F. M. & MacGregor, J. G.*: Statistical Analysis of the Compressive Strength of Concrete in Structures. ACI Materials Journal, 1996, 93(2), 158-168.
12. *Bartlett, F. M. & MacGregor, J. G.*: Variation of In-Place Concrete Strength in Structures. ACI Materials Journal, 1999, 96(2), 261-270.
13. *Bartlett, F. M.*: Precision of in-place concrete strengths predicted using core strength correction factors obtained by weighted regression analysis. Structural Safety, 1997, 19(4), 397-410.
14. *Chin, M. S., Mansur, M. A. & Wee, T. H.*: Effects of Shape, Size, and Casting Direction of Specimens on Stress-Strain Curves of High-Strength Concrete. ACI Materials Journal, 1997, 94(3), 209-218.
15. *Wisniewski, D. F., Cruz, P. J. S., Henriques, A. A. R. & Simões, R. A. D.*: Probabilistic models for mechanical properties of concrete, reinforcing steel and pre-stressing steel. Structure and Infrastructure Engineering, 2012, 8(2), 111-123.
16. *Rackwitz, R.*: Predictive distribution of strength under control. Materials and Structures, 1983, 16(4), 259-267.
17. *JCSS*: Probabilistic Model Code. 12th draft, Joint Committee on Structural Safety, 2001.
18. *Taerwe, L.*: The influence of autocorrelation on OC-lines of compliance criteria for concrete strength. Materials and Structures, 1987, 20(6), 418-427.
19. *Taerwe, L.*: Evaluation of compound compliance criteria for concrete strength. Materials and Structures, 1988, 21(1), 13-20.
20. *Caspeele, R. & Taerwe, L.*: Probabilistic evaluation of conformity criteria for concrete families. Materials and Structures, 2011, 44(7), 1219-1231.
21. *Caspeele, R. & Taerwe, L.*: Statistical comparison of data from concrete families in ready-mixed concrete plants. Structural Concrete, 2011, 12(3), 148-154.
22. *Caspeele, R. & Taerwe, L.*: Numerical Bayesian updating of prior distributions for concrete strength properties considering conformity control. Advances in Concrete Construction, 2013, 1(1), 85-102.
23. *Caspeele, R.*: From quality control to structural reliability: where Bayesian statistics meets risk analysis. Heron, 2014, 59(2/3), 79-100.
24. *Caspeele, R., Sykora, M. & Taerwe, L.*: Influence of quality control of concrete on structural reliability: assessment using a Bayesian approach. Materials and Structures, 2014, 47(1-2), 105-116.
25. *Caspeele, R. & Taerwe, L.*: Influence of concrete strength estimation on the structural safety assessment of existing structures. Construction and Building Materials, 2014, 62, 77-84.
26. *Foster, S. J., Stewart, M. G., Loo, M., Ahammed, M. & Sirivivatnanon, V.*: Calibration of Australian Standard AS3600 Concrete Structures: part I statistical analysis of material

properties and model error. Australian Journal of Structural Engineering, 2016, 17(4), 242-253.

27. *Rashid, M. A., Mansur, M. A. & Paramasivam, P.*: Correlations between Mechanical Properties of High-Strength Concrete. Journal of Materials in Civil Engineering, 2002, 14(3), 230-238.
28. *Strauss, A.*, *Zimmermann, T.*, *Lehký, D.*, *Novák, D.* & *Kersner, Z.*: Stochastic fracture-mechanical parameters for the performance-based design of concrete structures. Structural Concrete, 2014, 15(3), 380-394.
29. *Zimmermann, T., Lehký, D. & Strauss, A.*: Correlation among selected fracture-mechanical parameters of concrete obtained from experiments and inverse analyses. Structural Concrete, 2016, 17(6), 1094-1103.
30. *Evans, R. H.*: The Plastic Theories for the Ultimate Strength of Reinforced Concrete Beams. Journal of the Institution of Civil Engineers, 1943, 21(2), 98-121.
31. *Elwell, D. J. & Fu, G.*: Compression Testing of Concrete: Cylinders vs. Cubes. Special Report 119. Transport Research and Development Bureau, New York State Department of Transportation, 1995.
32. *Mansur, M. A. & Islam, M. M.*: Interpretation of Concrete Strength for Nonstandard Specimens. Journal of Materials in Civil Engineering, 2002, 14(2), 151-155.
33. *Graybeal, B. & Davis, M.*: Cylinder or Cube: Strength Testing of 80 to 200 MPa (11.6 to 29 ksi) Ultra-High-Performance Fiber-Reinforced Concrete. ACI Materials Journal, 2008, 105(6), 603-609.
34. *Van Der Vurst, F., Boel, V., Craeye, B., Desnerck, P. & De Schutter, G.*: Influence of the composition of powder-type SCC on conversion factors for compressive strength. Magazine of Concrete Research, 2014, 66(6), 295-304.
35. *Van Der Vurst, F., Caspeele, R., Desnerck, P., De Schutter, G. & Peirs, J.*: Modification of existing shape factor models for self-compacting concrete strength by means of Bayesian updating techniques. Materials and Structures, 2015, 48(4), 1163-1176.
36. *CEN TC250/SC2*: Eurocode 2 – Commentary. European Concrete Platform, 2008.
37. fib: *fib* Model Code for Concrete Structures 2010, Ernst & Sohn, 2013.
38. *Müller, H. S., Anders, I., Breiner, R. & Vogel, M.*: Concrete: treatment of types and properties in *fib* Model Code 2010. Structural Concrete, 2013, 14(4), 320-334.
39. *Gelman, A., Carlin, J. B., Stern, H. S., Dunson, D. B., Vehtari, A. & Rubin, D. B.*: Bayesian Data Analysis. 3. ed., CRC Press, 2014.
40. *Caspeele, R.*: Probabilistic Evaluation of Conformity Control and the Use of Bayesian Updating Techniques in the Framework of Safety Analyses of Concrete Structures. PhD thesis, Ghent University, 2010.
41. *Torrent, R. J.*: The log-normal distribution: A better fitness for the results of mechanical testing of materials. Materials and Structures, 1978, 11(4), 235-245.
42. *Caspeele, R. & Taerwe, L.*: Bayesian assessment of the characteristic concrete compressive strength using combined vague-informative priors. Construction and Building Materials, 2012, 28(1), 342-350.
43. *Steenbergen, R. D. J. M. & Vervuurt, A. H. J. M.*: Determining the in situ concrete strength of existing structures for assessing their structural safety. Structural Concrete, 2012, 13(1), 27-31.

Paper II

Solution strategy for non-linear finite element analyses of large reinforced concrete structures

Engen, M., Hendriks, M. A. N., Øverli, J. A. & Åldstedt, E.
Structural Concrete, 2015, 16(3), 389-397

Technical Paper

DOI: 10.1002/suco.201400088

Morten Engen*
Max A. N. Hendriks
Jan Arve Øverli
Erik Åldstedt

Solution strategy for non-linear finite element analyses of large reinforced concrete structures

When performing non-linear finite element analyses during the design of large reinforced concrete structures, there is a need for a general, robust and stable solution strategy with a low modelling uncertainty which comprises choices regarding force equilibrium, kinematic compatibility and constitutive relations. In this paper, analyses of experiments with a range of structural forms, loading conditions, failure modes and concrete strengths show that an engineering solution strategy is able to produce results with good accuracy and low modelling uncertainty. The advice is to shift the attention from a detailed description of the post-cracking behaviour of concrete to a rational description of the pre-cracking compressive behaviour for cases where large elements are used and the ultimate limit capacity is sought.

Keywords: large reinforced concrete structures, non-linear finite element analysis, modelling uncertainty, structural design, engineering solution strategy

1 Introduction

The design of large concrete structures such as dams and offshore oil and gas platforms is normally carried out using linear finite element analyses (LFEA) followed by post-processing and non-linear section design [1]. Owing to the size of the structure and the high number of load cases that might need to be analysed, the sizes of the finite elements are normally in the order of the member dimensions, and could be termed **large-scale**. Solid elements are normally used due to the accuracy required at structural joints. Fig. 1 shows an example of a global finite element model with a typical element size of approx. 1 m. In order to take advantage of the principle of superposition, reinforced concrete is treated as an isotropic, linear elastic material during the LFEA, and the non-linear material properties of concrete and reinforcement are taken into account during the non-linear section design. Owing to the cracking of concrete and yielding of reinforcement, a redistribution of internal forces occurs even at low load levels. Such effects cannot be revealed by the LFEA due to the lack of realistic connection between load and material response during calculation of the internal forces. Despite this inconsistency, the present design method is considered safe when equilibrium is satisfied, the material strengths are not exceeded and sufficient ductility is provided. To compensate for the inconsistency, non-linear finite element analyses (NLFEA), where the non-linear material behaviour is taken into account directly, could be carried out to verify the reliability of the design. *Engen*, *Hendriks*, *Øverli* and *Åldstedt* [2] outline the application of NLFEA in the design process.

One of the main challenges when taking the step to using NLFEA in reliability analyses of concrete structures is the large modelling uncertainty possibly associated with the solution strategy selected for NLFEA [3]. A solution strategy for NLFEA consists of choices regarding force equilibrium, kinematic compatibility and constitutive relations. A review of results from blind prediction competitions shows that predictions of beams in bending and shear can result in coefficients of variation (COV) of 5–30 % and 10–40 % respectively [3]. Such scatter can be attributed to the solution strategy selected and has been found to increase as the skills of the analyst decrease [4–7]. In order to use NLFEA in practical design, a general, robust and stable solution strategy should thus be selected. This is of particular importance in the design of offshore concrete structures owing to the wide range of loading conditions encountered during their lifetime.

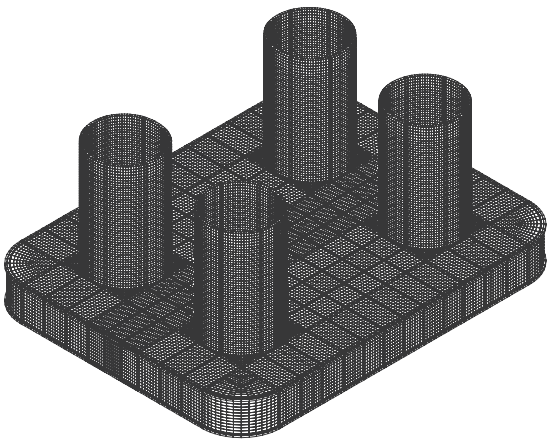

Fig. 1. Global finite element model used during the design of a typical offshore concrete platform (Roar Lie)

* Corresponding author: morten.engen@multiconsult.no

Submitted for review: 6 October 2014
Revised: 4 Dezember 2014
Accepted for publication: 2 January 2015

Several guidelines have been produced to help analysts select suitable solution strategies, but still leaving the analyst with a number of choices to make [8–10]; however, large-scale element sizes are treated only briefly. The objective of the present study is to develop a solution strategy for large-scale NLFEA in verifications of the global reliability of concrete structures. The objective of this paper is to select a proper solution strategy with a low COV for further development.

In this paper, the results from benchmark analyses on material and structural level, using two different solution strategies, are compared in order to reveal strengths and weaknesses. Three experiments on material level and ten relatively simple experiments on structural level, with a range of loading conditions, failure modes and concrete strengths, were chosen for this comparative study.

2 Solution strategy for large-scale NLFEA

A solution strategy for NLFEA consists of choices regarding force equilibrium, kinematic compatibility and constitutive relations, e.g. iteration method and convergence criteria, finite element type and integration scheme, and material models for concrete and reinforcement. The two solution strategies compared on material and structural level in this paper are more or less similar when it comes to equilibrium and kinematic compatibility, and the material model for concrete constitutes the main difference.

In a uniaxial compressive test, failure is initiated at the critical volume point where the test specimen has its smallest volume and starts to expand [11]. Due to the heterogeneity of concrete, one material point can reach the critical volume point before neighbouring material points. When this happens, the surrounding concrete will have a confining effect on the critically loaded concrete, leading to local triaxial compression at the critically loaded material point and transverse tension in the surrounding concrete. Failure is initiated when the tensile stresses in the surrounding concrete exceed the tensile capacity of the concrete. This phenomenon could be termed **splitting** due to the resulting cracks parallel to the maximum applied compressive stress. In contrast to splitting, **crushing**, or collapse of the void system of the concrete, happens due to extreme hydrostatic pressures [12], and is normally only observed as a post-peak phenomenon. Following this simple terminology, the failure modes at structural level are defined as either brittle or ductile. The brittle failure mode is associated with tensile stresses causing failure of the flow of compressive stresses from the load point to the supports, and the ductile failure mode is characterized by yielding of the reinforcement. Since the focus of this paper is on the ultimate capacity of structures, less attention was paid to the descending branch, all analyses were stopped at the peak level and no attempt was made to trace the post-peak behaviour. In order to reduce the analysis time, the load steps for the analyses on structural level were adjusted so that the ultimate load was reached in approx. 20 load increments.

The first solution strategy was based on the Dutch guidelines (DG) [10]. In the design phase, limited information is normally available regarding the concrete mix, and often the designer can only specify the compressive strength. The second solution strategy was based on a fully triaxial material model needing only **one** material input parameter, namely the uniaxial cylinder compressive strength [13, 14]. The solution strategy is well suited to engineering design problems, and is called the **engineering** solution strategy. The two solution strategies are summarized in Table 1.

Modified *Newton-Raphson* with a force convergence criterion of 10^{-2} and an energy convergence criterion of 10^{-3} was used in the DG solution strategy. The engineering solution strategy used a slightly amended version of the modified *Newton-Raphson* method, called *Newton-Raphson* Plus [15, 16], where the material stiffness matrices for concrete and reinforcement at each integration point were updated at the beginning of each load increment and kept constant throughout this load increment unless strong non-linearities, i.e. cracking of concrete and yielding of reinforcement, occurred. Convergence criteria dependent on stress and strain residuals were used, but were usually not met due to a relatively strict force convergence criterion of 10^{-3}. A trilinear constitutive law, as proposed by *González Vidosa*, *Kotsovos* and *Pavlovic* [15], was chosen for all reinforcement in both of the solution strategies in order to reduce bias. Both of the solution strategies used 20-node solid elements and three-node truss elements for concrete and reinforcement respective-

Table 1. Summary of the two solution strategies; ε_R and ε_E are the convergence criteria for residual force and energy respectively and the reference value used for convergence check is the square root of the sum of squares

	DG	**Engineering**
Force equilibrium	Modified *Newton-Raphson* with $\varepsilon_R = 10^{-2}$ and $\varepsilon_E = 10^{-3}$	*Newton-Raphson* Plus with $\varepsilon_R = 10^{-3}$
Kinematic compatibility	– 20-node solid elements for concrete and three-node bar elements for reinforcement – Reduced integration	
Constitutive relation	Concrete: – Fixed, orthogonal, smeared cracking – Uniaxial behaviour models generalized to triaxial stress states Reinforcement: – Trilinear relation	Concrete: – Fixed, non-orthogonal, smeared cracking with max. three cracks per integration point – Fully triaxial, empirically based material model Reinforcement: – Trilinear relation

ly. Despite the dangers of under-integration discussed in the literature [17], reduced integration was selected based on the recommendations published by *González Vidosa*, *Kotsovos* and *Pavlovic* [18].

In the guidelines published by *fib* [9], modelling the tensile behaviour of concrete and the interface between concrete and reinforcement receive special attention when discussing element size scales. Following these guidelines, bond slip and tension softening should be used in medium-scale analyses, i.e. when the element size is in the order of the reinforcing bar diameter, and perfect bond and tension stiffening should be used for large-scale analyses, recalling that tension stiffening represents the integrated response of uncracked concrete between cracks. In a recent study [19], results from medium- and large-scale analyses were compared. At the large scale, a fracture energy-based tension softening relation was modified in order to include the energy released during bond slip at the medium scale; see the work by *Lackner* and *Mang* [20] for a thorough discussion of the method. In [19] this approach was found to have only a limited effect on the global response, and it was suggested that this is due to the low relative contribution of concrete in tension to the total strain energy of the system. With this in mind, the tensile behaviour of concrete was not modified in the present study, where the elements were relatively large, and most of the focus was shifted towards the physical representation of cracking.

A fixed, orthogonal, total strain-based, smeared crack model was chosen for the DG solution strategy. When using a fixed crack model, it is necessary to assign a shear retention factor (SRF). The SRF reflects the relative amount of shear stiffness that should be retained at an integration point after cracking, and should be assigned a sufficiently high value to avoid numerical instabilities due to ill-conditioning of the material stiffness matrix and a sufficiently low value to reduce the transfer of shear stresses across cracks due to rotation of the stress field after cracking [18]. The Dutch guidelines propose the use of a variable SRF, but this has resulted in predicted capacities being too low. It has been suggested that the variable SRF mainly applies to medium-scale analyses, and a constant value of 0.1 was assigned in all analyses in the present study [21].

The DG solution strategy used a parabolic expression in compression [22] and an exponential softening expression in tension [23]. The effects of lateral stresses were taken into account by the model for strength reduction due to cracking published by *Vecchio* and *Collins* [24] and the confinement model published by *Selby* and *Vecchio* [25]. *Poisson*'s ratio was gradually decreased after cracking. Note that a constant value of 0.15 was assigned to *Poisson*'s ratio prior to cracking. A secant formulation was used for unloading and reloading. The chosen models required a set of material parameters that were all calculated based on relevant expressions in the *fib* Model Code for Concrete Structures 2010 [26] using a reported mean cylinder strength as input.

The material model used in the DG solution strategy was thus based on a uniaxial formulation and generalized by adopting extensions based on biaxial and triaxial experimental data. This is convenient when the effects of different behaviour models have to be studied, but models for material behaviour are often developed in combination with other complementary models and should not be separated [27]. Instead, fully triaxial material models could be developed directly based on biaxial and triaxial experimental results. This is the case for the material model used in the engineering solution strategy.

The material model used in the engineering solution strategy is described in full elsewhere [13, 14] and will only be outlined here. Decomposing the response of biaxially and triaxially loaded test specimens into octahedral stresses and strains led to the development of simple expressions for secant and tangent bulk and shear moduli only dependent on stress level and compressive strength, realizing that the deviatoric deformation due to pure hydrostatic loading is negligible and pure deviatoric loading results in both deviatoric and volumetric deformation. The state of strain corresponding to any state of stress can thus be calculated from *Hooke*'s law using the secant moduli for that particular state of stress and a coupling term for the volumetric response to deviatoric loading. By using this approach, the effects of confinement and varying *Poisson*'s ratio are automatically included, and the influence of lateral stresses on the strength is included in the three-dimensional fracture criterion. A criterion for loading or unloading is determined based on the critical deviatoric component of the octahedral stresses at an integration point and unloading and reloading follows a branch using the initial elastic moduli. For stress levels below the critical volume point, the response can be predicted using the non-linear moduli described above. For stress levels beyond the critical volume point, additional expansion in the directions transverse to the maximum principal compressive stress due to unstable formation of continuous microcracking could be calculated and added to the deformation calculated using the non-linear moduli [28]. Note that this effect was excluded from the present study following recommendations presented elsewhere [13].

Upon cracking, all stiffness and stress across the crack are reduced to zero, leaving the concrete as a fully brittle material. A total of three non-orthogonal, fixed cracks can be formed at each integration point, and a constant SRF is used [18]. The simplicity of the material model is achieved by neglecting any softening in both compression and tension and applying a constant tangential material stiffness in the uncracked directions after crack-

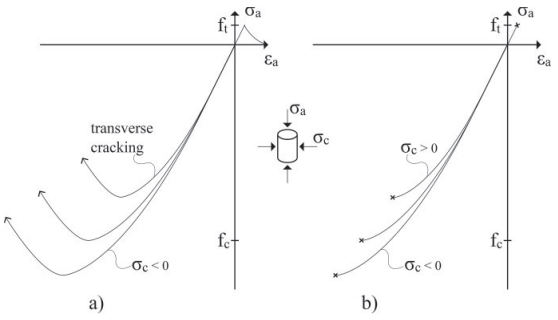

Fig. 2. Simplified presentation of the material models used in a) the DG solution strategy and b) the engineering solution strategy – shown for a cylinder subjected to an axial stress σ_a and a confining stress σ_c (ε_a = axial strain, f_c = compressive strength, f_t = tensile strength)

ing. A simplified presentation of the material models for the two solution strategies is shown in Fig. 2. In the present study, a review of nearly 70 benchmark analyses covering a wide range of structural forms, loading conditions and concrete strengths reported in the literature [13] revealed a mean ratio of numerical to experimental capacity of 1.0 with a COV of 14 %, which is good compared with the results collected by *Schlune* et al. [3] mentioned in the introduction. In this paper, ten of the 70 experiments on structural level were selected for a more thorough investigation.

3 Case studies on material level

In this section, results from experiments on plain concrete subjected to well-defined stress states are compared with results from NLFEA of single elements in order to compare the solution strategies on the material level. At this level it is important to select experiments that were not included in the databases to which the material models were calibrated during the development. The following benchmark experiments were selected with this in mind. Compressive stresses and strains are assigned negative values. It should be noted that the analyses were stopped at peak level and that no attempt was made to trace post-peak behaviour. The results are thus independent of, for example, the crack bandwidth and the variable post-cracking *Poisson*'s ratio as these parameters relate to the post-peak behaviour. No cracks were observed before the peak level in any of the analyses on material level. All the results were extracted from the integration points.

Fig. 3 shows a biaxial failure surface as a result of experiments on plain concrete with compressive strength f_c = 57.6 MPa [29]. The DG solution strategy produced somewhat unconservative results in the tension/compression regime, which could lead to somewhat stiffer structural behaviour before cracking. The engineering solution strategy showed a close fit with the experimental results and was somewhat conservative for equibiaxial compression and tension.

Fig. 4 shows the response to triaxial compression, $\sigma_3 \le \sigma_2 = \sigma_1$, for plain concrete with f_c = 56.9 MPa subjected to confining pressures of $\sigma_2 = \sigma_1 = -20$ MPa and $\sigma_2 = \sigma_1 = -40$ MPa [30]. At both levels of confinement the engineering solution strategy produced results with both stiffness and capacity closer to the experimental results than the DG solution strategy. The engineering solution strategy underestimated the strain at ultimate capacity,

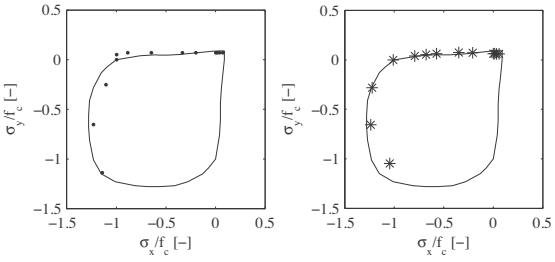

Fig. 3. Biaxial failure surface for plain concrete with f_c = 57.6 MPa [29] compared with results from NLFEA using (left) the DG solution strategy and (right) the engineering solution strategy

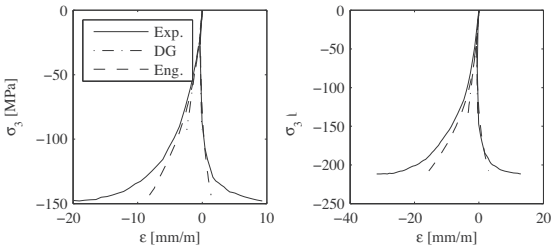

Fig. 4. Response of plain concrete with f_c = 56.9 MPa to triaxial compression $\sigma_3 \le \sigma_2 = \sigma_1$ [30] subjected to confining pressure (left) $\sigma_2 = \sigma_1 = -20$ MPa and (right) $\sigma_2 = \sigma_1 = -40$ MPa (compressive stress s_3 shown as a function of compressive strain ε_3 and lateral strains $\varepsilon_2 = \varepsilon_1$)

but predicted values closer to the experimental results compared with the DG solution strategy despite the brittleness of the engineering solution strategy. Note the significant increase in the ultimate strains resulting from a higher confining pressure.

The volumetric strain development for plain concrete with f_c = 32.1 MPa subjected to three different biaxial loading ratios, σ_2/σ_3 = 0, 0.52 and 1, is shown in Fig. 5 [29] and compared with results from NLFEA. For the uniaxial case, the two solution strategies agree well with the experimental results. At the intermediate confinement level the DG solution strategy tends to underestimate the volumetric strain and the engineering solution strategy tends to overestimate the strain. At the highest confinement level the engineering solution strategy overestimates the volumetric strain development, and it can be seen that the capacity is somewhat underestimated, as was also shown in Fig. 3.

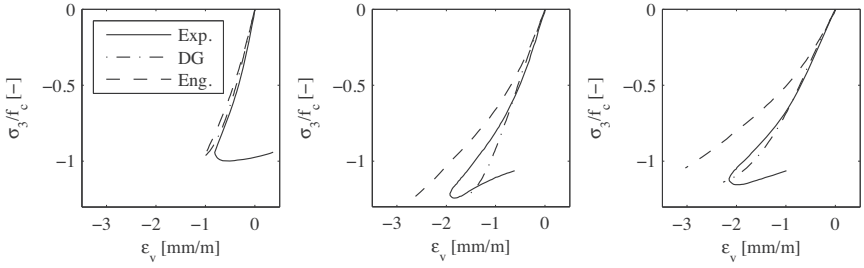

Fig. 5. Volumetric strain development for concrete with f_c = 32.1 MPa [29] subjected to (left) uniaxial compression, (centre) biaxial compression with σ_2/σ_3 = 0.52 and (right) equibiaxial compression

4 Case studies on structural level

Ten case studies on structural level are presented in this section. The cases were evaluated in terms of the predicted load-displacement curves and failure modes. The predicted ultimate loads correspond to the loads from the last converged load step. The case studies were selected in order to have variations in concrete strengths, structural forms, failure modes and loading conditions. Details of the finite element meshes are shown in Fig. 6, where it can be seen that the sizes of the finite elements were in the order of the member dimensions and that all reinforcement was lumped to the element borders. Details of the experiments can be found in the references below. In cases 1, 2, 3 and 9, only the effective depth of the beam was modelled, neglecting the cover. In all other cases the complete depth was modelled, but the reinforcement was still lumped to the element borders maintaining the total reinforcement area and internal lever arm. Note that the analyses using the engineering solution strategy were not performed by the authors; the results were collected from the literature referred to in Table 2. The finite element meshes and the simple reinforcement representation was adopted from this literature in order to reduce bias. The following cases were studied:

CS1: Reinforced concrete beam with stirrups under two-point loading (B1) [31]
CS2: Reinforced concrete beam without stirrups under one-point loading (OA-1) [32]
CS3: Reinforced concrete beam with stirrups under one-point loading (A-1) [32]
CS4: Reinforced concrete T-beam under four-point loading (beam C) [33]
CS5: Short structural wall subjected to horizontal and vertical loads (SW15) [34]

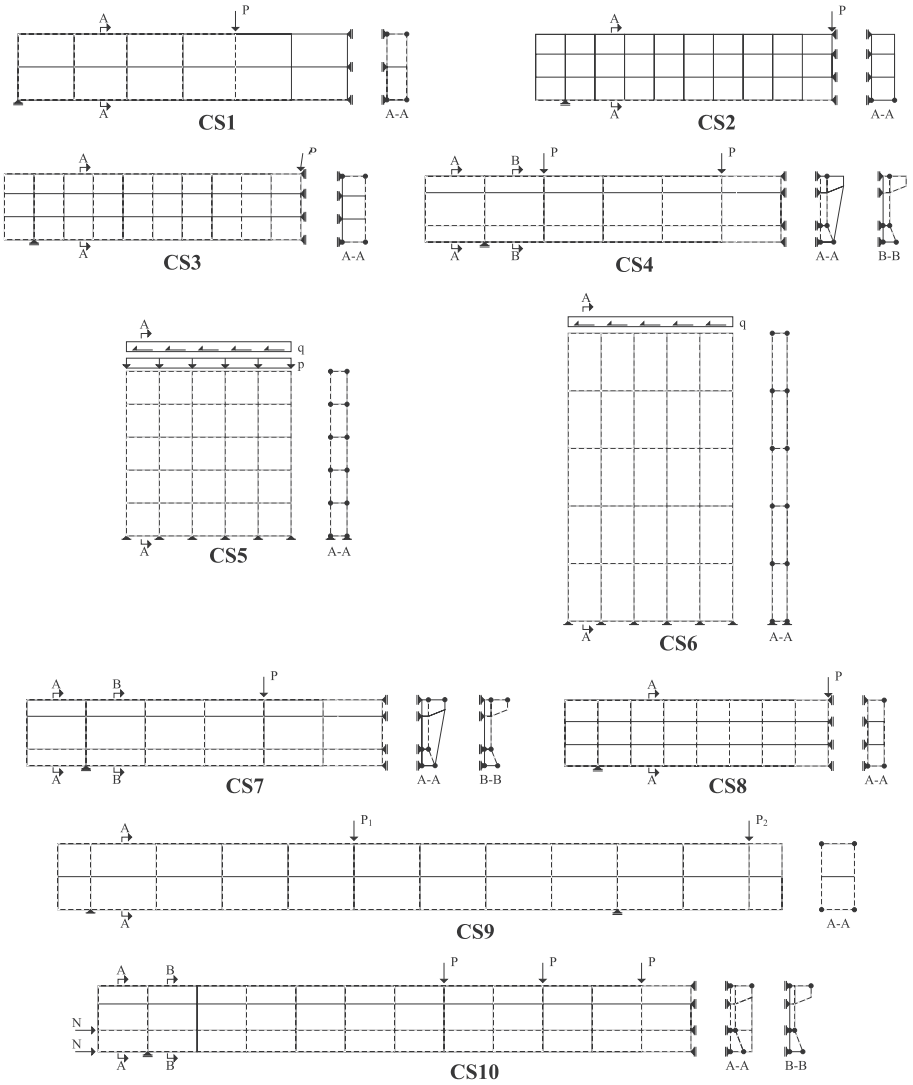

Fig. 6. Finite element meshes for all case studies on structural level (dashed lines and solid circles indicate reinforcement locations)

Table 2. Summary of ultimate load predictions compared with experimental results; numbers and letters in parentheses indicate ratio of predicted to experimental result (R_{NLFEA}/R_{exp}) and failure mode (B = brittle, D = ductile) respectively

Case study	R_{exp}	$R_{NLFEA,eng}$	$R_{NLFEA,DG}$
1	13.6 kN (D)	14 kN (1.03 D) [15]	16 kN (1.18 D)
2	334 kN (B)	300 kN (0.90 B) [15]	274 kN (0.82 B)
3	467 kN (B)	450 kN (0.96 B) [16]	467 kN (1.00 B)
4	240 kN (D)	195 kN (0.82 D) [39]	202 kN (0.84 D)
5	320 kN (D)	273 kN (0.85 D) [13]	217 kN (0.68 D)
6	127 kN (D)	115 kN (0.91 D) [13]	90 kN (0.71 D)
7	200 kN (D)	187 kN (0.94 D) [39]	189 kN (0.95 D)
8	323 kN (B)	360 kN (1.11 B) [39]	376 kN (1.16 B)
9	156 kN (D)	156 kN (1.00 D) [40]	120 kN (0.77 B)
10	94 kN (D)	84 kN (0.90 D) [41]	88 kN (0.94 D)
Mean ratio		0.94	0.90
Standard deviation		0.09	0.17
COV		9 %	19 %

CS6: Slender structural wall subjected to horizontal load (SW21) [34]
CS7: High-strength reinforced concrete T-beam under two-point loading (HSB2) [35]
CS8: High-strength reinforced concrete beam under one-point loading (B 150-11-3) [36]
CS9: Reinforced concrete beam with cantilever subjected to two-point sequential loading (B2CFP) [37]
CS10: Prestressed T-beam subjected to six-point loading (PCB6) [38]

The predicted load-displacement curves are shown in Fig. 7 and Table 2 compares the ultimate load predictions with the values established experimentally. The mean ratio of predicted to experimental ultimate load and the corresponding standard deviation and COV were calculated. Both solution strategies yielded adequate results. The engineering solution strategy yielded results with the lowest systematic error and variation – well within the limits of the results collected by *Schlune* et al. [3] presented in the introduction. The DG solution strategy predicted the stiffest behaviour in most cases.

5 Discussion

Solution strategies applicable for NLFEA of concrete structures with large finite elements are studied in the present paper. The cases are evaluated in terms of the predicted load-displacement curves and failure modes. During post-processing of the results, however, a detailed study of the stress and strain distributions and the crack patterns was necessary. Detailed plots of, for example, stress and strain contours and crack patterns were omitted from this paper in order to focus attention on the global behaviour. In general, the crack patterns obtained with the DG solution strategy corresponded well with those obtained with the engineering solution strategy, for which references can be found in section 4. Both solution strategies were able to predict results with accuracy well within the limits that were collected by *Schlune* et al. [3] mentioned in the introduction. One of the analyses with the DG solution strategy predicted a wrong failure mode. The results from the NLFEA with the engineering solution strategy had the lowest systematic error and the lowest modelling uncertainty.

When comparing the two solution strategies used in the present study, one distinct difference is the simple post-cracking behaviour in the engineering solution strategy. *Kotsovos* [42] points out that tensile fracture is characterized by a sudden loss of capacity in a force-controlled experiment due to the lack of possibility of stress redistributions within the concrete specimen upon formation of microcracks. On the other hand, *Reinhardt*, *Cornelissen* and *Hordijk* [23] mention that stress transfer is still possible after the tensile strength is reached in deformation-controlled experiments, and that this softening is a result of gradual degradation within a discrete crack band. Brittle cracking could seem too crude at large scale because the volume assigned to each integration point where the material behaviour is evaluated inevitably comprises both cracked and uncracked concrete. Nevertheless, the results from the analyses using the engineering solution strategy yield adequate accuracy even at lower load levels. It should be noted that when large elements are used, the resulting high value for the crack bandwidth results in a relatively steep descending branch, turning the softening material model into a more brittle one. The somewhat stiffer behaviour at structural level predicted by the DG solution strategy shown in Fig. 7 could be a combination of the larger amount of strain energy available in direct tension and the unconservative failure criterion in tension-compression shown in Fig. 3.

Large hydrostatic compressive stress states give rise to increased capacity and strains at ultimate load level [29, 30, 42]. The results of the triaxial benchmark analyses on the material level, shown in Fig. 4, show that the engineering solution strategy predicts a capacity and deformation in close agreement with the experimental results despite the brittle post-peak behaviour of the material model. The slightly underestimated strains obtained with the engineering solution strategy can be attributed to the expansion effects close to ultimate load levels which were neglected in the present study. In fact this effect was demonstrated by *Kotsovos* and *Newman* [28] for triaxial compression, resulting in underestimated strains similar to those shown in Fig. 4. The low capacity predicted by the DG solution strategy under triaxial compression is suggested to be due to the constant *Poisson*'s ratio before cracking. *Selby* and *Vecchio* [25] analysed the same experiment with a solution strategy similar to DG, but including a variable *Poisson*'s ratio, and the predicted capacity was found to be much closer to the experimental value.

The number of cases studied was too small to observe any systematic error as a function of the number of elements or integration points over the depths of the members. If – within the limits for large-scale elements – a finer mesh is chosen, a higher total number of integration

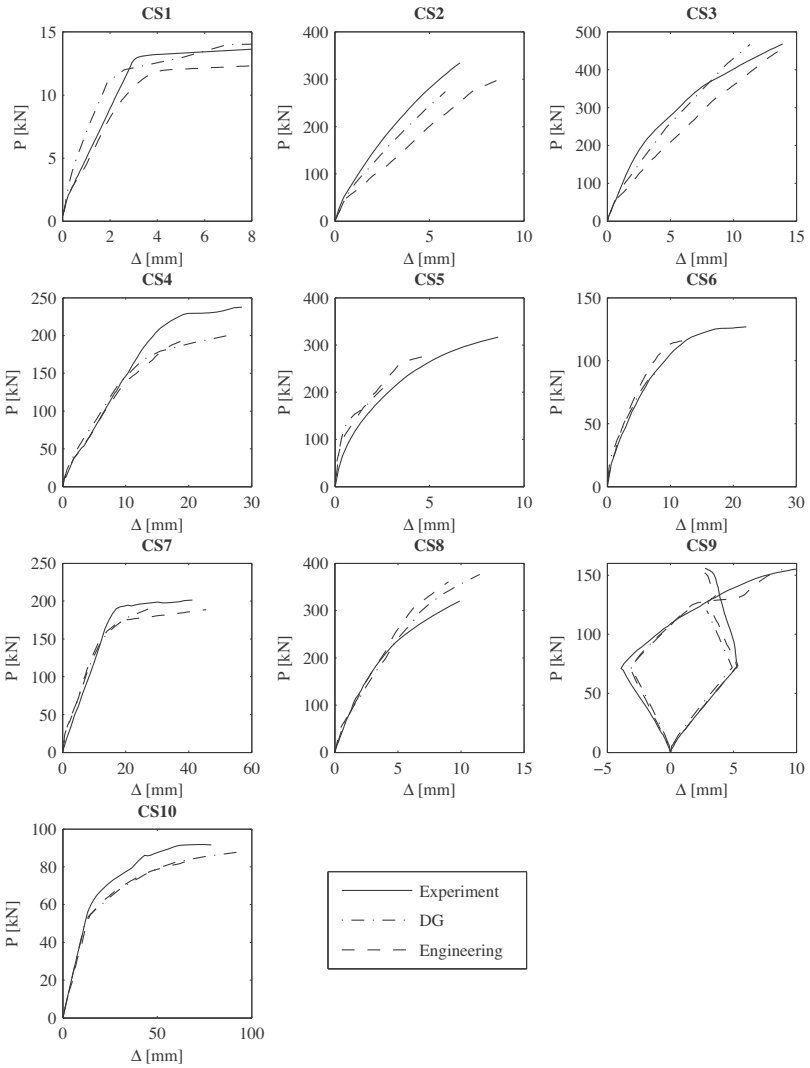

Fig. 7. Force-displacement curves for all case studies on structural level with total force plotted against displacement and positive displacement measured in direction of applied load in all cases

points where the stresses and strains are calculated is introduced. With a higher number of such sampling points, the stress field, and especially gradients over the cross-section due to, for example, bending or local effects, could be predicted with a higher degree of accuracy and critical points could be revealed. One question that remains to be answered is the level of local accuracy that is needed in order to predict the ultimate load with adequate global accuracy. In the further work, the effect of the ratio of element size to member size on the modelling uncertainty should be addressed.

Simple structural forms with a range of loading conditions and failure modes were chosen for this study. The estimated modelling uncertainty is thus based on different failure modes, and we do not have enough data to distinguish between the uncertainties for the specific failure modes. In a complex structure, the global failure could be a mixture of failures in several areas, a failure mode where in-plane and out-of-plane forces interact or it could be dominated by one specific failure mode in one specific area. The role of the NLFEA is to predict the global load and the failure mode unknown in advance, so a **general** modelling uncertainty of a solution strategy applied to a range of failure modes could seem most rational for complex structures. On the other hand, if the solution strategy turns out to have a higher modelling uncertainty when applied to a certain failure mode, and this failure mode dominates the global behaviour of the structure, the modelling uncertainty of that certain failure mode should have a larger influence on the estimated design capacity of the structure. In the further work, the modelling uncertainty of specific failure modes should be addressed, aiming for a uniform uncertainty independent of the failure mode. More complex structural forms should also be included.

6 Conclusion

Despite coarse finite element meshes, simple representations of reinforcement and boundary conditions and relatively large load increments, both solution strategies performed well, with results within the expected limits for modelling uncertainty discussed in the literature.

Based on the results from the present study, a shift in attention from a detailed description of the post-cracking behaviour of concrete to a rational description of the pre-cracking compressive behaviour is advised. This holds especially true for cases where large elements are used and the ultimate limit capacity is sought. Further work will be based on the engineering solution strategy, also considering associated recent developments [43, 44].

A thorough investigation of the effect of element size and failure mode on the modelling uncertainty should be carried out. More complex structural forms and loading conditions should also be included in this, still keeping the element sizes within the limits for large-scale elements.

Acknowledgements

The present industrial PhD is funded by Multiconsult AS and The Research Council of Norway. Morten Engen would like to thank his supervisors and all colleagues in the Marine Structures Department at Multiconsult for the valuable discussions and especially *Per Horn*, Senior Vice President of Multiconsult, for having the courage to initiate the research project.

References

1. *Brekke, D.-E., Åldstedt, E., Grosch, H.*: Design of Offshore Concrete Structures Based on Postprocessing of Results from Finite Element Analysis (FEA): Methods, Limitations and Accuracy. Proc. of 4th Intl. Offshore & Polar Engineering Conf., 1994.
2. *Engen, M., Hendriks, M. A. N., Øverli, J. A., Åldstedt, E.*: Application of NLFEA in the Design of Large Concrete Structures. Proc. of XXII Nordic Concrete Research Symp., Reykjavik, Iceland, 2014.
3. *Schlune, H., Plos, M., Gylltoft, K.*: Safety formats for nonlinear analysis tested on concrete beams subjected to shear forces and bending moments. Engineering Structures, 2011, 33 (8), pp. 2350–2356.
4. *Rots, J. G., Belletti, B., Damoni, C., Hendriks, M. A. N.*: Development of Dutch guidelines for nonlinear finite element analyses of shear critical bridge and viaduct beams. *fib* Bulletin 57: Shear and punching shear in RC and FRC elements, Workshop, 15–16 Oct 2010, Salò, Italy, pp. 139–154.
5. *Belletti, B., Damoni, C., Hendriks, M. A. N.*: Development of guidelines for nonlinear finite element analyses of existing reinforced and pre-stressed beams. Engineering Journal of Environmental and Civil Engineering, 2011, 15 (9), pp. 1361–1384.
6. *Belletti, B., Damoni, C., den Uijl, J. A., Hendriks, M. A. N.* and *Walraven, J. C.* (2013), Shear resistance evaluation of prestressed concrete bridge beams: *fib* Model Code 2010 guidelines for level IV approximations. Structural Concrete, 14: 242–249. doi: 10.1002/suco.201200046.
7. *Belletti, B., Damoni, C., Hendriks, M. A. N.* and *de Boer, A.* (2014), Analytical and numerical evaluation of the design shear resistance of reinforced concrete slabs. Structural Concrete, 15: 317–330. doi: 10.1002/suco.201300069.
8. *Broo, H., Lundgren, K., Plos, M.*: A guide to non-linear finite element modelling of shear and torsion in concrete bridges. Technical report, Chalmers University of Technology, 2008.
9. *fib* Bulletin 45: Practitioner's guide to finite element modelling of reinforced concrete structures. International Federation for Structural Concrete (*fib*), 2008.
10. *Hendriks, M. A. N., den Uijl, J. A., de Boer, A., Feenstra, P. H., Belletti, B., Damoni, C.*: Guidelines for Nonlinear finite element analysis of Concrete Structures, RTD 1016:2012. Technical report, Rijkswaterstaat – Ministerie van Infrastructuur en Milieu, 2012.
11. *Kotsovos, M. D.*: Consideration of Triaxial Stress Conditions in Design: A Necessity. ACI Structural Journal, 1987, 84 (3), pp. 266–273.
12. *fib* Bulletin 70: Code-type models for concrete behaviour. Background of MC2010. International Federation for Structural Concrete (*fib*), 2013.
13. *Kotsovos, M. D., Pavlovic, M. N.*: Structural Concrete: Finite-element analysis for limit-state design. Thomas Telford, 1995.
14. *Kotsovos, M. D., Pavlovic, M. N., Cotsovos, D. M.*: Characteristic features of concrete behaviour: Implications for the development of an engineering finite-element tool. Computers and Concrete, 2008, 5 (3), pp. 243–260.
15. *González Vidosa, F., Kotsovos, M. D., Pavlovic, M. N.*: Three-dimensional non-linear finite-element model for structural concrete. Part 1: main features and objectivity study. Proc. of ICE – Structures and Buildings, 1991, 91, pp. 517–544.
16. *González Vidosa, F., Kotsovos, M. D., Pavlovic, M. N.*: Three-dimensional non-linear finite-element model for structural concrete. Part 2: generality study. Proc. of ICE – Structures and Buildings, 1991, 91, pp. 545–560.
17. *Crisfield, M. A.*: Snap-through and snap-back response in concrete structures and the dangers of under-integration. International Journal for Numerical Methods in Engineering, 1986, 22 (3), pp. 751–767.
18. *González Vidosa, F., Kotsovos, M. D., Pavlovic, M. N.*: On the Numerical Instability of the Smeared-Crack Approach in the Non-Linear Modelling of Concrete Structures. Communications in Applied Numerical Methods, 1988, 4 (6), pp. 799–806.
19. *Engen, M., Hendriks, M. A. N., Øverli, J. A., Åldstedt, E.*: Large scale non-linear finite element analyses of reinforced concrete structures. Proc. of 10th *fib* Intl. PhD Symp. in Civil Engineering, 21–23 Jul 2014, Université Laval, Québec, Canada.
20. *Lackner, R., Mang, H. A.*: Scale Transitions in Steel-Concrete Interaction. I: Model. Journal of Engineering Mechanics, 2003, 129 (4), pp. 393–402.
21. *Bédard, C., Kotsovos, M. D.*: Fracture Processes of Concrete for NLFEA Methods. Journal of Structural Engineering, 1986, 112 (3), pp. 573–587.
22. *Feenstra, P. H.*: Computational aspects of biaxial stress in plain and reinforced concrete. PhD thesis, TU Delft, 1993.
23. *Reinhardt, H. W., Cornelissen, H. A. W., Hordijk, D. A.*: Tensile Tests and Failure Analysis of Concrete. Journal of Structural Engineering, 1986, 112 (11), pp. 2462–2477.
24. *Vecchio, F. J., Collins, M. P.*: Compressive Response of Cracked Reinforced Concrete. Journal of Structural Engineering, 1993, 119 (12), pp. 3590–3610.
25. *Selby, R. G., Vecchio, F. J.*: Three-dimensional constitutive relations for reinforced concrete, Pub. No. 93-02. Technical report, University of Toronto, Dept. of Civil Engineering, 1993.
26. *fib* Model Code for Concrete Structures 2010. Ernst & Sohn, 2013.

27. *Vecchio, F. J.*: Non-linear finite element analysis of reinforced concrete: at the crossroads? Structural Concrete, 2001, 2 (4), pp. 201–212.
28. *Kotsovos, M. D., Newman, J. B.*: A mathematical description of the deformational behaviour of concrete under complex loading. Magazine of Concrete Research, 1979, 31 (107), pp. 77–90.
29. *Kupfer, H., Hilsdorf, H. K., Rusch, H.*: Behavior of Concrete Under Biaxial Stresses. Journal of the American Concrete Institute, 1969, 66 (8), pp. 656–666.
30. *Ferrara, G., Rossi, P., Rossi, P. P., Ruggeri, L.*: Dispositivi di prova per l'analisis sperimentale del comportamento de conglomerati cementizi sottoposti a stati triassiali de sollecitazione. Proc. of 4th AIAS Congress, Rome, 1976.
31. *Kotsovos, M. D.*: A fundamental explanation of the behaviour of reinforced concrete beams in flexure based on the properties of concrete under multiaxial stress. Materials and Structures, 1982, 15 (90), pp. 529–537.
32. *Bresler, B., Scordelis, A. C.*: Shear Strength of Reinforced Concrete Beams. Journal of the American Concrete Institute, 1963, 60 (1), pp. 51–74.
33. *Kotsovos, M. D., Lefas, I. D.*: Behaviour of Reinforced Concrete Beams Designed in Compliance with the Concept of Compressive-Force Path. ACI Structural Journal, 1990, 87 (2), pp. 127–139.
34. *Lefas, I. D., Kotsovos, M. D., Ambraseys, N. N.*: Behaviour of Reinforced Concrete Structural Walls: Strength, Deformation Characteristics, and Failure Mechanism. ACI Structural Journal, 1990, 87 (1), pp. 23–31.
35. *Seraj, S. M.*: Reinforced and prestressed concrete members designed in accordance to the compressive-force path concept and fundamental material properties. PhD thesis, Imperial College, London, 1991.
36. *Mphonde, A. G., Frantz, G. C.*: Shear Strength of high strength concrete beams. Report No. CE 84-157. Technical report, Dept. of Civil Engineering, University of Connecticut, 1984.
37. *Kotsovos, M. D., Michelis, P.*: Behaviour of Structural Concrete Elements Designed to the Concept of the Compressive Force Path. ACI Structural Journal, 1996, 93 (4), pp. 428–436.
38. *Seraj, S. M., Kotsovos, M. D., Pavlovic, M. N.*: Compressive-force path and behaviour of prestressed concrete beams. Materials and Structures, 1993, 26 (2), pp. 74–89.
39. *Seraj, S. M., Kotsovos, M. D., Pavlovic, M. N.*: Three-dimensional finite-element modelling of normal- and high-strength concrete members, with special reference to T-beams. Computers & Structures, 1992, 44 (4), pp. 699–716.
40. *Kotsovos, M. D., Spiliopoulos, K. V.*: Modelling of crack closure for finite-element analysis of structural concrete. Computers & Structures, 1998, 69 (3), pp. 383–398.
41. *Seraj, S. M., Kotsovos, M. D., Pavlovic, M. N.*: Non-linear finite-element analysis of prestressed concrete members. Proc. of ICE – Structures and Buildings, 1992, 94, pp. 403–418.
42. *Kotsovos, M. D.*: Fracture processes of concrete under generalised stress states. Materials and Structures, 1979, 12 (72), pp. 431–437.
43. *Spiliopoulos, K. V., Lykidis, G. C.*: An efficient three-dimensional solid finite element dynamic analysis of reinforced concrete structures. Earthquake Engineering and Structural Dynamics, 2006, 35 (2), pp. 137–157.
44. *Lykidis, G. C., Spiliopoulos, K. V.*: 3D Solid Finite-Element Analysis of Cyclically Loaded RC Structures Allowing Embedded Reinforcement Slippage. Journal of Structural Engineering, 2008, 134 (4), pp. 629–638.

Morten Engen
MSc, Industrial PhD candidate
Dept. of Structural Engineering
Norwegian University of Science
& Technology
Rich. Birkelandsvei 1A, 7491 Trondheim, Norway
Multiconsult AS
Postboks 265 Skøyen, 0213 Oslo, Norway
Tel.: +47 40211511
morten.engen@multiconsult.no

Max A. N. Hendriks
PhD, Professor
Dept. of Structural Engineering
Norwegian University of Science
& Technology
Rich. Birkelandsvei 1A, 7491 Trondheim, Norway
max.hendriks@ntnu.no
Assistant Professor
Faculty of Civil Engineering & Geosciences
Delft University of Technology
Stevinweg 1, 2628CN Delft, The Netherlands

Jan Arve Øverli
PhD, Associate Professor
Dept. of Structural Engineering
Norwegian University of Science
& Technology
Rich. Birkelandsvei 1A, 7491 Trondheim
Norway
jan.overli@ntnu.no

Erik Åldstedt
PhD, Senior Consultant
Multiconsult AS
Postboks 265 Skøyen
0213 Oslo
Norway
erik.aaldstedt@multiconsult.no

Non-linear finite element analyses applicable for the design of large reinforced concrete structures

Engen, M., Hendriks, M. A. N., Øverli, J. A. & Åldstedt, E.

Accepted for publication in European Journal of Environmental and Civil Engineering, 2017

Paper III

Non-linear finite element analyses applicable for the design of large reinforced concrete structures

M. Engen[a,b,*], M. A. N. Hendriks[b,c], J. A. Øverli[b] and E. Åldstedt[a]

[a]Multiconsult ASA, Postboks 265 Skøyen, 0213 Oslo, Norway; [b]Dept. of Structural Engineering, NTNU, Norwegian University of Science and Technology, Rich. Birkelandsvei 1A, 7491 Trondheim, Norway, [c]Faculty of Civil Engineering & Geosciences, Delft University of Technology, Steinweg 1, 2628CN Delft, The Netherlands

ARTICLE HISTORY
Compiled June 16, 2017

ABSTRACT
In order to make non-linear finite element analyses applicable during assessments of the ultimate load capacity or the structural reliability of large reinforced concrete structures, there is need for an efficient solution strategy with a low modelling uncertainty. A solution strategy comprises choices regarding force equilibrium, kinematic compatibility and constitutive relations. This contribution demonstrates four important steps in the process of developing a proper solution strategy: 1) definition, 2) verification by numerical experiments, 3) validation by benchmark analyses and 4) demonstration of applicability. A complete solution strategy is presented in detail, including a fully triaxial material model for concrete, which was adapted to facilitate its implementation in a standard finite element software. Insignificant sensitivity to finite element discretization, load step size, iteration method and convergence tolerance were found by numerical experiments. A low modelling uncertainty, denoted by the ratio of experimental to predicted capacity, was found by comparing the results from a range of experiments to results from non-linear finite element predictions. The applicability to large reinforced concrete structures is demonstrated by an analysis of an offshore concrete shell structure.

KEYWORDS
non-linear finite element analyses; large concrete shell structures; practical applications; ultimate load capacity; modelling uncertainty; structural design

1. Introduction

With the introduction of the semi-probabilistic safety formats in fib *Model Code 2010 for Concrete Structures* (*fib*, 2013), non-linear finite element analyses (NLFEA) are receiving increased interest from the engineering community. This paper addresses the topic of NLFEA applicable for the design of large reinforced concrete structures, where the main scope of the analyses are accurate predictions of the ultimate load capacity.

The design of large reinforced concrete shell structures like dams and offshore oil and gas platforms is normally based on global linear finite element analyses (LFEA). This allows for using the principle of superpositioning in order to handle the vast number of design load combinations (Brekke, Åldstedt, and Grosch, 1994; Engen, Hendriks,

*Corresponding author. E-mail: morten.engen@multiconsult.no

Øverli, and Åldstedt, 2015). For such large shell structures it is important to perform global analyses due to the interaction between global and local load effects. In order to reduce the computational cost, the finite elements are normally large compared to the sectional dimensions. Sufficient capacity is assured by performing local sectional design based on the sectional forces obtained from the LFEA.

In order to better take into account the real physical behaviour of reinforced concrete, non-linear finite element analyses (NLFEA) could be carried out in the design phase. The NLFEA should then be used in combination with methods for global reliability assessments, e.g. the semi-probabilistic safety formats suggested in fib *Model Code for Concrete Structures 2010* (*fib*, 2013). Due to cracking of concrete and yielding of reinforcement, a redistribution of the internal forces can be expected.

In order to perform NLFEA, the analyst needs to make proper choices regarding force equilibrium, kinematic compatibility and constitutive relations. Collectively, the choices constitute a strategy for obtaining a solution from NLFEA, or short, a *solution strategy* for NLFEA (Engen et al., 2015). Previous research has led to the development of a set of guidelines for NLFEA of reinforced or prestressed concrete beams, girders and slabs (Belletti, Damoni, and Hendriks, 2011; Belletti, Damoni, den Uijl, Hendriks, and Walraven, 2013; Belletti, Damoni, Hendriks, and de Boer, 2014; Belletti, Pimentel, Scolari, and Walraven, 2015; Hendriks, de Boer, and Belletti, 2017). However, the applicability to large reinforced concrete shell structures has not been demonstrated.

This contribution is part of an ongoing research project and complements the findings reported by the authors in two separate publications (Engen et al., 2015; Engen, Hendriks, Köhler, Øverli, and Åldstedt, 2017). Engen et al. (2015) compared results obtained with the mentioned guidelines to results reported elsewhere in the literature in order to select a solution strategy for further development. Engen et al. (2017) adapted the selected solution strategy and assessed the modelling uncertainty by comparing results obtained with NLFEA to experimental results reported in the literature. The modelling uncertainty can be defined as the ratio between the experimental and the predicted capacity, $\theta = R_{\text{exp}}/R_{\text{NLFEA}}$. The modelling uncertainty is mainly related to simplifications of the mathematical models compared to the real physical behaviour that is modelled, either for practical reasons or due to a lack of knowledge. This can be related to e.g. modelling of the material behaviour as a function of a limited number of variables, or a simplified representation of the real loading or boundary conditions. For reinforced concrete, the material model for concrete is considered the largest source of modelling uncertainties.

In this paper the selected solution strategy from Engen et al. (2015, 2017) is further developed and discussed in detail. The solution strategy includes a fully triaxial material model for concrete which was adapted to facilitate its implementation in a standard finite element software. The accuracy of the solution strategy should be assessed by verification and validation, where verification answers the question *are we solving the equations right?*, and validation answers the question *are we solving the right equations?* (Engen et al., 2017; Roache, 1998). The complete solution strategy was verified by comparing results obtained with different finite element discretizations, load step sizes and iterative solution procedures. Validation was performed by comparison of experimental and predicted results from a range of benchmark analyses. Results from two benchmark analyses are presented in this paper and the applicability to large concrete structures is demonstrated by NLFEA of an offshore concrete shell structure. It will be demonstrated that the ultimate load capacity and load-displacement relations can be efficiently predicted with reasonable accuracy in spite of using relatively simple material models and coarse finite element meshes. It should be noted that problems

related to e.g. durability or mechanical degradation, where a precise prediction of the crack pattern is important, might call for other and more detailed solution strategies.

2. Solution strategy for NLFEA

2.1. *Material model for concrete*

A common way of selecting material models for concrete is to use a uniaxial material model as basis, extended with additional models that take into account other material effects such as the effects of confinement and lateral cracking. Such an approach can be convenient when the structural effects of different material effects are to be studied, but additional models are normally developed in combination with other complementary models and should not be separated (Vecchio, 2001). Alternatively, fully triaxial material models where all material effects are treated, could be used. One such material model has been developed by Kotsovos and co-workers since the 1970s and is still subject to improvements (Bédard and Kotsovos, 1985; Cotsovos and Pavlovic, 2006; González Vidosa, Kotsovos, and Pavlovic, 1991a,b; Kotsovos, 1979a, 1980; Kotsovos and Pavlovic, 1995; Kotsovos and Spiliopoulos, 1998; Kotsovos, Pavlovic, and Cotsovos, 2008; Lykidis and Spiliopoulos, 2008; Markou and Papadrakakis, 2013; Spiliopoulos and Lykidis, 2006). Recently, the model was also adapted to light-weight aggregate concrete (Øverli, 2016). In the literature, it is stated that this model is particularly suited for structural engineering NLFEA. Demonstrations of the computational efficiency and comparisons to commercially available algorithms can be found in the literature (Bark, Markou, Mourlas, and Papadrakakis, 2016; Markou, Sabouni, Suleiman, and El-Chouli, 2015; Markou and Papadrakakis, 2013; Mourlas, Papadrakakis, and Markou, 2016).

The early versions of the fully triaxial material model are implemented in special purpose finite element software that allowed the user to interfer with the program on several levels. In order to make the material model available for practising engineers, it was adapted to facilitate its implementation in a standard finite element software in the present work. In the following, the basic ingredients, i.e. the constitutive relation and the fracture criterion, will be presented, the central parts of the implemented algorithms will be outlined and two improvements to the earlier versions of the model are highlighted.

In this section, the subscripts i and j are reserved for tensor components, while k and l are used for the load step and iteration number respectively. Thorough reviews of other constitutive relations and crack models for concrete can be found elsewhere (Cotsovos, 2004; González Vidosa, 1989; Rots, 1988; Rots and Blaauwendraad, 1989). It is emphasized that the objective of the present work was not to contribute to a detailed discussion about how concrete as a material *should* be modelled, but how it *could* be modelled in NLFEA performed by practising engineers where the purpose of the analysis is to assess the ultimate load capacity or structural reliability of large reinforced concrete structures. The material model did not include regularization of the constitutive relation in terms of e.g. crack bandwidth and fracture energy in order to obtain results that are objective with respect to the size of the finite elements (Bazant and Oh, 1983). It will be demonstrated that this sensitivity was insignificant when relatively large elements were used in analyses of reinforced concrete.

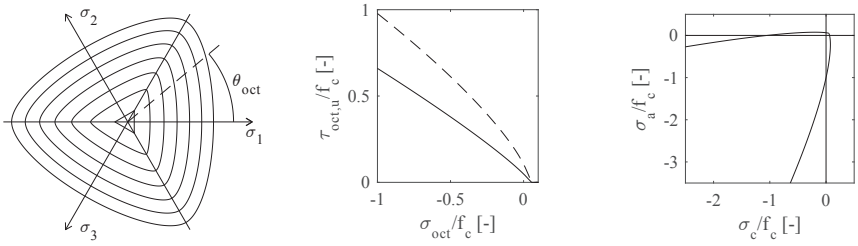

(a) Deviatoric sections of the fracture criterion for different levels of hydrostatic stress.

(b) $\tau_{\mathrm{oct,u}}$ for $\theta_{\mathrm{oct}} = 0°$ (solid) and $\theta_{\mathrm{oct}} = 60°$ (dashed).

(c) Hydrostatic section of the fracture criterion showing the axial strength σ_{a} as a function of the lateral confining stress σ_{c}.

Figure 1. Demonstration of the shape of the fracture criterion for concrete with $f_{\mathrm{c}} = 50$ MPa.

2.1.1. Constitutive relation and fracture criterion

When concrete is subjected to an increasing state of stress, the non-linear deformational response *below the ultimate stress level* can be described in terms of the internal fracture process which reduces tensile stress concentrations near the tips of internal microcracks (Kotsovos, 1979b). The response under multiaxial states of stress can be decomposed into three parts: 1) the change in volume due to hydrostatic loading, 2) the change of shape due to deviatoric loading and 3) the change in volume due to deviatoric loading (Kotsovos, 1980). Part 1 can be modelled by superimposing an internal hydrostatic stress, which is statically equivalent to the stress reduction due to microcracking, or by continuously degrading the bulk modulus, K, which is depending on the hydrostatic stress level. Similar reasoning can be used of parts 2 and 3. Due to this decomposition, it is convenient to decompose the stress state into octahedral stress components: σ_{oct}, τ_{oct} and θ_{oct}. σ_{oct} is the hydrostatic stress, which is the projection of the point in principal stress space onto the hydrostatic axis along $\sigma_1 = \sigma_2 = \sigma_3$. The deviatoric plane is orthogonal to the hydrostatic axis, and intersects with σ_{oct}. The point which represents the state of stress in principal stress space lies in the deviatoric plane with a distance τ_{oct} to the hydrostatic axis. θ_{oct} is the lode-angle which is the angle between the point in the deviatoric plane and the projection of the positive σ_1-axis as indicated in Figure 1(a). σ_{oct} is a function of the first invariant of the stress tensor, τ_{oct} is a function of the second invariant of the deviatoric stress tensor and θ_{oct} is a function of the second and third invariant of the deviatoric stress tensor.

By assuming non-linear elastic isotropic material behaviour for uncracked concrete and using the secant values of the stiffness moduli, the total strains corresponding to a given stress level below the ultimate stress level, can be calculated by Hooke's law in Equation (1) which can be interpreted as the sum of the change of shape and the change in volume.

$$\epsilon_{ij} = \frac{\sigma_{ij} - \sigma_{\mathrm{oct}}\delta_{ij}}{2G_{\mathrm{s}}} + \frac{(\sigma_{\mathrm{oct}} + \sigma_{\mathrm{id}})\delta_{ij}}{3K_{\mathrm{s}}} \tag{1}$$

G and K is the shear modulus and the bulk modulus, respectively. K and G represent part 1 and 2, respectively, of the non-linear deformational response described above. The subscript s indicates that the respective modulus is a secant modulus.

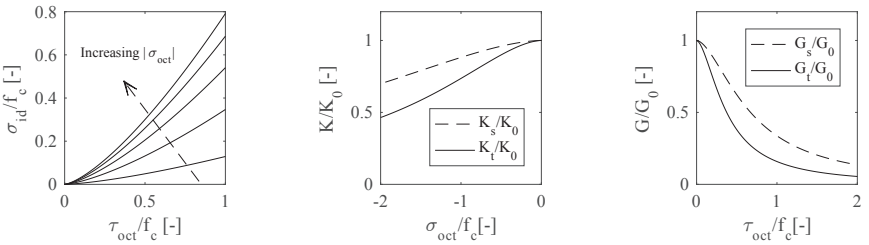

(a) Development of σ_{id} as a function of increasing deviatoric stress and compressive hydrostatic stress.

(b) Development of the bulk modulus as a function of increasing compressive hydrostatic stress.

(c) Development of the shear modulus as a function of increasing deviatoric stress.

Figure 2. Internal hydrostatic stress and non-linear bulk and shear moduli as functions of the stress level for concrete with $f_{\mathrm{c}} = 50$ MPa. The subscripts *0*, *s* and *t* indicate initial, secant and tangent values of the respective modulus.

σ_{id} is an equivalent internal hydrostatic stress which represents the change in volume due to deviatoric loading, i.e. part 3 of the non-linear deformational response, and is a function of the cylinder strength f_{c} and the current σ_{oct} and τ_{oct} (Kotsovos, 1980). The development of σ_{id} is shown in Figure 2(a). δ_{ij} is the *Kronecker delta* which is equal to unity for equal indices and zero elsewhere. Note that positive and negative values indicate tensile and compressive stresses and strains in the present work. With this type of formulation, the effects of confinement and *Poisson's ratio* on the stress-strain relation are automatically included. Initial, unloaded values of the shear and bulk modulus, G_0 and K_0, can be calculated from the cylinder strength, and expressions describing the dependency of the moduli on their initial values, the cylinder strength and the stress level are found in the literature (Kotsovos, 1980). Figures 2(b) and 2(c) show K and G respectively as functions of the stresses.

The ultimate stress level, given by a fracture criterion, is defined in terms of the critical octahedral shear stress, $\tau_{\mathrm{oct,u}}(\sigma_{\mathrm{oct}}, \theta_{\mathrm{oct}}, f_{\mathrm{c}})$, and expressions for $\tau_{\mathrm{oct,u}}$ dependent on σ_{oct}, θ_{oct} and f_{c} are found in the literature (Kotsovos, 1979a). The critical octahedral shear stresses for $\theta_{\mathrm{oct}} = 0°$ and $\theta_{\mathrm{oct}} = 60°$ are calculated using Equations (2) and (3) respectively, and shown in Figure 1(b). By ordering the principal stresses according to $\sigma_1 > \sigma_2 > \sigma_3$ it can be shown that all stress states have $0° \leq \theta_{\mathrm{oct}} \leq 60°$, and the relation proposed by Willam and Warnke (1974) can be used to calculate intermediate values of $\tau_{\mathrm{oct,u}}$ for given σ_{oct}, θ_{oct} and f_{c}. The fracture criterion can be interpreted as a limit beyond which the fracture process changes from internal microcracking to visible macrocracking. In the principal stress space, the fracture criterion can be visualized as a cone opening along the compressive hydrostatic axis, with a cross section approaching a triangle for hydrostatic tensile stresses, as demonstrated in Figure 1(a). Figure 1(c) demonstrates the significant effect of lateral stresses on the axial strength. If the fracture criterion is exceeded with at least one positive principal stress, a crack is formed on a plane with a normal parallel to the direction of the largest principal stress. If on the other hand the fracture criterion is exceeded with all principal stresses compressive, this corresponds to compressive failure, i.e. a complete loss of capacity in all directions.

$$\frac{\tau_{\mathrm{oct,u,0^\circ}}}{f_\mathrm{c}} = 0.633\left(0.05 - \frac{\sigma_\mathrm{oct}}{f_\mathrm{c}}\right)^{0.857} \tag{2}$$

$$\frac{\tau_{\mathrm{oct,u,60^\circ}}}{f_\mathrm{c}} = 0.944\left(0.05 - \frac{\sigma_\mathrm{oct}}{f_\mathrm{c}}\right)^{0.724} \tag{3}$$

Figure 3 shows the material response up to failure for a) uniaxial loading and b) 10% confining stresses. The effect of confinement on both deformations and capacity was a direct consequence of the stress-dependent non-linear stiffness moduli and fracture criterion. Following the approach presented in this section the material model depended on only one material parameter, the compressive cylinder strength. It is noted that the expressions for K, G, σ_id and $\tau_\mathrm{oct,u}$ found in the literature are results from fitting mathematical expressions to experimental results (Kotsovos, 1979a, 1980).

2.1.2. Outline of the implemented algorithm

The implemented material model consisted of three main parts: *A*) uncracked stress update algorithm, *B*) crack initiation and stress update algorithm for cracked integration points, and *C*) crack closing and stress update algorithm for closing integration points. Each part provided the appropriate material stiffness matrix. In part *A*, the non-linearities are mainly due to loading in compression, and in parts *B* and *C*, the non-linearities are due to opening and closing of cracks. Two improvements to the earlier versions of the material model were introduced: i) material stiffness matrix for uncracked integration points based on initial stiffness moduli, ii) and threshold angle for crack initiation.

A) Uncracked stress update algorithm. The stress-strain relationship up to the ultimate stress level given by Equation (1) is stress-driven, i.e. in the form $\boldsymbol{\epsilon} = \boldsymbol{\epsilon}(\boldsymbol{\sigma})$ where $\boldsymbol{\sigma}$ and $\boldsymbol{\epsilon}$ are the stress and strain vectors shown in Equation (4). Since typical strain-driven material models are required in standard finite element software, the relation should either be inverted or solved in an iterative manner. An iterative solution as proposed in the literature (González Vidosa, 1989; Kotsovos and Pavlovic, 1995) was used. In the iterative stress update, the fracture criterion was continuously monitored, and if $\tau_\mathrm{oct} > \tau_\mathrm{oct,u}$, $\tau_\mathrm{oct,u}$ was used in the calculation of G and σ_id in Equation (1). If this limitation was not used, G and σ_id could attain unrealistically low and high values respectively.

In a general case, the material stiffness matrix consists of partial derivatives of the constitutive relation in terms of the strains, or partial derivatives of the stress update algorithm in terms of the strains. Following the recommendations by Kotsovos and Pavlovic (1995) the material stiffness matrix, $\mathbf{C}$, was given in the form of Equation (5) corresponding to Hooke's law neglecting the coupling between deviatoric loading and hydrostatic deformation. The subscript t indicates that tangent stiffnesses were used, and $\lambda = K - 2G/3$ is *Lame's constant*. The material stiffness matrix according to Equation (5) with initial values for the material stiffness parameters was output from the material model. Compared to updated values for the stiffness parameters, this was found to have a slightly stiffening and stabilizing effect on the solution.

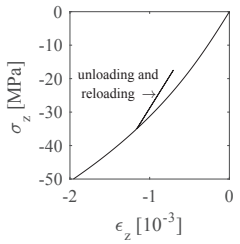

(a) Uniaxial compression: σ_x : $\sigma_y : \sigma_z = 0 : 0 : 1.0$.

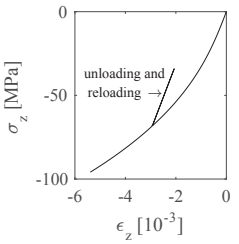

(b) Triaxial compression: σ_x : $\sigma_y : \sigma_z = 0.1 : 0.1 : 1.0$.

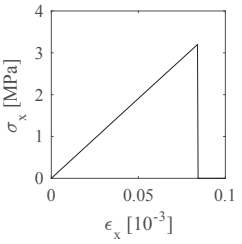

(c) Uniaxial tension $\sigma_x > 0$.

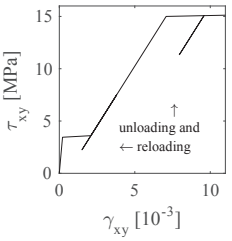

(d) Pure shear $\tau_{xy} > 0$.

Figure 3. Examples of loading, unloading and reloading of concrete with $f_c = 50$ MPa subjected to a) uniaxial compression, b) triaxial compression, c) uniaxial tension and d) pure shear. Note that no unloading and reloading is shown for the uniaxial tension case and that reinforcement $\rho_x = \rho_y = 3\%$ with yield stress $f_y = 500$ MPa was included in the pure shear case.

$$\boldsymbol{\sigma} = \{\sigma_x \ \sigma_y \ \sigma_z \ \tau_{xy} \ \tau_{yz} \ \tau_{xz}\}^T \ , \ \boldsymbol{\epsilon} = \{\epsilon_x \ \epsilon_y \ \epsilon_z \ \gamma_{xy} \ \gamma_{yz} \ \gamma_{xz}\}^T \tag{4}$$

$$\mathbf{C} = \begin{bmatrix} 2G_t + \lambda_t & \lambda_t & \lambda_t & 0 & 0 & 0 \\ & 2G_t + \lambda_t & \lambda_t & 0 & 0 & 0 \\ & & 2G_t + \lambda_t & 0 & 0 & 0 \\ & & & G_t & 0 & 0 \\ & \text{sym.} & & & G_t & 0 \\ & & & & & G_t \end{bmatrix} \tag{5}$$

As indicated in Figure 2(c), the non-linearities due to deviatoric loading dominate, and τ_{oct} can be regarded as the main contributor to the internal fracture process below the ultimate stress level. τ_{oct} was thus used as an indicator for loading and unloading. If τ_{oct} was found to be less than the previously maximum sustained τ_{oct}, indicating unloading, the stresses were simply updated linearly using initial values of the material stiffness parameters as shown in the unloading-reloading branches in Figure 3. A similar procedure is suggested in the literature (Bathe, Walczak, Welch, and Mistry, 1989; Kotsovos, 1984; Kotsovos and Spiliopoulos, 1998). The resulting stress update for an uncracked integration point can be seen in Figure 3 for loading, unloading and reloading. It is evident that confinement leads to a stiffer material

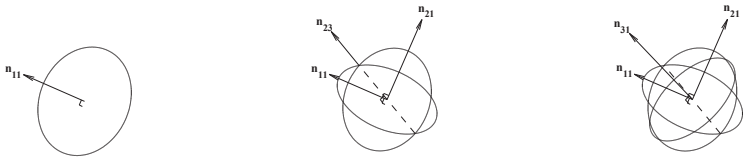

(a) One crack. The stress in the direction normal to the first crack plane, $\mathbf{n}_{11}$, is set to zero, and the stiffness is reduced.

(b) Two cracks. The stress in the direction of the intersection of the two crack planes, $\mathbf{n}_{23}$, is the only non-zero normal stress component.

(c) Three cracks. All normal stress components are set to zero.

Figure 4. Demonstration of possible crack states, where the plane of each open crack is visualized as a circle.

response, i.e. the strains are smaller in Figure 3(b) than in 3(a) for the same axial stress level, since due to a lower τ_{oct} the shear modulus is less degraded. Also, the axial stress at the ultimate stress level, and the corresponding strains are larger due to the stress dependent fracture criterion. If the confinement was further increased, the response would become more linear, but still non-linear due to the continuously degrading bulk modulus.

After the stresses were updated, the fracture criterion was checked, and if the stresses were found to exceed the ultimate stress level, i.e. if $\tau_{\text{oct}} > \tau_{\text{oct,u}}$, the crack initiation algorithm was called.

B) Crack initiation and cracked stress update algorithm. Upon cracking, the material model followed a smeared, non-orthogonal, fixed cracking approach with a maximum number of three cracks per integration point. The possible crack states are shown in Figure 4. In this context, the terms *fixed* and *non-orthogonal* refer to that the normal to a crack plane is kept constant after crack initiation and not rotated along the principal stress or strain directions, and that further cracking is not restricted to directions orthogonal to existing cracks. If the fracture criterion was exceeded with at least one principal tensile stress, a crack was initiated on a plane with a normal parallel to the largest principal stress, as shown by the vector $\mathbf{n}_{11}$ in Figure 4(a), resulting in a state of nearly plane stress. The stress normal to the crack plane was set equal to zero. If on the other hand the fracture criterion was exceeded with all principal stresses compressive, compressive failure was initiated by setting all normal stresses equal to zero, i.e. a complete loss of capacity in all directions. It should be noted that this way of treating cracking is non-standard as cracking is initiated in a brittle manner neglecting any softening both in tension and compression. Also, no measures were introduced on material level to ensure objectivity with respect to finite element size in terms of e.g. fracture energy and crack bandwidth (Bazant and Oh, 1983), but as will be demonstrated, the mesh size dependency was found to be insignificant for the coarse finite element meshes used in the present work.

$$\bar{\mathbf{C}}_1 = \begin{bmatrix} \beta_\sigma(2G_\mathrm{t}+\lambda_\mathrm{t}) & 0 & 0 & 0 & 0 & 0 \\ & 2G_\mathrm{t}+\lambda_\mathrm{t} & \lambda_\mathrm{t} & 0 & 0 & 0 \\ & & 2G_\mathrm{t}+\lambda_\mathrm{t} & 0 & 0 & 0 \\ & & & \beta_\tau G_\mathrm{t} & 0 & 0 \\ & \text{sym.} & & & G_\mathrm{t} & 0 \\ & & & & & \beta_\tau G_\mathrm{t} \end{bmatrix} \tag{6}$$

$$\bar{\mathbf{C}}_2 = \begin{bmatrix} \beta_\sigma(2G_\mathrm{t}+\lambda_\mathrm{t}) & 0 & 0 & 0 & 0 & 0 \\ & \beta_\sigma(2G_\mathrm{t}+\lambda_\mathrm{t}) & 0 & 0 & 0 & 0 \\ & & 2G_\mathrm{t}+\lambda_\mathrm{t} & 0 & 0 & 0 \\ & & & \beta_\tau G_\mathrm{t} & 0 & 0 \\ & \text{sym.} & & & \beta_\tau G_\mathrm{t} & 0 \\ & & & & & \beta_\tau G_\mathrm{t} \end{bmatrix} \tag{7}$$

$$\bar{\mathbf{C}}_3 = \begin{bmatrix} \beta_\sigma(2G_\mathrm{t}+\lambda_\mathrm{t}) & 0 & 0 & 0 & 0 & 0 \\ & \beta_\sigma(2G_\mathrm{t}+\lambda_\mathrm{t}) & 0 & 0 & 0 & 0 \\ & & \beta_\sigma(2G_\mathrm{t}+\lambda_\mathrm{t}) & 0 & 0 & 0 \\ & & & \beta_\tau G_\mathrm{t} & 0 & 0 \\ & \text{sym.} & & & \beta_\tau G_\mathrm{t} & 0 \\ & & & & & \beta_\tau G_\mathrm{t} \end{bmatrix} \tag{8}$$

The material stiffness matrix of a cracked integration point was evaluated in a local coordinate system defined by the crack direction, and transformed to global coordinates by an appropriate transformation rule. The stiffness parameters, G and λ, were assigned the values from the stress level upon first crack initiation, and kept constant for all remaining load steps regardless of further cracking and loading or unloading. The material stiffness matrix corresponding to one crack is given by Equation (6), which simply is a reduction of Equation (5), with the only remaining significant stiffnesses in the plane of the crack. The overbars in Equations (6) to (8) indicate that the matrices are established in a local coordinate system. The index *1* in Equation (6) indicates that the matrix represents one crack and that it is evaluated in the coordinate system defined by the vectors $\mathbf{n}_{11}$, $\mathbf{n}_{12}$ and $\mathbf{n}_{13}$, and similarly for the indices *2* and *3* in Equations (7) and (8). The normal retention factor, $\beta_\sigma = 0.0001$, followed the recommendations by Bathe et al. (1989), and was provided in order to avoid diagonal elements equal to zero. The shear retention factor, $\beta_\tau = 0.1$, followed the recommendations by Gonzlez Vidosa, Kotsovos, and Pavlovic (1988). It is emphasized that the off-diagonal terms that are set equal to zero in Equations (6) to (8) are equivalent to setting the corresponding Poisson's ratio equal to zero. This represents a simplified treatment of the gradual post-cracking reduction of the Poisson's ratio often recommended in the literature (Hendriks et al., 2017). The material stiffness matrix corresponding to compressive failure was set equal to the matrix corresponding to three cracks given by Equation (8).

When using a smeared crack approach, every crack represents an average crack state within the volume represented by the integration point. A rotation of the stress field and an increase of the stresses can lead to new cracks in the same integration point, but if the angle between the new and existing crack(s) is small, the new crack can

be interpreted as already represented by the existing crack(s), at least if the elements are relatively large. Hence, it is appropriate to introduce a *threshold angle* as a lower bound to the angle between the new and the existing crack(s). The effect of different values for the threshold angle between 0° and 90° is demonstrated in the literature (de Borst and Nauta, 1985; Rots and Blaauwendraad, 1989). A threshold angle of 45° was selected in the present work. Large threshold angles could lead to stress states exceeding the fracture criterion in critical integration points without initiating new cracks (de Borst and Nauta, 1985; Rots and Blaauwendraad, 1989). In order to ensure conservative results, this potential issue was avoided in the present work by proportionally scaling down the stress state in cases where the stresses exceeded the fracture criterion without initiating new cracks. The proportional stress scaling can be interpreted as a limitation of the stress state to a value given by the fracture criterion until new cracks are allowed to initiate.

If the fracture criterion was exceeded for the second time with at least one positive principal stress, a second crack could be formed on a plane with a normal parallel to the current largest principal stress, as indicated by the vector $\mathbf{n}_{21}$ in Figure 4(b). Note that $\mathbf{n}_{11}$ and $\mathbf{n}_{21}$ are non-orthogonal vectors separated by an angle larger than the threshold angle. The material stiffness matrix was reduced to Equation (7) with the only significant normal stiffness left in the direction of the intersection between the crack planes, indicated by the vector $\mathbf{n}_{23} = \mathbf{n}_{11} \times \mathbf{n}_{21}$ in Figure 4(b), resulting in a state of nearly uniaxial stress. The stresses in the directions $\mathbf{n}_{21}$ and $\mathbf{n}_{21} \times \mathbf{n}_{23}$ were set equal to zero. Finally, a third crack could be formed on a plane with a normal indicated by $\mathbf{n}_{31}$ in Figure 4(c) parallel to the current largest principal stress. With three cracks, the normal stresses in the directions corresponding to the principal stress directions upon formation of the third crack were all set equal to zero. The material stiffness matrix was given by Equation (8).

If the threshold angle was set equal to 0° and the stress scaling described above was left out, a possible outcome of initiating a new crack in a previously cracked integration point due to a small rotation of the stress field could be a spurious loss of capacity in a direction orthogonal to the normal to the new crack plane. Although not presented herein, the global results from analyses with values of the threshold angle below 45° showed no significant influence from the selected value, however, by introducing the threshold angle and the stress scaling, any potential spurious stress reduction was avoided.

The stress update of a cracked integration point followed a linear relation between the material stiffness matrices in Equations (6) to (8) and the total strain increment e.g. $\Delta\boldsymbol{\sigma} = \mathbf{C}_1\Delta\boldsymbol{\epsilon}$, where $\mathbf{C}_1$ is $\bar{\mathbf{C}}_1$ transformed to the global coordinate system, in addition to the stress reduction normal to the crack planes described above. The material stiffness matrices in Equations (6) to (8) are thus close approximations to the partial derivatives of the stress update algorithm, and will contribute to fast convergence. The resulting stress update is shown in Figures 3(c) and 3(d) for uniaxial tension and pure shear respectively. Before cracking in pure shear, the stresses are carried by the concrete as compression and tension in the principal directions. Upon cracking, the principal tensile stress is reduced to zero, and the concrete carries stresses in principal compression only, resulting in stresses in the coordinate directions that need to be equilibrated by reinforcement. Hence, the results for pure shear were obtained with reinforcement amounts $\rho_{\mathrm{x}} = \rho_{\mathrm{y}} = 3\%$ and a yield stress $f_{\mathrm{y}} = 500$ MPa.

C) Crack closing and closing stress update algorithm. In a cracked integration point, the strain(s) normal to the crack plane(s) were checked. If the total strain normal to a crack plane was found to turn negative, and less than its value upon cracking, the

crack was in a state of closing. It should be noted that the strain upon cracking could be negative if the integration point was unloading to cracking from a compressive state of stress.

The material stiffness matrix was restored for the appropriate number of cracks that remained open and evaluated locally according to the directions of the remaining crack(s). An integration point that had experienced compressive failure was not allowed to close, since compressive failure represented a complete loss of capacity in all directions.

The stresses in a closing integration point were first updated according to the algorithm for cracked integration points. If one crack was found to be closing, the total strains were transformed to the local directions of the closing crack and multiplied with a uniaxial stiffness in order to find the stresses due to closing, $\Delta\bar{\boldsymbol{\sigma}}$, according to Equation (9). The local closing stress was further transformed to global coordinates and added to the current stress. A similar procedure was applied to two and three closing cracks with plane stress and triaxial stiffnesses respectively, according to Equations (10) and (11). In Equations (9) to (11), the overbars indicate that the stresses and strains are transformed to local coordinates and the numerical subscripts indicate strains along the first, second and third local axis. By following this procedure it was ensured that the closing stress update was unified with the cracked stress update and that the correct stress components were updated for closing. This algorithm is similar to what was presented by Spiliopoulos and Lykidis (2006).

$$\Delta\bar{\sigma}_{\text{uniaxial}} = \frac{G_{\text{t}}(2G_{\text{t}} + 3\lambda_{\text{t}})}{G_{\text{t}} + \lambda_{\text{t}}}\bar{\epsilon}_1 \rightarrow \Delta\bar{\boldsymbol{\sigma}} = \begin{Bmatrix} \Delta\bar{\sigma}_{\text{uniaxial}} \\ 0 \\ 0 \\ 0 \\ 0 \\ 0 \end{Bmatrix} \tag{9}$$

$$\Delta\bar{\boldsymbol{\sigma}}_{\text{plane}} = \begin{bmatrix} \dfrac{4G_{\text{t}}(G_{\text{t}} + \lambda_{\text{t}})}{2G_{\text{t}} + \lambda_{\text{t}}} & \dfrac{2G_{\text{t}}\lambda_{\text{t}}}{2G_{\text{t}} + \lambda_{\text{t}}} \\ \text{sym.} & \dfrac{4G_{\text{t}}(G_{\text{t}} + \lambda_{\text{t}})}{2G_{\text{t}} + \lambda_{\text{t}}} \end{bmatrix} \begin{Bmatrix} \bar{\epsilon}_1 \\ \bar{\epsilon}_2 \end{Bmatrix} \rightarrow \Delta\bar{\boldsymbol{\sigma}} = \begin{Bmatrix} \Delta\bar{\boldsymbol{\sigma}}_{\text{plane}} \\ 0 \\ 0 \\ 0 \\ 0 \end{Bmatrix} \tag{10}$$

$$\Delta\bar{\boldsymbol{\sigma}}_{\text{triaxial}} = \begin{bmatrix} 2G_{\text{t}} + \lambda_{\text{t}} & \lambda_{\text{t}} & \lambda_{\text{t}} \\ & 2G_{\text{t}} + \lambda_{\text{t}} & \lambda_{\text{t}} \\ \text{sym.} & & 2G_{\text{t}} + \lambda_{\text{t}} \end{bmatrix} \begin{Bmatrix} \bar{\epsilon}_1 \\ \bar{\epsilon}_2 \\ \bar{\epsilon}_3 \end{Bmatrix} \rightarrow \Delta\bar{\boldsymbol{\sigma}} = \begin{Bmatrix} \Delta\bar{\boldsymbol{\sigma}}_{\text{triaxial}} \\ 0 \\ 0 \\ 0 \end{Bmatrix} \tag{11}$$

2.2. *Material model for reinforcement*

A bilinear elastic-plastic relation was used for the reinforcement. The initial slope of the stress-strain curve was fully defined by an elastic Young's modulus $E = 200000$ MPa. After yielding, the relation between stress and total strain was defined by a low hard-

ening modulus $E_{\mathrm{H}} = 2000$ MPa. Similar recommendations are found in the literature (Hendriks et al., 2017; Kotsovos and Pavlovic, 1995).

2.3. *Force equilibrium*

In the present work, results from analyses with modified and full Newton-Raphson were compared. Line search was applied in order to improve the iterative displacement increments. For reinforced concrete structures, a force based convergence criterion can be difficult, or even impossible, to satisfy in load steps where large forces need to be redistributed due to cracking. This is expected to be pronounced in analyses with large elements and large load steps. In the present work, a force criterion based on the change in the norm of the nodal residual forces given by Equation (12) was thus used in combination with an energy criterion given by Equation (13). $\mathbf{R}_{\mathrm{res}}$ is the vector of nodal residual forces, $\delta\mathbf{u}$ is the vector of nodal iterative displacement increments, and ϵ_{F} and ϵ_{E} are the convergence tolerances. The subscripts *l*, *1* and *0* indicate the current iteration, the first iteration of the current load step, and the last iteration of the previous load step respectively. According to recommendations published elsewhere (Hendriks et al., 2017) the tolerances were set to $\epsilon_{\mathrm{F}} = 0.01$ and $\epsilon_{\mathrm{E}} = 0.001$. Convergence was achieved with at least one of the criteria satisfied within a maximum number of 40 iterations per load step. The load was applied with constant load increments.

$$\frac{|\sqrt{\mathbf{R}_{\mathrm{res},l}^T\mathbf{R}_{\mathrm{res},l}} - \sqrt{\mathbf{R}_{\mathrm{res},l-1}^T\mathbf{R}_{\mathrm{res},l-1}}|}{|\sqrt{\mathbf{R}_{\mathrm{res},1}^T\mathbf{R}_{\mathrm{res},1}} - \sqrt{\mathbf{R}_{\mathrm{res},0}^T\mathbf{R}_{\mathrm{res},0}}|} \leq \epsilon_{\mathrm{F}} \tag{12}$$

$$\frac{\delta\mathbf{u}_l^T\mathbf{R}_{\mathrm{res},l}}{\delta\mathbf{u}_1^T\mathbf{R}_{\mathrm{res},1}} \leq \epsilon_{\mathrm{E}} \tag{13}$$

2.4. *Kinematic compatibility*

When analysing concrete shell structures, shell elements are often preferred due to their efficiency in modelling and computation. However, such elements usually require additional capacity control, since the interaction between in-plane forces and moments, and transverse shear forces is usually not accounted for in the NLFEA. Solid elements thus seem most applicable. This also allows the analyst to model the geometry and load application more accurately, and ensures correct modelling of the stiffness in structural joints. In LFEA with properly formulated hexahedral elements, the internal forces and bending moments in slender shells can be calculated with high accuracy even with only one element over the shell thickness or beam height. However, in NLFEA it is expected that there is need for evaluation of the internal stress state in a larger number of integration points over the thickness in order to capture the effect of cracking, and the interaction between in-plane forces, bending moments and transverse shear forces.

Markou and Papadrakakis (2013) have stated that the use of numerically unstable material models is one of the reasons for researchers to use higher order elements with higher order numerical integration rules. Bergan and Holand (1979) argues that higher order interpolation functions with artificially high differentiability should be avoided

due to the highly discrete and localized deformational behaviour of concrete. This is considered particularly relevant in analyses with relatively large finite elements, i.e. elements that are large relative to the cross sectional dimensions. Artificial straining should also be avoided in order to reduce the risk of premature cracking. The two-point Gauss rule calculates the exact values of stresses and strains for undistorted elements (Barlow, 1976), and the error is smaller with a two-point rule than with a three-point rule in case of distorted elements (Barlow, 1989). This was believed to be crucial in the present work in order to reduce artificial straining and the risk of premature cracking.

Based on these arguments, fully integrated *8-noded solid elements* were used in the present work. In order to avoid spurious shear strains in bending dominated areas, so-called *enhanced strains* were used (Simo and Rifai, 1990; Simo, Armero, and Taylor, 1993). A minimum number of three elements were used over the shell thickness or beam height. Compared to using *20-* or *27-noded solid elements* the size of the global stiffness matrix can be significantly reduced which in turn results in a faster solution of each equilibrium iteration and a lower amount of required memory.

The reinforcement was assumed fully bonded, i.e. neglecting any differential deformation between the concrete and the reinforcement. This assumption was justified by the size of the elements, prohibiting any detailed modelling of local variations in the interface. The reinforcement was modelled as elements overlaying the solid concrete elements, providing strength and stiffness embedded within the volume of the concrete element according to the material model of the reinforcement steel, the cross sectional area of the bars, the orientation in space and the size of the cover. This functionality, referred to as embedded reinforcement in most commercial finite element software, is an efficient way of modelling reinforcement in engineering applications, without the need for adapting the mesh of solid elements to the reinforcement layout.

3. Verification by numerical experiments

Verification is related to how the mathematical problem is solved, and the sensitivity to the selected solution method. The sensitivity to size of finite elements, Newton-Raphson procedure and size of load steps were assessed by performing numerical experiments of two setups that were designed for the purpose. In the crack plots of this section and Section 5, each crack is visualized as a circular plane with a normal parallel to the largest principal tensile stress upon cracking. If the normal lies in the drawing plane, the crack appears as a line, but if the normal forms an angle with the drawing plane, the crack appears as an ellipse approaching a circle. If the crack closes, the symbol is removed, and the integration point appears as uncracked in the figure.

3.1. *Description of the numerical experiment setups*

One *slender* and one *short* beam was designed for the verification of the solution strategy. The cross section and reinforcement layout is shown in Figure 5(a). The concrete had a cylinder strength of 40 MPa and all reinforcement had a yield strength of 500 MPa. The slender and the short beam had a total length of 6 m and 3 m respectively. The beams were simply supported and were subjected to a constant distributed load, as shown schematically in Figure 5(b). Unless explicitly specified, the load steps were adjusted in order to reach yielding of the tensile reinforcement after 30 load steps. In the Figures 6, 9 and 10 the total load, $R = R_1 + R_2$, is plotted against the vertical displacement, Δ, at the midspan.

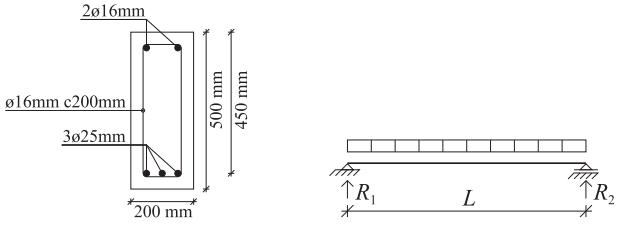

(a) Cross section. (b) Loading and boundary conditions.

Figure 5. Details of the numerical experiment setups.

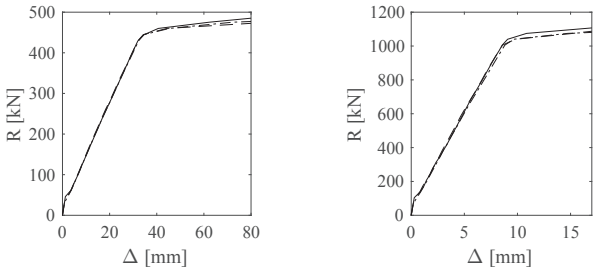

(a) Slender case. (b) Short case.

Figure 6. Comparison of results obtained with modified Newton-Raphson with three (solid), six (dashed) and nine (dash-dotted) elements over the beam height for a) slender case and b) short case.

3.2. *Sensitivity to size of finite elements*

The sensitivity to finite element discretization was checked by performing analyses of the two experimental setups with three different element sizes. Three, six and nine elements were used over the beam height, and the number of elements along the beam length was adjusted in order to keep the elements square. Two elements were used over the width in all analyses. Figure 6 shows the resulting load-displacement curves from analyses with modified Newton-Raphson, and no significant element size dependency can be observed. Similar results were obtained with full Newton-Raphson. Figures 7 and 8 show examples of the resulting crack patterns. For each load level, the crack directions were comparable. The element size in the coarsest meshes was comparable to the crack spacing that can by estimated using e.g. fib *Model Code 2010* (*fib*, 2013). The observed cracks in the results from the analyses with the coarsest meshes should thus be interpreted as average states of cracking within the volume corresponding to each integration point. With smaller elements, it can be seen that the crack patterns were gradually localizing, and the crack spacing can be found as a result of the analysis. This topic of gaining more details from the results upon mesh refinement has been elaborated on in the literature (*fib*, 2008), but will not be taken further here. As the mesh was refined, the cracks were found to propagate deeper towards the compressive zone, although this had no significant effect on the load-displacement curves as shown in Figure 6. The coarsest meshes in Figures 7 and 8 are comparable to the element sizes that were used in the validation in Section 4 and the demonstrations in Section 5.

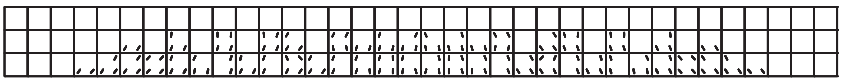

(a) Three elements over the beam height.

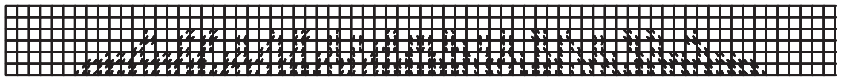

(b) Six elements over the beam height.

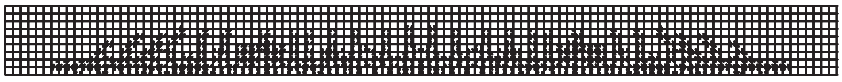

(c) Nine elements over the beam height.

Figure 7. Crack patterns for the slender case at load step 10: $R = 153$ kN. All the analyses were performed with two elements over the width of the beam.

(a) Three elements over the beam height.

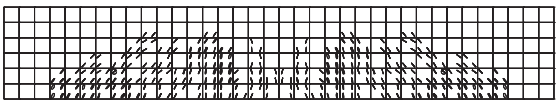

(b) Six elements over the beam height.

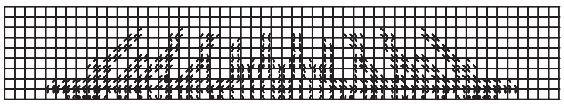

(c) Nine elements over the beam height.

Figure 8. Crack patterns for the short case at load step 10: $R = 347$ kN. All the analyses were performed with two elements over the width of the beam.

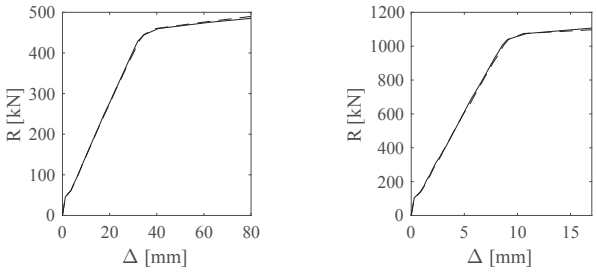

(a) Slender case. (b) Short case.

Figure 9. Comparison of results obtained with three elements over the beam height with modified (solid) and full (dashed) Newton-Raphson for a) slender case and b) short case.

3.3. *Sensitivity to Newton-Raphson procedure*

The sensitivity to the method for updating the tangent stiffness matrix during equilibrium iterations was checked by comparing results from analyses with full and modified Newton-Raphson. All of the analyses were performed with three elements over the beam height. The resulting load-displacement curves are shown in Figure 9. No significant sensitivity was observed in either of the cases. For the slender case, a total number of 409 iterations with modified Newton-Raphson taking approximately 115 s was needed to reach yielding of the longitudinal reinforcement in 30 load steps. These numbers were reduced to 214 iterations and 60 s using full Newton Raphson. Similarly for the short case, 277 iterations in 40 s and 173 iterations in 30 s was needed with modified and full Newton-Raphson respectively. A slight increase of the calculation time per iteration with full Newton-Raphson was thus compensated for by requiring a lower number of iterations for reaching convergence. The sensitivity to the selected convergence tolerances were also assessed by decreasing the tolerance of the force-based convergence criterion, however no significant influence on the resulting load-displacement curve could be observed.

3.4. *Sensitivity to size of load steps*

The sensitivity to the size of the load steps was checked by performing analyses of both the slender and the short case with three elements over the beam height, modified Newton-Raphson and applying the load corresponding to yielding of the longitudinal reinforcement in 30, 20 and ten load steps. The resulting load-displacement curves are shown in Figure 10, where no significant sensitivity can be observed.

4. Validation by benchmark analyses

Validation is related to how well the numerical predictions correspond to real observations. In the present work, validation was performed by comparing experimental and predicted capacities from 38 benchmark analyses. The sample of benchmark analyses contained beams (Bresler and Scordelis, 1963; Jelic, Pavlovic, and Kotsovos, 2004; Kotsovos, 1982), walls (Cervenka and Gerstle, 1972; Lefas, Kotsovos, and Ambraseys, 1990) and frames (Ernst, Smith, Riveland, and Pierce, 1973; Vecchio and Balopoulou,

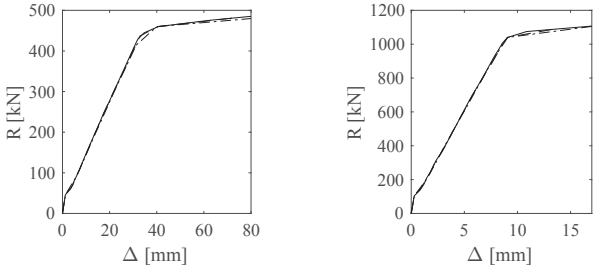

(a) Slender case. (b) Short case.

Figure 10. Comparison of results obtained with modified Newton-Raphson and three elements over the beam height with 30 (solid), 20 (dashed) and ten (dash-dotted) load steps for a) slender case and b) short case.

1990; Vecchio and Emara, 1992) with failure modes ranging from fully brittle to fully ductile. The sample could have been separated in smaller samples depending on the failure mode or type of structural component, but since the failure mode of large concrete shell structures most likely is due to an interaction between different sectional forces, the collection seems justified. During post-processing of the results from the benchmark analyses, the nodal displacement increments were plotted as deformed shapes, and if the displacement increments were found to significantly change from step to step, this was treated as a warning of failure. The last converged load step before failure was selected as the predicted capacity. Failure can thus be interpreted as the load level where the materials are degraded to such an extent, either due to cracking, yielding or both, that a further internal redistribution of forces is not possible.

Figure 11 shows the relation between experimental and predicted capacity. It is evident that the capacity is properly predicted with a small scatter in most of the cases. Based on these results, the modelling uncertainty, $\theta = R_{\text{exp}}/R_{\text{NLFEA}}$ can be assessed. By using the Bayesian inference technique suggested by (Engen et al., 2017) and assuming that θ can be modelled as a log-normally distributed random variable, a mean $\mu_\theta = 1.07$ and a coefficient of variation $V_\theta = 0.09$ was found. This can be regarded as being within the requirements suggested in the literature (Pimentel, Brühwiler, and Figueiras, 2014; Schlune, Plos, and Gylltoft, 2012). Engen et al. (2017) analysed the same set of benchmark experiments with the same solution strategy as used herein, however using modified Newton-Raphson, a force-based convergence criterion, $||\mathbf{R}_{\text{res}}||/||\mathbf{R}_{\text{ext}}|| < 0.01$, and not continuously monitoring the fracture criterion during the stress update algorithm for uncracked integration points as mentioned in Section 2.1.2. $\mathbf{R}_{\text{res}}$ is the vector of nodal residual forces, $\mathbf{R}_{\text{ext}}$ is the vector of nodal external loads, and $||\cdot||$ is the L_2-norm of the vectors. With these settings, $\mu_\theta = 1.10$ and $V_\theta = 0.11$ was obtained. Assuming a 5% level of significance, the modelling uncertainty obtained using the two versions of the solution strategy can not be rejected to come from the same population, i.e. having the same mean and coefficient of variation. This finding underlines the conclusions from the previous section where no sensitivity to Newton-Raphson procedure was found.

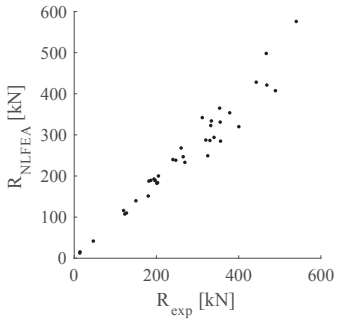

Figure 11. Predicted and experimental capacities, R_{NLFEA} and R_{exp}, for the 38 benchmark analyses.

Table 1. Summary of computational performance in the three demonstration cases.

Case	Solid elements	Reinf. elements	Equations	Iterations	Solution time
MDCB3	162	378	974	763	178 s
2D18H	720	1764	4286	775	764 s
Large structure	5547	10554	22351	662	3965 s

5. Demonstration of performance

In this section, the performance of the solution strategy is demonstrated by two benchmark analyses from the previous section involving sequential loading and an analysis of an offshore concrete shell structure that was specially designed in the present work. The focus of the present work was on the structural behaviour at the ultimate load level, and the presented results were thus limited to load-displacement curves and crack plots for the benchmark analyses and displacement plots and indications of internal load redistributions for the shell structure. It is noted again that all of the analyses were performed using solid elements.

Table 1 shows a summary of the number of elements, equilibrium equations, total number of iterations and the time spent computing the solutions of the NLFEA in this section. All analyses were performed on a Windows PC with an Intel Xeon E5620 CPU with 2.39 GHz and 16 GB RAM. No parallel processing was used. The average solution time per iteration and equilibrium equation was 0.23 ms to 0.27 ms in all analyses. This number should only be treated as indicative, since the solution time highly depends on the computer specifications and how data are transferred by the solver.

5.1. *Continuous beam MDCB3 by* Jelic, Pavlovic & Kotsovos

Jelic et al. (2004) tested simply supported beams subjected to sequential loading. The beam MDCB3 was selected for the present paper. The loading and supports are shown schematically in Figure 12(b), where the loads R_1 and R_2 were applied as pressures over the full width and two elements along the length, and the supports were modelled by multi-point constraints in order to mimic the load and support plates. The load at the midspan, R_1, was applied first, and while keeping $R_1 = 90$ kN, the load at the tip of the cantilever, R_2, was increased until failure. R_2 was applied with constant load steps so that the experimental capacity of $R_2 = 103.9$ kN was reached in 30 load

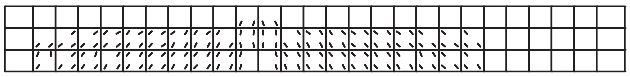

(a) Full intensity of the load at midspan: $R_1 = 90$ kN, $R_2 = 0$ kN.

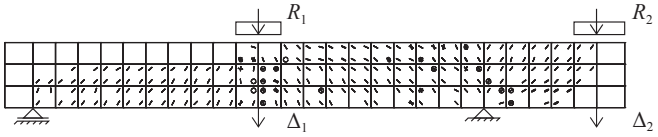

(b) Load step 2 substep 30: $R_1 + R_2 = 192.6$ kN.

Figure 12. Crack patterns for the beam MDCB3 tested by Jelic et al. for a) full intensity of the load at midspan and b) failure. The analysis was performed with two elements over the width of the beam.

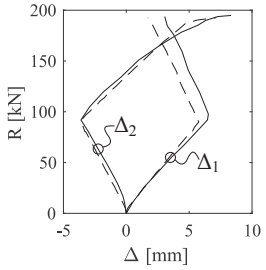

(a) Experimental and predicted load-displacement curve for the beam MDCB3 tested by Jelic et al.

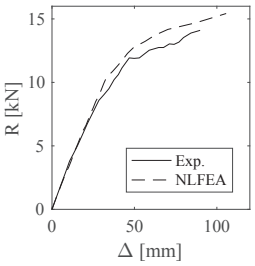

(b) Experimental and predicted load-displacement curves for the frame 2D18H tested by Ernst et al.

Figure 13. Load-displacement curves from the two benchmark analyses.

steps. The predicted total failure load was $R_{\mathrm{NLFEA}} = R_1 + R_2 = 192.6$ kN, giving a modelling uncertainty $\theta = 1.01$. The resulting load-displacement curve is shown in Figure 13(a) where the total reaction is plotted against the deflections below the two point loads. Crack patterns for selected load steps are shown in Figure 12, where it can be seen that several cracks were closing during application of the second point load. The predicted failure mode was characterized by diagonal cracking between the point load at the tip of the cantilever and the right support, combined with yielding of the longitudinal reinforcement over the support, corresponding to the failure mode described by Jelic et al. (2004).

5.2. *Portal frame 2D18H by* Ernst, Smith, Riveland & Pierce

Ernst et al. (1973) tested the portal frame 2D18H subjected to three vertical point loads and one horizontal point load. While keeping the total vertical load constant with a value $3V = 24.6$ kN, the horizontal load, R, was increased until failure. The loading and supports are shown schematically in Figure 14(b), where the horizontal and vertical loads were applied as distributed pressures over three and two elements along the height and length respectively, and the supports were modelled by multi-point constraints in order to mimic the load and support plates. R was applied with constant load steps so that the experimental capacity of $R = 14.1$ kN was reached in

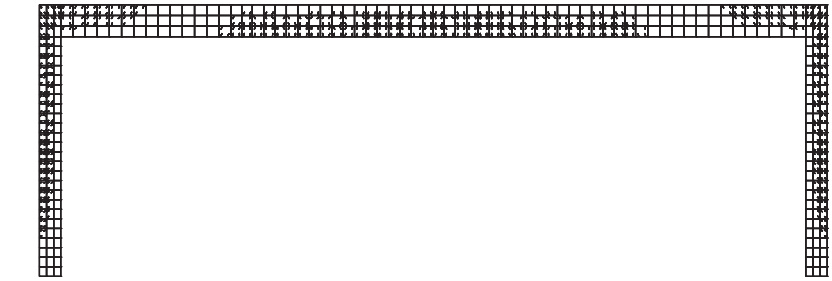

(a) Full intensity of the vertical loads: $V = 8.2$ kN, $R = 0$.

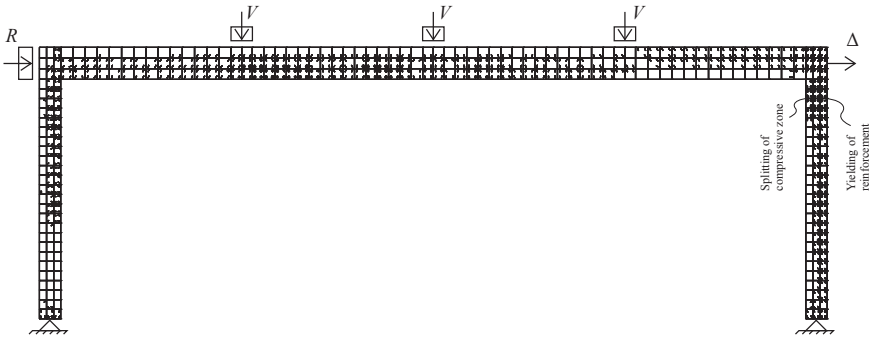

(b) Load step 2 substep 32: $V = 8.2$ kN, $R = 15.4$ kN.

Figure 14. Crack patterns for the frame 2D18H tested by Ernst et al. for a) full intensity of the vertical loads and b) failure. The analysis was performed with two elements over the width of the cross sections.

30 load steps. The predicted failure load was $R_{\mathrm{NLFEA}} = 15.4$ kN, giving $\theta = 0.92$. The resulting load-displacement curve is shown in Figure 13(b), where the total horizontal reaction is plotted against the horizontal deflection at the top. Crack plots for selected load steps are shown in Figure 14. Due to the reversed bending in the left leg of the frame resulting from application of the horizontal load, several cracks were closing when approaching the ultimate load level. The predicted failure mode was characterized by yielding of the outer longitudinal reinforcement of the right leg, followed by splitting of the compressive zone in the inner right corner and compressive failure, in close agreement with what was reported by Ernst et al. (1973).

5.3. *Offshore concrete shell structure*

A large offshore concrete shell structure suitable for oil or gas production was specially designed during this work. A thorough description of e.g. the design procedure, resulting reinforcement layout and geometry is beyond the scope of this paper, and only a brief description is provided in the following. A description of the design, construction and performance of offshore concrete structures for oil and gas fields can be found in the literature (*fib*, 2009).

The structure consisted of a 90 m tall shaft supported on a 10 m tall circular caisson as shown in Figure 15(a). The outer radii of the shaft and caisson were 6 m and 18 m respectively. The purpose of the structure is to support a topside with production

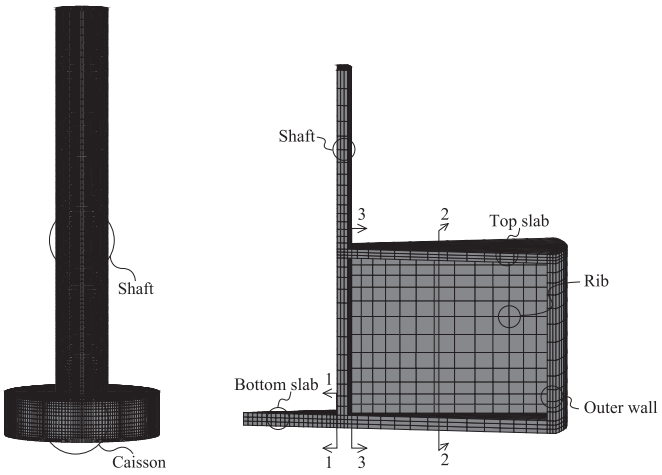

(a) Complete structure.

(b) The sector covering 30° and a total height of 20 m which was studied in the present work.

Figure 15. Offshore concrete structure.

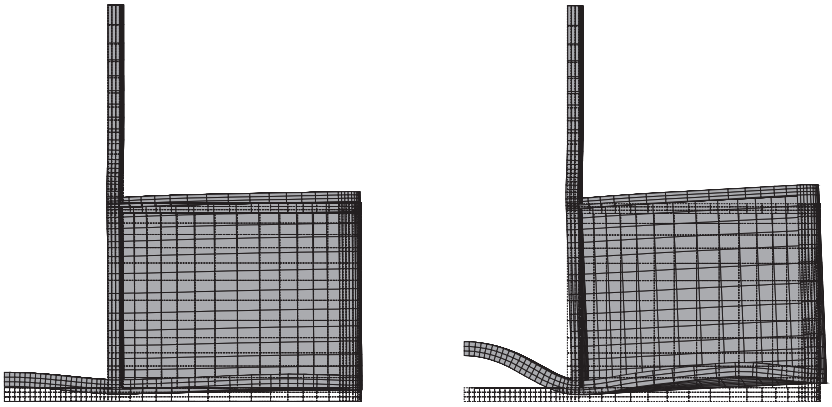

(a) LFEA.

(b) NLFEA.

Figure 16. Deformed shape at full characteristic intensity of all applied loads. The displacements are scaled with a factor of 100.

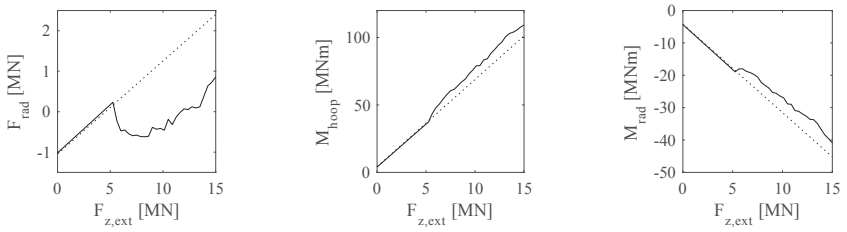

(a) Radial force resultant in the bottom slab in section 1-1, F_{rad}.

(b) Global bending moment in the caisson in hoop direction in section 2-2, M_{hoop}.

(c) Global bending moment in the caisson in radial direction in section 3-3, M_{rad}.

Figure 17. Force resultants and global bending moments in sections as functions of the total applied load from the topside carried by the studied part of the structure, $F_{\mathrm{z,ext}}$, from NLFEA (solid) and LFEA (dotted). The bending moments are calculated around the mid-height of the caisson, and the sections are shown in Figure 15(b).

facilities and living quarters with an assumed total weight of 18000 t, and to guide riser pipes from the sea-bed through the caisson and shaft. A mean water depth of 80 m was assumed to be applicable, and the structure was assumed to be completely waterfilled during operation. The caisson was stiffened with twelve equally spaced ribs as shown in Figure 15(b). A concrete strength of B55 and reinforcement steel strength of B500NC according to NS 3473 (Norges Standardiseringsforbund, 2003) was assumed. In order to demonstrate the applicability of the presented solution strategy to a large structure, a sector corresponding to one twelfth of the structure was studied in the present work as shown in Figure 15(b). The studied finite element model had a total height of 20 m. In the finite element model, all the nodes at the top of the shaft were constrained in the vertical direction, and the nodes along the radial symmetry edges were constrained in the hoop direction. The structure was assumed supported on soft soil, so that the vertical load could be applied as a constant outer pressure on the bottom slab.

Based on results from LFEA, the structure was designed with a special post-processor and non-linear sectional design software (Brekke et al., 1994) according to NS 3473 and EN-ISO 19903 (CEN, 2006; Norges Standardiseringsforbund, 2003). Only the dead weight of the concrete, the external and internal static water pressure and the total vertical load from the topside were considered in the present work in order to be able to reduce the complexity of the problem. The structure was designed for the applicable load combinations in the operation phase in the ultimate limit state.

The resulting reinforcement amounts from the non-linear sectional design were transferred back to the finite element model used in the NLFEA, and were modelled similarly as in the benchmark analyses described above. It should be noted that the complete structure could easily have been modelled, analysed and designed, but due to the symmetry with respect to load and geometry, and due to the mechanism of load transfer in circular shafts, a limited amount of information would have been gained compared to the smaller model that was used.

In a real design situation other static and dynamic loads and other limit states will require global modelling of the complete structure and are expected to have significant influence on the required shell thicknesses and reinforcement amounts. Also, the reinforcement amounts are normally adjusted in local areas due to e.g. constructability, continuity in reinforcement layout and required anchorage. However, in the present work, only the required amounts found directly from the ultimate limit design checks

were included.

A combination of local bending moments and transverse shear forces, and global membrane forces, results in a relatively complex distribution of internal sectional forces. The vertical load is transferred through the upper parts of the shaft as vertical compressive forces. When approaching the caisson, the shaft is subjected to additional local bending in the vertical direction, compressive forces in the hoop direction and transverse shear forces. The ribs provide stiffness to the caisson, and ensures that the caisson deforms as one unit, and that the vertical load is carried as a combination of global bending in the hoop and radial direction. The ribs are subjected to in-plane forces, while the top and bottom slab and the outer wall and the lower parts of the shaft within the caisson are subjected to in-plane forces, bending moments in two principal directions and transverse shear forces. Because the structure was assumed completely waterfilled, the internal and external water pressure mainly resulted in a slight prestressing of the structure due to the difference in internal and external area for load application.

In the NLFEA the dead weight of the concrete and the internal and external water pressure was first applied in five load steps, before the total load from the topside was applied in 40 load steps. It should be noted that in the present paper it was not attempted to perform a reliability assessment of the structure; the materials were assigned their characteristic strengths and the loads were applied with their characteristic intensities. Ideally, the results from the NLFEA should have been compared to experimental results, but for obvious reasons, no relevant results are available for such structures. Instead it would be valuable to study the difference in calculated response between a LFEA and a NLFEA, since the design is based on the former, and a possible global reliability assessment would be based on the latter. Hence, the global and local structural effects of material non-linearity are presented in the following comparing results from LFEA and NLFEA following the same load histories. The deformed shapes in the final load step of the LFEA and NLFEA shown in Figure 16 are provided as physical evidence for the discussion.

At 37.5% and 40% of the total vertical load, $F_{\mathrm{z,ext}}$, cracks appeared on the outer and inner face of the central parts of the bottom slab. The cracks resulted in a translation of the neutral axis in the central parts of the bottom slab, an elongation of the midplane and the significant radial displacement of the joint between the shaft and the bottom slab that can be seen in Figure 16(b). This effect, known in the literature as the *compressive membrane effect*, gave a reduction of the radial resultant tensile forces in section 1-1 in the central parts of the bottom slab as shown in Figure 17(a), but also an increase in hoop tension in the lower parts of the shaft, the outer wall and the rest of the bottom slab.

From 52.5% to 67.5% of the total vertical load, cracks appeared at the outer face of the bottom slab along the rib, the inner face of the bottom slab along the radial symmetry edge and in lower parts of the shaft along the rib. The cracking in the bottom slab led to a compressive membrane effect in hoop direction, slightly reducing the hoop tension in the bottom slab. The cracking in the shaft reduced the stiffness of the shaft, leading to a reduction of horizontal forces transferred from the rib to the shaft and a slight redistribution of global bending of the caisson from radial direction in section 3-3 to hoop direction in section 2-2 as shown in Figures 17(b) and 17(c). The global resultant moments M_{hoop} and M_{rad} were calculated by summing the moment contributions around the mid-height of the caisson from the nodal forces in hoop direction in section 2-2 and radial direction in section 3-3 respectively. Due to the reduction of horizontal force transfer from the rib to the shaft, the tensile and

compressive resultants due to global radial bending of the caisson were localized in the bottom and top slab respectively. As the vertical load was further increased to the characteristic level, cracking propagated in the described cracked areas, and only minor cracking appeared in the outer wall and in the lower parts of the rib close to the joint between the shaft and the bottom slab. The reinforcement did not yield in any direction. The compressive membrane effect in the two directions in the bottom slab resulted in crack closure, where some of the closed cracks remained closed during the rest of the load application, but some also reopened. At the final load level 11757 cracks had appeared in the structure, of which 153 were closed.

Due to the global force redistribution, a change of local behaviour was observed, e.g. the principal compressive stress, σ_3, in the shaft above the top slab increased from -23.5 MPa to -25.7 MPa, and σ_3 in the rib close to the joint between the shaft and the top slab increased from -10.0 MPa to -10.6 MPa. A beneficial reduction of tensile forces in the bottom slab thus came with the expense of increased compressive stresses in the shaft and the rib.

6. Discussion

The level of detail which is required for the material model depends on the phenomena that are to be studied in the analysis. In the present work, the ultimate load capacity was sought, and for this application the simple material models for concrete and reinforcement was appropriate. The results were supporting the conclusions from Engen et al. (2015) advising a shift of the attention from a detailed description of the post-cracking tensile behaviour to a rational description of the pre-cracking compressive behaviour of concrete in analyses where large finite elements are used. The assumed brittleness in tension and compression was considered a useful simplification which resulted in a material model with only one material parameter needed. If on the other hand a tensile softening relation based on crack bandwidth and fracture energy was used, results from Bazant and Oh (1983) and Hendriks et al. (2017) show that the element size should be limited to 100-400 mm depending on the cylinder strength in order to avoid snap-backs in the constitutive relation. The limiting values correspond to a sudden vertical drop in the stress-strain relation upon cracking (Bazant and Oh, 1983). Because the size of the elements used in the present work was in the order of these limiting values and the results indicated insignificant sensitivity to finite element size, the simplified brittle behaviour was justified. With the scope of the present work being focused on large *reinforced* concrete structures, the brittle degradation of one local point is not expected to significantly influence the ultimate load capacity, since the stresses released due to cracking of the concrete are directly supported by the reinforcement. If however, lightly reinforced or unreinforced concrete was studied, a more detailed description of the post-cracking tensile behaviour might become necessary.

Although not presented in detail in the present paper, the tolerances of the convergence criteria and the maximum number of iterations were observed not to significantly influence the predicted global behaviour, but influenced which load was treated as the predicted capacity in the benchmark analyses. This result indicates that the solutions were converged to a *stable* state close to equilibrium, and that the remaining force unbalance in unconverged load steps might be due to local self-equilibrating unbalances as discussed by Bergan and Holand (1979). In most of the load steps of the presented NLFEA, the energy convergence criterion was governing, i.e. it was satisfied before the force criterion, even though a tighter tolerance was used for the energy criterion.

The two criteria are fundamentally different, and the tolerances are not directly comparable, but the results indicate that different criteria require different tolerances in order to obtain comparative levels of accuracy, and that it is important to state both the selected tolerance and the mathematical expression of the criterion when results from NLFEA are presented.

The cylinder strength reported in the references was used directly as the only input material parameter for the concrete material model in the benchmark analyses, and was not calibrated in order to improve the results. This was considered particularly important in engineering applications where the results are not known on beforehand. The results from the benchmark analyses did not show exact crack patterns, but the failure modes and the ultimate limit loads were close to what was experimentally obtained. Finite elements of the size that was used in the present study are typically in the order of the crack spacing and localized crack patterns can not be expected.

The results from the NLFEA of the large shell structure show that a global analysis is required for a realistic assessment of such structures. If only local analyses were performed, the analyst should pay close attention to the applied boundary conditions. If the central part of the bottom slab was modelled locally, the compressive membrane effect could be overestimated if the slab was fully constrained in the radial direction. Also, if only the rib was modelled, the effect of redistribution of resultants from global bending could not be predicted, and too large horizontal force transfer from the rib to the shaft might be predicted, which could lead to an overestimation of crack widths and stresses in the horizontal reinforcement. With a solution time of approximately 6 s per equilibrium iteration, the solution strategy presented in the present paper is considered applicable for NLFEA of large concrete structures in the design phase.

7. Conclusions

Development of a solution strategy for NLFEA should as a minimum include the four steps 1) definition, 2) verification, 3) validation and 4) demonstration of applicability. This contribution complements findings published by the authors in two separate publications (Engen et al., 2015, 2017). In spite of relatively simple material models and large finite elements, the results from the present work indicate that the presented solution strategy has a low modelling uncertainty and a low element size and load step size dependency. With the presented solution strategy, the practising engineer is equipped with an efficient tool for performing detailed assessments of the ultimate load capacity and the structural reliability of new and existing large reinforced concrete structures. This will be elaborated on in the further work of the present research project.

Acknowledgments

The work presented in this paper is part of an industrial PhD funded by Multiconsult ASA and The Research Council of Norway. Morten Engen thanks his supervisors and all colleagues in the Marine Structures Department at Multiconsult for valuable discussions and particularly Per Horn, former Senior Vice President of Multiconsult, for having the courage to initiate the research project.

References

H. Bark, G. Markou, C. Mourlas, and M. Papadrakakis. Seismic assessment of a 5-storey retrofitted rc building. In *ECCOMAS Congress 2016, VII European Congress on Computational Methods in Applied Sciences and Engineering, Crete Island, Greece, 5-10 June 2016*, 2016.

J. Barlow. More on Optimal Stress Points - Reduced Integration, Element Distortions and Error Estimations. *International Journal for Numerical Methods in Engineering*, 28:1487–1504, 1989.

J. Barlow. Optimal Stress Locations in Finite Element Models. *International Journal for Numerical Methods in Engineering*, 10:243–251, 1976.

K.-J. Bathe, J. Walczak, A. Welch, and N. Mistry. Nonlinear Analysis of Concrete Structures. *Computers & Structures*, 32(3/4):563–590, 1989.

Z. P. Bazant and B. H. Oh. Crack band theory for fracture of concrete. *Materials and Structures*, 16(3):155–177, 1983.

C. Bédard and M. D. Kotsovos. Application of NLFEA to Concrete Structures. *Journal of Structural Engineering*, 111(12):2691–2707, 1985.

B. Belletti, C. Damoni, and M. A. N. Hendriks. Development of guidelines for nonlinear finite element analyses of existing reinforced and pre-stressed beams. *European Journal of Environmental and Civil Engineering*, 15(9)(9):1361–1384, 2011.

B. Belletti, C. Damoni, J. A. den Uijl, M. A. N. Hendriks, and J. Walraven. Shear resistance evaluation of prestressed concrete bridge beams: *fib* Model Code 2010 guidelines for level IV approximations. *Structural Concrete*, 14(3):242–249, 2013.

B. Belletti, C. Damoni, M. A. N. Hendriks, and A. de Boer. Analytical and numerical evaluation of the design shear resistance of reinforced concrete slabs. *Structural Concrete*, 15(3): 317–330, 2014.

B. Belletti, M. Pimentel, M. Scolari, and J. C. Walraven. Safety assessment of punching shear failure according to the level of approximation approach. *Structural Concrete*, 16(3): 366–380, 2015.

P. G. Bergan and I. Holand. Nonlinear finite element analysis of concrete structures. *Computer Methods in Applied Mechanics and Engineering*, 17/18(2):443–467, 1979.

D.-E. Brekke, E. Åldstedt, and H. Grosch. Design of Offshore Concrete Structures Based on Postprocessing of Results from Finite Element Analysis (FEA): Methods, Limitations and Accuracy. In *Proceedings of the Fourth (1994) International Offshore and Polar Engineering Conference*, 1994.

B. Bresler and A. C. Scordelis. Shear Strength of Reinforced Concrete Beams. *Journal of the American Concrete Institute*, 60(1):51–74, 1963.

V. Cervenka and K. H. Gerstle. Inelastic Analysis of Reinforced Concrete Panels: Experimental Verification and Application. *IABSE Publications*, 32:31–45, 1972.

D. M. Cotsovos. *Numerical Modelling of Structural Concrete under Dynamic (Earthquake and Impact) Loading*. PhD thesis, Imperial College London, 2004.

D. M. Cotsovos and M. N. Pavlovic. Simplified FE model for RC structures under earthquakes. *Proceedings of the ICE - Structures and Buildings*, 159(SB2):87–102, 2006.

R. de Borst and P. Nauta. Non-orthogonal cracks in a smeared finite element model. *Engineering Computations*, 2(1):35–46, 1985.

fib. Bulletin 45: Practitioner's guide to finite element modelling of reinforced concrete structures. International Federation for Structural Concrete (*fib*), 2008.

fib. Bulletin 50: Concrete structures for oil & gas fields. International Federation for Structural Concrete (*fib*), 2009.

fib. fib *Model Code for Concrete Structures 2010*. Ernst & Sohn, 2013.

M. Engen, M. A. N. Hendriks, J. A. Øverli, and E. Åldstedt. Application of NLFEA in the Design of Large Concrete Structures. In *Proceedings of the XXII Nordic Concrete Research Symposium, Reykjavik, Iceland 2014*, 2014.

M. Engen, M. A. N. Hendriks, J. A. Øverli, and E. Åldstedt. Solution strategy for non-linear

Finite Element Analyses of large reinforced concrete structures. *Structural Concrete*, 16(3): 389–397, 2015.

M. Engen, M. A. N. Hendriks, J. Köhler, J. A. Øverli, and E. Åldstedt. A Quantification of the Modelling Uncertainty of Non-linear Finite Element Analyses of Large Concrete Structures. *Structural Safety*, 64:1–8, 2017.

G. C. Ernst, G. M. Smith, A. R. Riveland, and D. N. Pierce. Basic Reinforced Concrete Frame Performance Under Vertical and Lateral Loads. *ACI Journal*, 70(4):261–269, 1973.

CEN. EN ISO 19903: Petroleum and natural gas industries. Fixed concrete offshore structures, 2006.

F. González Vidosa. *Three-dimensional finite element analysis of structural concrete under static loading*. PhD thesis, University of London, 1989.

F. González Vidosa, M. D. Kotsovos, and M. N. Pavlovic. On the Numerical Instability of the Smeared-Crack Approach in the Non-Linear Modelling of Concrete Structures. *Communications in Applied Numerical Methods*, 4(6):799–806, 1988.

F. González Vidosa, M. D. Kotsovos, and M. N. Pavlovic. Three-dimensional non-linear finite-element model for structural concrete. Part 1: main features and objectivity study. *Proceedings of the ICE - Structures and Buildings*, 91:517–544, 1991a.

F. González Vidosa, M. D. Kotsovos, and M. N. Pavlovic. Three-dimensional non-linear finite-element model for structural concrete. Part 2: generality study. *Proceedings of the ICE - Structures and Buildings*, 91:545–560, 1991b.

M. A. N. Hendriks, A. de Boer, and B. Belletti. Guidelines for Nonlinear Finite Element Analysis of Concrete Structures. Rijkswaterstaat Centre for Infrastructure, Report RTD:1016-1:2017, 2017.

I. Jelic, M. N. Pavlovic, and M. D. Kotsovos. Performance of structural-concrete members under sequential loading and exhibiting points of inflection. *Computers and Concrete*, 1(1): 99–113, 2004.

M. D. Kotsovos. A mathematical description of the strength properties of concrete under generalized stress. *Magazine of Concrete Research*, 31(108):151–158, 1979a.

M. D. Kotsovos. Fracture processes of concrete under generalised stress states. *Materials and Structures*, 12(72):431–437, 1979b.

M. D. Kotsovos. A mathematical model of the deformational behavior of concrete under generalised stress based on fundamental material properties. *Materials and Structures*, 13(76):289–298, 1980.

M. D. Kotsovos. A fundamental explanation of the behaviour of reinforced concrete beams in flexure based on the properties of concrete under multiaxial stress. *Materials and Structures*, 15(90):529–537, 1982.

M. D. Kotsovos. Concrete. A brittle fracturing material. *Materials and Structures*, 17(98): 107–115, 1984.

M. D. Kotsovos and M. N. Pavlovic. *Structural Concrete: Finite-element analysis for limit-state design*. Thomas Telford, 1995.

M. D. Kotsovos and K. V. Spiliopoulos. Modelling of crack closure for finite-element analysis of structural concrete. *Computers & Structures*, 69(3):383–398, 1998.

M. D. Kotsovos, M. N. Pavlovic, and D. M. Cotsovos. Characteristic features of concrete behaviour: Implications for the development of an engineering finite-element tool. *Computers and Concrete*, 5(3):243–260, 2008.

I. D. Lefas, M. D. Kotsovos, and N. N. Ambraseys. Behaviour of Reinforced Concrete Structural Walls: Strength, Deformation Characteristics, and Failure Mechanism. *ACI Structural Journal*, 87(1):23–31, 1990.

G. C. Lykidis and K. V. Spiliopoulos. 3D Solid Finite-Element Analysis of Cyclically Loaded RC Structures Allowing Embedded Reinforcement Slippage. *Journal of Structural Engineering*, 134(4):629–638, 2008.

G. Markou, R. Sabouni, F. Suleiman, and R. El-Chouli. Full-Scale Modeling of the Soil-Structure Interaction Problem Through the use of Hybrid Models (HYMOD). *International Journal of Current Engineering and Technology*, 5(2):885–899, 2015.

G. Markou and M. Papadrakakis. Computationally efficient 3D finite element modeling of RC structures. *Computers and Concrete*, 12(4):443–498, 2013.

C. Mourlas, M. Papadrakakis, and G. Markou. Accurate and efficient modeling for the cyclic behavior of rc structural members. In *ECCOMAS Congress 2016, VII European Congress on Computational Methods in Applied Sciences and Engineering, Crete Island, Greece, 5-10 June 2016*, 2016.

Norges Standardiseringsforbund. NS 3473.E: Design of concrete structures. Design and detailing rules. 6th edition, September 2003.

M. Pimentel, E. Brühwiler, and J. A. Figueiras. Safety examination of existing concrete structures using the global resistance safety factor concept. *Engineering Structures*, 70: 130–143, 2014.

P. J. Roache. Verification of Codes and Calculations. *AIAA Journal*, 36(5):696–702, 1998.

J. G. Rots. *Computational modeling of concrete fracture*. PhD thesis, Technische Universiteit Delft, 1988.

J. G. Rots and J. Blaauwendraad. Crack models for concrete: Discrete or smeared? Fixed, multidirectional or rotating? *Heron*, 34(1):1–59, 1989.

H. Schlune, M. Plos, and K. Gylltoft. Safety formats for non-linear analysis of concrete structures. *Magazine of Concrete Research*, 64(7):563–574, 2012.

J. C. Simo and M. S. Rifai. A Class of Mixed Assumed Strain Methods and the Method of Incompatible Modes. *International Journal for Numerical Methods in Engineering*, 29: 1595–1638, 1990.

J. C. Simo, F. Armero, and R. L. Taylor. Improved versions of assumed enhanced strain trilinear elements for 3D finite deformation problems. *Computer Methods in Applied Mechanics and Engineering*, 110:359–386, 1993.

K. V. Spiliopoulos and G. Ch. Lykidis. An efficient three-dimensional solid finite element dynamic analysis of reinforced concrete structures. *Earthquake Engineering and Structural Dynamics*, 35(2):137–157, 2006.

F. J. Vecchio. Non-linear finite element analysis of reinforced concrete: at the crossroads? *Structural Concrete*, 2(4):201–212, 2001.

F. J. Vecchio and S. Balopoulou. On the Nonlinear Behaviour of Reinforced Concrete Frames. *Canadian Journal of Civil Engineering*, 17(5):698–704, 1990.

F. J. Vecchio and M. B. Emara. Shear Deformations in Reinforced Concrete Frames. *ACI Structural Journal*, 89(1):46–56, 1992.

J. A. Øverli. A density-dependent failure criterion for concrete. *Construction and Building Materials*, 124:566–574, 2016.

K. J. Willam and E. P Warnke. Constitutive Model for the Triaxial Behaviour of Concrete. *IABSE reports of the working commissions*, 19:1–30, 1974.

A quantification of the modelling uncertainty of non-linear finite element analyses of large concrete structures

Engen, M., Hendriks, M. A. N., Köhler, J., Øverli, J. A. & Åldstedt, E.
Structural Safety, 2017, 64(1), 1-8

Paper IV

Structural Safety 64 (2017) 1–8

Contents lists available at ScienceDirect

Structural Safety

journal homepage: www.elsevier.com/locate/strusafe

A quantification of the modelling uncertainty of non-linear finite element analyses of large concrete structures

Morten Engen [a,b,*], Max A.N. Hendriks [b,c], Jochen Köhler [b], Jan Arve Øverli [b], Erik Åldstedt [a]

[a] Multiconsult ASA, Postboks 265 Skøyen, 0213 Oslo, Norway
[b] Dept. of Structural Engineering, Norwegian University of Science & Technology, Rich. Birkelandsvei 1A, 7491 Trondheim, Norway
[c] Faculty of Civil Engineering & Geosciences, Delft University of Technology, Steinweg 1, 2628CN Delft, The Netherlands

ARTICLE INFO

Article history:
Received 1 March 2016
Received in revised form 25 August 2016
Accepted 26 August 2016
Available online 24 September 2016

Keywords:
Non-linear finite element analyses
Bayesian inference
Large concrete shell structures
Modelling uncertainty
Global resistance
Characterization of failure mode

ABSTRACT

In order to make non-linear finite element analyses applicable during assessment of the global resistance of large concrete structures, there is need for a solution strategy with a low modelling uncertainty. A solution strategy comprises choices regarding force equilibrium, kinematic compatibility and constitutive relations. Relatively large solid finite elements and a fully triaxial material model for concrete were used in the present work. Bayesian inference was applied to results from 38 benchmark analyses. The results indicated that the modelling uncertainty could be represented as a log-normally distributed random variable with mean 1.10 and standard deviation of 0.12. A new method for characterizing the failure mode was developed. The results indicated that the physical uncertainties influenced the estimated parameters of the modelling uncertainty, and that this should be considered when other uncertainties are included in a reliability assessment.

1. Introduction

The design of large concrete shell structures like dams and offshore oil and gas platforms is normally based on global linear finite element analyses. This allows for using the principle of superpositioning in order to handle the vast number of design load combinations [1,2]. For such large shell structures it is important to perform global analyses due to the interaction between global and local load effects. Solid elements are normally used due to the required accuracy in structural joints, and the elements are large compared to the sectional dimensions.

In order to better take into account the real physical behaviour of reinforced concrete, non-linear finite element analyses (NLFEA) could be carried out. The results of such analyses are global in nature due to all sections contributing to the load carrying capacity [3,4]. Due to the global nature of NLFEA, the capacity should be assessed in a global manner, in contrast to the local sectional design based on linear finite element analyses. fib *Model Code 2010 for concrete structures* [5] introduces probabilistic methods and the semi-probabilistic concept of global resistance methods for assessing the structural reliability. Demonstrations of the global resistance methods are reported in the literature for relatively simple structural forms [3,4,6–12] and also for larger structural systems [13,14]. For such assessments to be accurate, all relevant sources of uncertainties should be considered. As described by Zhang and Mahadevan [15], there are basically three sources of uncertainties in engineering analyses: *physical uncertainties*, *modelling uncertainties* and *statistical uncertainties*.

In this paper, the different sources of uncertainties are discussed. The modelling uncertainty is further quantified by use of Bayesian inference, and a new method for characterization of the failure mode is presented in order to study the influence from the physical uncertainties on the modelling uncertainty. The results indicate that the modelling uncertainty includes contributions from the physical uncertainties, and that this should be considered when other uncertainties are included in a reliability assessment.

2. Uncertainties in engineering analyses

The *physical uncertainties* are related to the measured strength and deformation properties of concrete and reinforcement. The physical uncertainties of concrete and reinforcement on material level is studied by several authors, e.g. Rackwitz [16], and a summary of the results is found in the *Probabilistic Model Code* [17]. The variation of material properties can be studied on several hierarchical levels and can be quantified in terms of the uncertain

* Corresponding author at: Multiconsult ASA, Postboks 265 Skøyen, 0213 Oslo, Norway.
E-mail address: morten.engen@multiconsult.no (M. Engen).

http://dx.doi.org/10.1016/j.strusafe.2016.08.003
0167-4730/

mean of the gross supply, the variability of the production line of one producer, the variability within one batch and the mean and standard deviation of the material property in a reference volume. By investigation of such results, it can be seen that the variation of the compressive cylinder strength of concrete, denoted by the coefficient of variation, is in the range of 5–15% depending on the cylinder strength, compared to a value of typically 5% for the yield strength of the reinforcement steel. The correlation between the cylinder strength and other properties of concrete is studied by e.g. Rashid et al. [18], where the splitting tensile strength of 499 tested specimens was found to vary within a bandwidth of approximately 30–40% when presented as a function of the compressive cylinder strength.

Ideally, the physical uncertainty on structural level should be assessed by performing a large number of experiments on nominally equivalent components. However, in reality, only a limited amount of results from repeated experiments are reported, and the results are typically normalized in order to assess the physical uncertainty from a range of experiments. The uncertainty found from such a study would also include a contribution from modelling uncertainty due to the selected normalizing factor. Based on the different uncertainties on material level it is expected that the physical uncertainties on structural level depend on whether the failure mode is governed by the concrete or the reinforcement, and expected to be particularly high if the failure mode is governed by the tensile strength of the concrete. This statement is supported in the work of Ellingwood and Galambos [19] where the resistance of reinforced concrete beams failing in bending is found to have a lower coefficient of variation than beams failing in shear. Fig. 1a and b shows normalized results from experiments with ductile [20–24] and brittle [25] failure modes respectively. By investigation of the variation, the uncertainty of the ductile failure modes is smaller than the uncertainty of the brittle failure modes. A significant *statistical uncertainty* is present in the case of the ductile failure modes due to the limited amount of observations collected in the present study.

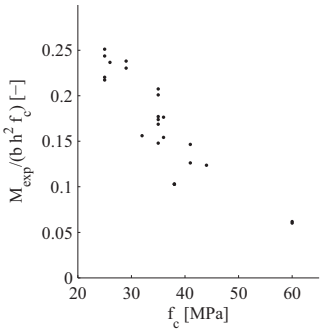

(a) Experimentally obtained moment capacity M_{exp} for ductile beams and walls [20–24] normalized by the width b, height h and cylinder strength f_c plotted against the cylinder strength.

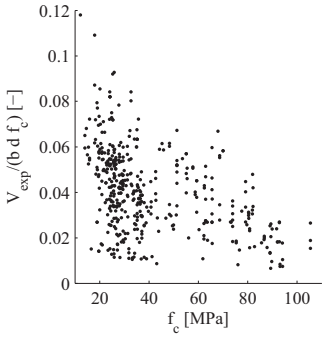

(b) Experimentally obtained shear capacity V_{exp} for brittle beams [25] normalized by the width b, depth d and cylinder strength f_c plotted against the cylinder strength.

Fig. 1. Visualization of the physical uncertainty on structural level for (a) ductile and (b) brittle experiments.

Modelling uncertainties, or model uncertainties, in engineering analyses are related to model selection and the accuracy of the selected model, and apply to both statistical and mechanical models. Only the contribution from the accuracy of the mechanical model to the modelling uncertainty was considered in the present work. Models in engineering analyses are never right or wrong, but they can be more or less useful for a certain problem if the modelling uncertainty is appropriately accounted for. The accuracy of the mechanical model depends on the approximations in the numerical solution procedure and the mathematical idealization of the problem. According to Ditlevsen [26] the uncertainties related to the mathematical idealization are due to a limitation of the possible infinite number of basic variables to a finite number and idealizations of the mathematical equations, both for pragmatic reasons and due to a lack of detailed knowledge about the variation or the behaviour of the problem at hand. There are aspects that we know that we do not consider in the model, but also features that we do not know, i.e. the unknown unknowns. The modelling uncertainty thus covers implicitly everything that is not explicitly considered in the model.

The modelling uncertainty can be quantified by *verification* and *validation* [27]. Verification is related to how the equations of the mechanical model are solved, i.e. a quantification of the accuracy without questioning the relation between the equations and the physical problem at hand. With regard to NLFEA, verification thus relates to the iterative solution of the equilibrium equations and the discretization into finite elements. Validation, on the other hand, relates to how well the equations capture the true physical behaviour. In the NLFEA context, validation thus relates to idealization of the geometry and the material behaviour. In other words, verification answers the question *Are we solving the equations right?*, and validation answers the question *Are we solving the right equations?* [27].

This distinction is useful. One cannot expect improved results by refining the element discretization or the iterative solution scheme if the material model is inadequate. The same holds for refinement of the material model with an improper element discretization. Following the multiplicative formulation in the Probabilistic Model Code [17], the modelling uncertainty was defined as the ratio of the experimental to the predicted capacity, $\Theta = R_{exp}/R_{NLFEA}$.

3. Solution strategy for NLFEA

All of the choices regarding force equilibrium, kinematic compatibility and constitutive relations influence the modelling uncertainty of NLFEA. Collectively, these choices constitute a strategy for obtaining a solution from NLFEA, or short, a *solution strategy* for

NLFEA [2]. For reinforced concrete, the material model for concrete is considered the largest source of modelling uncertainties.

A common way of selecting material models for concrete is to use a uniaxial material model as basis and extend this with additional models that take into account other material effects such as the effects of confinement and lateral cracking. Such an approach can be convenient when the structural effects of different material effects are to be studied, but additional models are normally developed in combination with other complementary models and should not be separated [28]. Alternatively, fully triaxial material models where all material effects are treated, could be used directly. One such fully triaxial material model has been developed by Kotsovos and co-workers since the 1970s and is still subject to improvements [29–38]. In order to make the material model available for practising engineers, it was adapted to a commercial finite element software in the present work. The details are presented in a separate paper [39]. The material model required only one input parameter, the compressive cylinder strength of concrete. A bilinear, elastoplastic model was used for the reinforcement.

Relatively large solid 8-noded finite elements were used for the concrete and the reinforcement was represented by fully bonded embedded reinforcement elements. Due to the size of the concrete elements, the length of the reinforcement elements corresponding to one integration point was typically in the order of magnitude of the expected crack spacing, and the assumption of perfect bond was thus justified. It should be noted that this is a valid approach specially for NLFEA with large finite elements, where the ultimate limit capacity is sought assuming properly anchored reinforcement. If, on the other hand, the crack pattern at the serviceability limit state is to be studied, a more detailed description of the interface between concrete and reinforcement steel and thus a finer finite element mesh might be needed. Modified Newton–Raphson in combination with line search was used for the iterative solution of the equilibrium equations. A convergence criterion given by $||\mathbf{R}_{\mathbf{res}}||/||\mathbf{R}_{\mathbf{ext}}|| < 0.01$ was used for the equilibrium iterations. $\mathbf{R}_{\mathbf{res}}$ is the vector of nodal residual forces, $\mathbf{R}_{\mathbf{ext}}$ is the vector of nodal external loads and $||\cdot||$ indicates that the L_2-norm was used. The loads were applied with constant increment, so that the experimental capacity was reached in 30 load steps.

The solution strategy is discussed in detail in a separate paper, where verification is performed by comparing solutions with different element discretizations, load step sizes and iterative solution procedures [39]. The results show insignificant sensitivity to finite element size and load step size. Validation was performed by comparison of experimental results and results from NLFEA, and the results are presented in the present paper.

4. Characterization of the failure mode

The classical way of characterizing the failure mode of a concrete structure both experimentally and numerically is a matter of subjective judgement. By assessing crack patterns and stress and strain fields at the ultimate limit load, the failure mode can be described as e.g. *diagonal tension*, *shear compression* or *flexure-compression* [40]. Such distinctions are convenient in classical sectional design methods, but have limited applicability to global resistance assessments of large concrete structures where the failure mode could be due to interaction between different sectional forces. For this reason, a more objective characterization to be used in numerical assessments of the failure mode was proposed in the present work.

When a reinforced concrete structure is loaded, cracking of concrete will be initiated at some load level. Upon cracking, the internal forces need to be redistributed. Such redistribution can be associated with the plastic dissipation, i.e. the absorbed non-recoverable strain energy, in the system. If the load is further increased, cracking can either propagate and stabilize if sufficient reinforcement is provided, or propagate progressively to failure. Eventually, also cracking of the sufficiently reinforced structure will propagate to failure when the global redistribution capacity of the reinforcement is exhausted. Hence, reinforcement provides ductility to the brittle concrete by controlling crack propagation and providing sufficient capacity for redistribution of internal forces. This statement was formulated mathematically according to the following expression, where $W_{\text{pl,tot}}$ and $W_{\text{pl,steel}}$ are the plastic dissipation of the system and the reinforcement at failure respectively:

$$X_{\text{ductility}} = \frac{W_{\text{pl,steel}}}{W_{\text{pl,tot}}} \tag{1}$$

The *ductility index*, $X_{\text{ductility}}$, takes values between 0 and 1, and indicates to which degree the failure mode is governed by the reinforcement, and thus the degree of ductility of the failure mode.

5. Statistical inference

According to the definition in the Probabilistic Model Code [17] the modelling uncertainty of benchmark analysis i was defined as the ratio of the experimental to the predicted capacity $\theta_i = R_{\text{exp},i}/R_{\text{NLFEA},i}$. In order to incorporate the modelling uncertainty in a probabilistic analysis, we need to decide the type and parameters of the probability distribution by statistical inference.

5.1. Bayesian data analysis

In Bayesian data analysis both the variable to be modelled and the parameters of the distribution are treated as unknown random variables. The method allows for incorporation of both prior knowledge and observed data, and the statistical uncertainty of the parameters can be estimated from the respective probability distributions. Demonstrations of use can be found in the literature [15,41,42] and a thorough treatment of the technique can be found in the work by Gelman et al. [43]. Although not all of the information provided in this section was used in the rest of the paper, it was included for completeness. All the resulting expressions in this section are valid for normally distributed random variables and were adapted from Gelman et al. [43].

The probability distribution of a normally distributed random variable y is fully described as soon as the mean μ and the variance σ^2 is known. According to Bayes' theorem, the conditional distribution of the mean and variance given a set of n observations y_i collected in the array $\mathbf{y}$ can be expressed as:

$$\mathrm{P}(\mu, \sigma^2|\mathbf{y}) \propto \mathrm{P}(\mu, \sigma^2)\mathrm{P}(\mathbf{y}|\mu, \sigma^2) \tag{2}$$

$\mathrm{P}(\mu, \sigma^2|\mathbf{y})$ is called the *joint posterior distribution* of μ and σ^2 given the observations $\mathbf{y}$. The posterior distribution of μ and σ^2 is thus proportional to the product of the *prior distribution* $\mathrm{P}(\mu, \sigma^2)$ and the *likelihood* $\mathrm{P}(\mathbf{y}|\mu, \sigma^2)$. Any known information about the random variable, both qualitative and quantitative can be included in the prior distribution.

Having established the joint posterior distribution $\mathrm{P}(\mu, \sigma^2|\mathbf{y})$, a natural extension is to establish the posterior predictive distribution $\mathrm{P}(\tilde{y}|\mathbf{y})$ where $\tilde{y}$ is a future prediction of the outcome of the variable y. In Sections 5.2 and 5.3 estimates for μ and σ^2, and posterior predictions of $\tilde{y}$ are given for two different prior distributions.

For non-normally distributed random variables, only a limited selection of analytical solutions, the so-called conjugate priors, exist for some distributions, e.g. Poisson or gamma distributions.

If these solutions do not exist, the joint posterior and the posterior predictive distributions should be approximated by e.g. numerical integration methods such as Markov Chain Monte Carlo simulation methods or deterministic quadrature rules [43].

5.2. Inference using a non-informative prior distribution

If no information is given about the variable, a non-informative prior distribution can be assumed. An important property of a non-informative prior distribution is that it should be objective, and thus not influence the posterior distribution in any direction. Based on the marginal posterior distributions the expected values and the variances for the mean and the variance are given by (3)–(6), where $\bar{y} = \frac{1}{n}\sum_{i=1}^{n} y_i$ is the sample mean and $s^2 = \frac{1}{n-1}\sum_{i=1}^{n}(y_i - \bar{y})^2$ is the sample variance. Note how the statistical uncertainty, i.e. $\mathrm{Var}[\mu|\mathbf{y}]$ and $\mathrm{Var}[\sigma^2|\mathbf{y}]$, decrease as the number of observations increase.

$$\mathrm{E}[\mu|\mathbf{y}] = \bar{y} \tag{3}$$

$$\mathrm{Var}[\mu|\mathbf{y}] = \frac{n-1}{n-3}\frac{s^2}{n} \tag{4}$$

$$\mathrm{E}[\sigma^2|\mathbf{y}] = \frac{n-1}{n-3}s^2 \tag{5}$$

$$\mathrm{Var}[\sigma^2|\mathbf{y}] = \frac{2(n-1)^2}{(n-3)^2(n-5)}s^4 \tag{6}$$

It can be shown that the posterior prediction $\tilde{y}$ can be modelled as a t-distributed random variable with location $\bar{y}$, scale $s^2(1+1/n)$ and $n-1$ degrees of freedom. A future observation can thus be modelled by (7) where t_{n-1} is a centrally t-distributed random variable with $n-1$ degrees of freedom. For large n the t-distribution approaches the normal distribution.

$$\tilde{y} = \bar{y} + t_{n-1}s\sqrt{1+\frac{1}{n}} \tag{7}$$

5.3. Inference using a conjugate prior distribution

If prior information exists, this can be included in the prior distribution. One technique that ensures closed form solutions is to select a joint prior distribution of the same form as the likelihood. This is called a *conjugate prior distribution*. The parameters of the resulting posterior distribution are given in (8)–(11), where n_0 is the number of samples that forms the basis of the prior knowledge and $\nu_0 = n_0 - 1$ is the prior number of degrees of freedom.

$$\mu_n = \frac{n_0\mu_0 + n\bar{y}}{n_0 + n} \tag{8}$$

$$n_n = n_0 + n \tag{9}$$

$$\nu_n = \nu_0 + n = n_0 + n - 1 \tag{10}$$

$$\nu_n\sigma_n^2 = \nu_0\sigma_0^2 + (n-1)s^2 + \frac{n_0 n}{n_0+n}(\bar{y}-\mu_0)^2 \tag{11}$$

The expected values and variances are given in (12)–(15). Notice how (12) and (14) approach (3) and (5) if no prior information exists.

$$\mathrm{E}[\mu|\mathbf{y}] = \mu_n \tag{12}$$

$$\mathrm{Var}[\mu|\mathbf{y}] = \frac{\nu_n}{\nu_n - 2}\frac{\sigma_n^2}{n_n} \tag{13}$$

$$\mathrm{E}[\sigma^2|\mathbf{y}] = \frac{\nu_n}{\nu_n - 2}\sigma_n^2 \tag{14}$$

$$\mathrm{Var}[\sigma^2|\mathbf{y}] = \frac{2\nu_n^2}{(\nu_n-2)^2(\nu_n-4)}\sigma_n^4 \tag{15}$$

It can be shown that the posterior prediction $\tilde{y}$ can be modelled as a t-distributed random variable with location μ_n, scale $\sigma_n^2(1+1/n_n)$ and ν_n degrees of freedom. A future observation can thus be modelled by (16) where t_{ν_n} is a centrally t-distributed random variable with ν_n degrees of freedom.

$$\tilde{y} = \mu_n + t_{\nu_n}\sigma_n\sqrt{1+\frac{1}{n_n}} \tag{16}$$

5.4. The probability distribution of the modelling uncertainty

The probability distribution of the modelling uncertainty is generally not known in advance, however, it is suggested to represent it as a log-normally distributed random variable [17]. The relation between the parameters of a log-normal distribution $\mu_{\ln}$ and $\sigma_{\ln}$ and the mean and variance of the variable itself are given in (17) and (18), where $V = \sigma/\mu$ is the coefficient of variation.

$$\mu_{\ln} = \ln\mu - \frac{1}{2}\ln(V^2+1) \tag{17}$$

$$\sigma_{\ln} = \sqrt{\ln(V^2+1)} \tag{18}$$

In order to perform Bayesian inference on a normally distributed random variable, each observation of the modelling uncertainty θ_i is assigned to y_i. If, on the other hand, the random variable is log-normally distributed, the natural logarithm of each observation $\ln\theta_i$ is assigned to y_i. In order to verify the selected distribution type, the Shapiro–Wilk test for normality [44] with the improvements proposed by Royston [45] was applied. A test statistic was calculated and used as input for a hypothesis test where the null-hypothesis stated that the sample was normally distributed. The *P*-value was calculated and compared to a 5% level of significance.

6. Quantification of the modelling uncertainty

The global results from 38 benchmark analyses are summarized in Table 1 and Fig. 2. The sample consisted of seven short and five slender walls by Lefas et al. [24], one beam by Kotsovos [20], 12 beams by Bresler and Scordelis [40], two frames by Ernst et al. [46], two frames by Vecchio and Balopoulou [47] and Vecchio and Emara [48], one deep beam by Cervenka and Gerstle [49] and eight beams by Jelic et al. [50]. All of the references reported the nominal geometries, and the cylinder strength of the concrete and the yield strength of the reinforcement steel based on a number of material samples. The cylinder strength was used directly as the only input material parameter for the concrete material model, and was not calibrated in order to improve the results in any of the analyses. It was assumed that the concrete within one structural component, i.e. one beam, frame or wall, originated from one batch, and that the reported cylinder strength was measured on samples from the same batch. No information about the spatial variability of the strength was reported, and was thus not considered in the analyses.

Most model predictions were slightly underestimating the experimental capacity, denoted by $\theta_i > 1.0$, and the variation was small. The results from the Shapiro–Wilk test on either $y_i = \theta_i$ or $y_i = \ln\theta_i$, i.e. testing for either normality or log-normality, are summarized in Table 2, where the *P*-value was compared to a 5% level

Table 1
Summary of the results from the benchmark analyses. f_c is the cylinder strength in MPa, $R_{exp,i}$ and $R_{NLFEA,i}$ are the experimental and predicted capacities in kN, θ_i is the modelling uncertainty and $x_{ductility,i} = W_{pl,steel}/W_{pl,tot}$ is the ductility index given by the ratio of the plastic dissipation of the reinforcement and the total plastic dissipation.

Ref.	Experiment	f_c	$R_{exp,i}$	$R_{NLFEA,i}$	θ_i	$x_{ductility,i}$
[24]	SW11	42.3	260.00	274.94	0.95	0.914
	SW12	43.6	340.00	293.20	1.16	0.331
	SW13	32.3	330.00	252.35	1.31	0.000
	SW14	33.2	265.00	253.92	1.04	0.839
	SW15	33.9	320.00	298.39	1.07	0.946
	SW16	41.7	355.00	271.46	1.31	0.000
	SW17	41.1	247.00	238.22	1.04	0.841
	SW21	33.6	127.00	113.99	1.11	0.863
	SW22	40.6	150.00	139.94	1.07	0.704
	SW23	37.8	180.00	151.38	1.19	0.464
	SW24	38.3	120.00	120.01	1.00	0.920
	SW26	25.1	123.00	90.20	1.36	0.526
[20]	B1	37.8	13.60	12.69	1.07	0.680
[40]	OA-1	22.5	333.60	378.53	0.88	0.000
	OA-2	23.7	355.84	320.40	1.11	0.000
	OA-3	37.6	378.08	277.93	1.36	0.000
	A-1	24.1	467.04	466.96	1.00	0.235
	A-2	24.3	489.28	423.80	1.15	0.132
	A-3	35.0	468.37	405.60	1.15	0.130
	B-1	24.8	442.58	443.00	1.00	0.179
	B-2	23.2	400.32	320.00	1.25	0.183
	B-3	38.7	353.62	377.17	0.94	0.103
	C-1	29.6	311.36	290.27	1.07	0.147
	C-2	23.8	324.70	238.33	1.36	0.253
	C-3	35.0	269.10	224.72	1.20	0.088
[46]	2D18	40.8	46.40	41.72	1.11	0.848
	2D18H	28.8	14.10	13.24	1.07	0.824
[47]	BF1	29.0	540.00	521.98	1.03	0.888
[48]	BF2	30.0	332.00	301.31	1.10	0.000
[49]	W2	26.8	240.00	240.00	1.00	0.967
[50]	HDCB3	30.0	202.70	180.16	1.13	0.024
	HDCB4	30.0	196.50	182.29	1.08	0.037
	MDCB3	28.0	193.90	189.98	1.02	0.881
	MDCB4	28.0	196.40	193.14	1.02	0.919
	LDCB3	30.0	181.60	178.54	1.02	0.185
	LDCB4	30.0	186.20	179.70	1.04	0.292
	G21	34.3	204.80	185.53	1.10	0.069
	G22	34.3	200.80	197.01	1.02	0.958

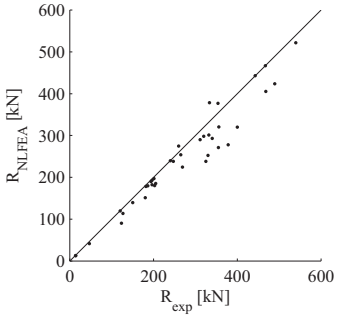

Fig. 2. Experimental capacity and predicted capacity for the 38 benchmark analyses.

Table 2
Summary of results from the Shapiro–Wilk test for normality of Θ. *W* is the Shapiro–Wilk test statistic and the *P*-value is the probability of making the current observation given that the observations are normally distributed.

y_i	W	*P*-value	
θ_i	0.9232	0.012 < 0.05	⇒ Reject
$\ln\theta_i$	0.9461	0.066 > 0.05	⇒ Do not reject

of significance. The test did not reject that Θ could be represented as a log-normally distributed random variable. The results were confirmed by the probability plots in Fig. 3 where the scatter plot is slightly more concentrated along the straight line for the log-normal distribution than for the normal distribution. Note that the straight lines are indicative only, as they are based on the sample mean and sample variance.

Based on these results, Bayesian inference with a non-informative prior was performed on the sample **y** where $y_i = \ln\theta_i$. The expressions in Section 5.2 resulted in $\mu_{\ln\Theta} = 0.092$ and $\sigma_{\ln\Theta} = 0.108$, and by using the expressions in Section 5.4 a mean $\mu_\Theta = 1.10$, a standard deviation $\sigma_\Theta = 0.12$ and a coefficient of variation $V_\Theta = 10.9\%$ was calculated.

Fig. 4a shows the modelling uncertainty plotted against the cylinder strength. No simple linear trend can be observed, and the resulting linear correlation coefficient was 0.013 which confirms that observation. It might be interesting also to check the correlation to other input parameters, but as the sample contained benchmark experiments with varying reinforcement layouts and structural forms, no parameters except the cylinder strength were directly comparable. Fig. 4b shows the modelling uncertainty plotted against the ductility index, as defined in Section 4, for all the benchmark analyses. Depending on the ductility index, the observations might be grouped in two separate domains: one brittle and one ductile.

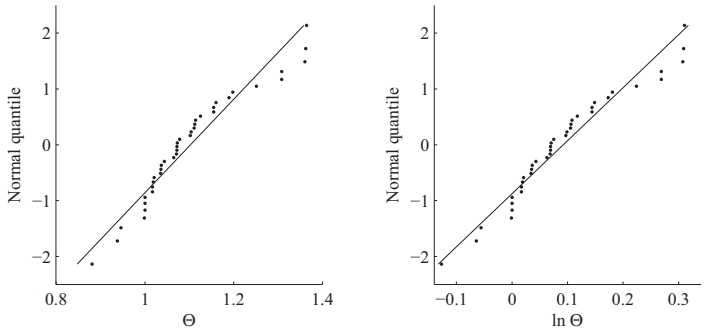

(a) Normal distribution. (b) Log-normal distribution.

Fig. 3. Probability plot for the modelling uncertainty Θ assuming (a) normal and (b) log-normal distribution.

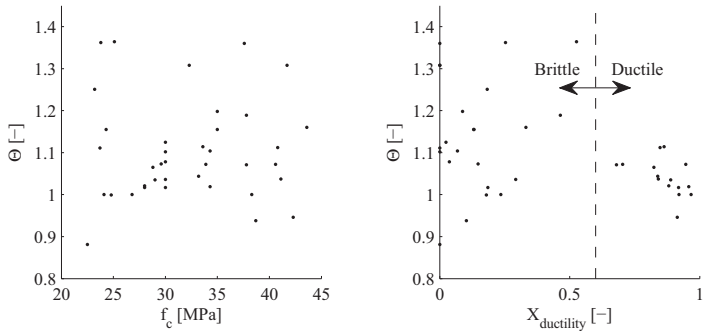

(a) Cylinder strength. (b) Ductility index.

Fig. 4. Correlation between modelling uncertainty Θ and (a) cylinder strength f_c and (b) ductility index $X_{\text{ductility}} = W_{\text{pl,steel}}/W_{\text{pl,tot}}$.

7. Discussion

The level of detail which is needed for the material model depends on the phenomena that are to be studied in the analysis. In the present study, the ultimate limit capacity was sought, and for this application the simple fully triaxial material model [29,30] was appropriate. The results were supporting the conclusions from Engen et al. [2] advising a shift of the attention from a detailed description of the post-cracking tensile behaviour to a rational description of the pre-cracking compressive behaviour of concrete in analyses where large finite elements are used. Despite the simple form of the material model and the coarse meshes of linear solid elements, the resulting modelling uncertainty had a low standard deviation, and the mean value close to one indicated a small model bias.

A new method for characterization of the failure mode was presented. The method characterized the failure mode in terms of the ductility index, $X_{\text{ductility}}$, defined as the ratio between the plastic dissipation of the reinforcement and the total plastic dissipation of the system. It was regarded as an advantage of the method that it was objective and unambiguous compared to traditional characterizations based on subjective judgement. This seemed to be particularly relevant for failure modes where the interaction between several sectional forces was governing. The objective characterization should be complemented by a description of the failure mode, e.g. in terms of the crack pattern, stress and strain contours and displacements.

If all the redistribution, i.e. the plastic dissipation, is assigned to the concrete, the structure is likely to fail in a brittle manner due to the low redistribution capacity of the concrete. The brittle failure modes governed by the concrete have a higher inherent physical uncertainty and are often more difficult to predict with a high accuracy compared to the ductile counterpart of failure modes governed by the reinforcement. The sources for the high inherent uncertainty of the brittle failure modes are the spatial variability and the mean and standard deviation of the material properties within the concrete batch, and the correlation between the cylinder strength and other parameters of the concrete as described in Section 2. Because these variations were not controlled in the uncerlying experiments, they were not considered explicitly in the analyses, thus they were implicitly included in the modelling uncertainty. The modelling uncertainty of the ductile failure modes, on the other hand, would have a lower contribution from physical uncertainties due to the lower physical uncertainties inherent to the reinforcement steel. This statement serves as a rational explanation to the results from earlier studies of the modelling uncertainty in connection to prediction of the capacity of reinforced concrete [3,19]. As an indication on the dependency of Θ on the failure mode, the benchmark analyses could be separated in two domains, e.g. a brittle domain for $X_{\text{ductility}} < 0.6$ and a ductile domain for $X_{\text{ductility}} \geqslant 0.6$, as shown in Fig. 4b. Bayesian inference resulted in $\mu_\Theta = 1.14$ and $\sigma_\Theta = 0.14$, and $\mu_\Theta = 1.04$ and $\sigma_\Theta = 0.05$, for the brittle and ductile domain respectively, and the standard deviation of the modelling uncertainty thus got its largest contribution from the brittle domain.

Based on the discussion above, the separation of uncertainties such that a pure modelling uncertainty is obtained is not straight forward and it is reasonable to keep the present definition and note that the estimated modelling uncertainty also includes contributions from the physical uncertainties. With the present definition of the modelling uncertainty, and treating the physical uncertainties on hierarchical levels, the only contribution to the physical uncertainties that should be included in a reliability assessment are those related to the variability of the material supply between different producers. However, reasonable assumptions for the quantification of this variability is beyond the scope of this paper and calls for further research.

If the capacity of a ductile experiment was underestimated, the calculated ductility index would also be underestimated, resulting in a low $x_{\text{ductility},i}$, a low predicted capacity and a high θ_i. This represented a slight weakness of the characterization of the failure mode presented in the present paper. It should be noted that the underestimation could be both due to solving the wrong equations, i.e. inadequate material modelling or geometric idealization, or due to wrong solution of the equations, i.e. inadequate finite element discretization or iterative solution of the non-linear equilibrium equations. On the other hand, if the capacity of a brittle experiment was properly estimated, this resulted in a low $x_{\text{ductility},i}$ and $\theta_i \approx 1.0$, and a high $x_{\text{ductility},i}$ would in all cases indicate that the failure mode is indeed ductile.

In order to perform all the benchmark analyses in a consistent manner, the external load was applied with constant load increments such that the experimental capacity was reached in 30 load steps. This was the main reason for several of the points in Fig. 4a and b being horizontally aligned. Due to the discretized load application, a higher load could in principle be reached if the load was continuously increased to failure. If several benchmark analyses in reality could have yielded higher capacities, this would influence the estimated parameters of the modelling uncertainty. A resulting theoretical deviation was found to be in the order of magnitude of the statistical uncertainty of the estimated parameters, and was thus not studied further in detail.

Ditlevsen and Madsen [51] note that whatever degree of refinement of the mechanical model, some modelling uncertainty will remain, and at some degree of refinement, the physical and statistical uncertainty will dominate the total uncertainty of the problem. This indicates that a reasonable target for the modelling uncertainty could be in the order of the dominating physical or statistical uncertainty. In the recommendations published by *fib* [52] it is stated that the coefficient of variation of the modelling uncertainty should be less than 30%. Assuming a target reliability level including sensitivity factors, the global safety factor for modelling uncertainty used in Model Code 2010 corresponds to a coefficient of variation of 5–15% depending on the assumed bias [5]. The coefficient of variation obtained in the present study was thus considered adequate. It should be noted that the resulting modelling uncertainty reported in the present paper is related to one specific solution strategy, i.e. one specific set of choices regarding force equilibrium, kinematic compatibility and constitutive relations. A change of solution strategy is expected to result in different parameters for the modelling uncertainty that need to be quantified.

The modelling uncertainty as treated in the present project can be incorporated in reliability assessments in several ways. In semi-probabilistic methods, the coefficient of variation can be included in the calculation of the total coefficient of variation following the approach suggested by Schlune et al. [3] or as a separate reduction factor as discussed by e.g. Kadlec and Cervenka [53]. Θ could be incorporated directly as a basic variable in a procedure based on e.g. a response surface and a first order reliability method as demonstrated by Belletti et al. [12]. In a full probabilistic method, Θ can be simulated by drawing random samples from a normal, log-normal or a t-distribution depending on which distribution is the most suitable.

8. Conclusions

Results from a range of benchmark analyses where a fully triaxial material model for concrete and relatively large solid elements were used, showed that the modelling uncertainty could be represented as a log-normally distributed random variable with a mean 1.10 and a standard deviation of 0.12. These results indicate that the global safety factor for modelling uncertainty suggested in Model Code 2010 for numerical models subjected to a high level of validation is valid. The new method for characterizing the failure mode that was developed was successfully applied, and the results indicated that the physical uncertainties influence the estimated parameters of the modelling uncertainty. Because the physical uncertainties related to variation of the concrete compressive strength within and between batches from one producer were not explicitly considered in the NLFEA in the present study, these uncertainties were implicitly included in the estimated modelling uncertainty. With the present definition of the modelling uncertainty, only the physical uncertainties related to the variability of the material supply between different producers should thus be included in a reliability assessment. It is worth noting that all the cases that were studied, relate to laboratory experiments with more or less well-defined boundary and loading conditions. In a real concrete structure, the physical uncertainties might increase e.g. due to inadequate curing conditions or variable quality of workmanship, and the modelling uncertainty might increase due to e.g. idealization of geometry, load application and boundary conditions. In the further work, different possibilities for including the modelling uncertainty in a reliability assessment will be studied. This is considered crucial for obtaining realistic estimates of the design load carrying capacity or the reliability of both new and existing concrete structures.

Acknowledgement

The work presented in this paper is part of an industrial PhD funded by Multiconsult ASA and The Research Council of Norway. Morten Engen would like to thank his supervisors and all colleagues in the Marine Structures Department at Multiconsult for valuable discussions and particularly *Per Horn*, former Senior Vice President of Multiconsult, for having the courage to initiate the research project.

References

[1] Brekke D-E, Åldstedt E, Grosch H. Design of offshore concrete structures based on postprocessing of results from finite element analysis (FEA): methods, limitations and accuracy. In: Proceedings of the fourth (1994) international offshore and polar engineering conference; 1994.
[2] Engen M, Hendriks MAN, Øverli JA, Åldstedt E. Solution strategy for non-linear Finite Element Analyses of large reinforced concrete structures. Struct Concr 2015;16(3):389–97.
[3] Schlune H, Plos M, Gylltoft K. Safety formats for non-linear analysis of concrete structures. Mag Concr Res 2012;64(7):563–74.
[4] Cervenka V. Reliability-based non-linear analysis according to fib Model Code 2010. Struct Concr 2013;14(1):19–28.
[5] *fib*, *fib*. Model code for concrete structures 2010, Ernst & Sohn; 2013.
[6] Belletti B, Damoni C, Hendriks MA. Development of guidelines for nonlinear finite element analyses of existing reinforced and pre-stressed beams. Eur J Environ Civil Eng 2011;15(9):1361–84.
[7] Schlune H, Plos M, Gylltoft K. Safety formats for nonlinear analysis tested on concrete beams subjected to shear forces and bending moments. Eng Struct 2011;33(8):2350–6.
[8] Allaix DL, Carbone VI, Mancini G. Global safety format for non-linear analysis of reinforced concrete structures. Struct Concr 2013;14(1):29–42.
[9] Belletti B, Damoni C, den Uijl JA, Hendriks MAN, Walraven J. Shear resistance evaluation of prestressed concrete bridge beams: fib Model Code 2010 guidelines for level IV approximations. Struct Concr 2013;14(3):242–9.

[10] B. Belletti, C. Damoni, M. A. Hendriks, J. A. den Uijl, Nonlinear finite element analyses of reinforced concrete slabs: comparison of safety formats, in: FraMCoS-8; 2013.
[11] Belletti B, Damoni C, Hendriks MAN, de Boer A. Analytical and numerical evaluation of the design shear resistance of reinforced concrete slabs. Struct Concr 2014;15(3):317–30.
[12] Belletti B, Pimentel M, Scolari M, Walraven JC. Safety assessment of punching shear failure according to the level of approximation approach. Struct Concr 2015;16(3):366–80.
[13] Pimentel M, Brühwiler E, Figueiras JA. Safety examination of existing concrete structures using the global resistance safety factor concept. Eng Struct 2014;70:130–43.
[14] Blomfors M, Engen M, Plos M. Evaluation of safety formats for non-linear Finite Element Analyses of statically indeterminate concrete structures subjected to different load paths. Struct Concr 2016;17(1):44–51.
[15] Zhang R, Mahadevan S. Model uncertainty and Bayesian updating in reliability-based inspection. Struct Saf 2000;22(2):145–60.
[16] Rackwitz R. Predictive distribution of strength under control. Mater Struct 1983;16(4):259–67.
[17] JCSS. Probabilistic Model Code, 12th draft. Joint Committee on Structural Safety; 2001.
[18] Rashid MA, Mansur MA, Paramasivam P. Correlations between mechanical properties of high-strength concrete. J Mater Civil Eng 2002;14(3):230–8.
[19] Ellingwood B, Galambos TV. Probability-based criteria for structural design. Struct Saf 1982;1(1):15–26.
[20] Kotsovos MD. A fundamental explanation of the behaviour of reinforced concrete beams in flexure based on the properties of concrete under multiaxial stress. Mater Struct 1982;15(90):529–37.
[21] Kotsovos GM. Assessment of the flexural capacity of RC beam/column elements allowing for 3d effects. Eng Struct 2011;33:2772–80.
[22] Kotsovos GM, Cotsovos DM, Kotsovos MD, Kounadis AN. Seismic behaviour of RC walls: an attempt to reduce reinforcement congestion. Mag Concr Res 2011;63(4):235–46.
[23] Kotsovos GM. Seismic design of RC beam-column structural elements. Mag Concr Res 2011;63(7):527–37.
[24] Lefas ID, Kotsovos MD, Ambraseys NN. Behaviour of reinforced concrete structural walls: strength, deformation characteristics, and failure mechanism. ACI Struct J 1990;87(1):23–31.
[25] Reineck K-H, Kuchma D, Kim KS, Marx S. Shear database for reinforced concrete members without shear reinforcement. ACI Struct J 2003;100(2):240–9.
[26] Ditlevsen O. Model uncertainty in structural reliability. Struct Saf 1982;1(1):73–86.
[27] Roache PJ. Verification of codes and calculations. AIAA J 1998;36(5):696–702.
[28] Vecchio FJ. Non-linear finite element analysis of reinforced concrete: at the crossroads? Struct Concr 2001;2(4):201–12.
[29] Kotsovos MD. A mathematical description of the strength properties of concrete under generalized stress. Mag Concr Res 1979;31(108):151–8.
[30] Kotsovos MD. A mathematical model of the deformational behavior of concrete under generalised stress based on fundamental material properties. Mater Struct 1980;13(76):289–98.
[31] Bédard C, Kotsovos MD. Application of NLFEA to concrete structures. J Struct Eng 1985;111(12):2691–707.
[32] González Vidosa F, Kotsovos MD, Pavlovic MN. Three-dimensional non-linear finite-element model for structural concrete. Part 1: main features and objectivity study. Proc ICE Struct Build 1991;91:517–44.
[33] González Vidosa F, Kotsovos MD, Pavlovic MN. Three-dimensional non-linear finite-element model for structural concrete Part 2: generality study. Proc ICE Struct Build 1991;91:545–60.
[34] Kotsovos MD, Pavlovic MN. Structural Concrete: Finite-element analysis for limit-state design. Thomas Telford; 1995.
[35] Kotsovos MD, Spiliopoulos KV. Modelling of crack closure for finite-element analysis of structural concrete. Comput Struct 1998;69(3):383–98.
[36] Cotsovos DM, Pavlovic MN. Simplified FE model for RC structures under earthquakes. Proc ICE Struct Build 2006;159(SB2):87–102.
[37] Spiliopoulos KV, Lykidis GC. An efficient three-dimensional solid finite element dynamic analysis of reinforced concrete structures. Earthq Eng Struct Dyn 2006;35(2):137–57.
[38] Markou G, Papadrakakis M. Computationally efficient 3D finite element modeling of RC structures. Comput Concr 2013;12(4):443–98.
[39] Engen M, Hendriks MAN, Øverli JA, Åldstedt E. Material model for non-linear finite element analyses of large concrete structures; 2016 (submitted for review).
[40] Bresler B, Scordelis AC. Shear strength of reinforced concrete beams. J Am Concr Inst 1963;60(1):51–74.
[41] Droguett EL, Mosleh A. Bayesian methodology for model uncertainty using model performance data. Risk Anal 2008;28(5):1457–76.
[42] Allaix DL, Carbone VI, Mancini G. Modelling uncertainties for the loadbearing capacity of corroded simply supported RC beams. Struct Concr 2015;16(3):333–41.
[43] Gelman A, Carlin JB, Stern HS, Dunson DB, Vehtari A, Rubin DB. Bayesian data analysis. 3rd ed. CRC Press; 2014.
[44] Shapiro SS, Wilk MB. An analysis of variance test for normality (complete samples). Biometrika 1965;52(3 and 4):591–611.
[45] Royston P. Approximating the Shapiro-Wilk W-test for non-normality. Statist Comput 1992;2(3):117–9.
[46] Ernst GC, Smith GM, Riveland AR, Pierce DN. Basic reinforced concrete frame performance under vertical and lateral loads. ACI J 1973;70(4):261–9.
[47] Vecchio FJ, Balopoulou S. On the nonlinear behaviour of reinforced concrete frames. Canad J Civil Eng 1990;17(5):698–704.
[48] Vecchio FJ, Emara MB. Shear deformations in reinforced concrete frames. ACI Struct J 1992;89(1):46–56.
[49] Cervenka V, Gerstle KH. Inelastic analysis of reinforced concrete panels: experimental verification and application. IABSE Publications 1972;32:31–45.
[50] Jelic I, Pavlovic MN, Kotsovos MD. Performance of structural-concrete members under sequential loading and exhibiting points of inflection. Comput Concr 2004;1(1):99–113.
[51] Ditlevsen O, Madsen HO. Structural reliability methods, coastal, maritime and structural engineering. Department for Mechanical Engineering, Technical University of Denmark; 2005 [internet edition, 2.2.5 ed.].
[52] fib. Bulletin 45: practitioner's guide to finite element modelling of reinforced concrete structures. Int Feder Struct Concr (fib), 2008.
[53] Kadlec L, Cervenka V. Uncertainty of numerical models for punching resistance of rc slabs. In: Concrete – innovation and design, fib symposium, Copenhagen May 18–20; 2015.

DEPARTMENT OF STRUCTURAL ENGINEERING
NORWEGIAN UNIVERSITY OF SCIENCE AND TECHNOLOGY

N–7491 TRONDHEIM, NORWAY
Telephone: +47 73 59 47 00 Telefax: +47 73 59 47 01

"Reliability Analysis of Structural Systems using Nonlinear Finite Element Methods",
C. A. Holm, 1990:23, ISBN 82-7119-178-0.

"Uniform Stratified Flow Interaction with a Submerged Horizontal Cylinder",
Ø. Arntsen, 1990:32, ISBN 82-7119-188-8.

"Large Displacement Analysis of Flexible and Rigid Systems Considering
Displacement-Dependent Loads and Nonlinear Constraints",
K. M. Mathisen, 1990:33, ISBN 82-7119-189-6.

"Solid Mechanics and Material Models including Large Deformations",
E. Levold, 1990:56, ISBN 82-7119-214-0, ISSN 0802-3271.

"Inelastic Deformation Capacity of Flexurally-Loaded Aluminium Alloy Structures",
T. Welo, 1990:62, ISBN 82-7119-220-5, ISSN 0802-3271.

"Visualization of Results from Mechanical Engineering Analysis",
K. Aamnes, 1990:63, ISBN 82-7119-221-3, ISSN 0802-3271.

"Object-Oriented Product Modeling for Structural Design",
S. I. Dale, 1991:6, ISBN 82-7119-258-2, ISSN 0802-3271.

"Parallel Techniques for Solving Finite Element Problems on Transputer Networks",
T. H. Hansen, 1991:19, ISBN 82-7119-273-6, ISSN 0802-3271.

"Statistical Description and Estimation of Ocean Drift Ice Environments",
R. Korsnes, 1991:24, ISBN 82-7119-278-7, ISSN 0802-3271.

“Properties of concrete related to fatigue damage: with emphasis on high strength concrete”,
G. Petkovic, 1991:35, ISBN 82-7119-290-6, ISSN 0802-3271.

"Turbidity Current Modelling",
B. Brørs, 1991:38, ISBN 82-7119-293-0, ISSN 0802-3271.

"Zero-Slump Concrete: Rheology, Degree of Compaction and Strength. Effects of Fillers as Part Cement-Replacement",
C. Sørensen, 1992:8, ISBN 82-7119-357-0, ISSN 0802-3271.

"Nonlinear Analysis of Reinforced Concrete Structures Exposed to Transient Loading",
K. V. Høiseth, 1992:15, ISBN 82-7119-364-3, ISSN 0802-3271.

"Finite Element Formulations and Solution Algorithms for Buckling and Collapse Analysis of Thin Shells",
R. O. Bjærum, 1992:30, ISBN 82-7119-380-5, ISSN 0802-3271.

"Response Statistics of Nonlinear Dynamic Systems",
J. M. Johnsen, 1992:42, ISBN 82-7119-393-7, ISSN 0802-3271.

"Digital Models in Engineering. A Study on why and how engineers build and operate digital models for decisison support",
J. Høyte, 1992:75, ISBN 82-7119-429-1, ISSN 0802-3271.

"Sparse Solution of Finite Element Equations",
A. C. Damhaug, 1992:76, ISBN 82-7119-430-5, ISSN 0802-3271.

"Some Aspects of Floating Ice Related to Sea Surface Operations in the Barents Sea",
S. Løset, 1992:95, ISBN 82-7119-452-6, ISSN 0802-3271.

"Modelling of Cyclic Plasticity with Application to Steel and Aluminium Structures",
O. S. Hopperstad, 1993:7, ISBN 82-7119-461-5, ISSN 0802-3271.

"The Free Formulation: Linear Theory and Extensions with Applications to Tetrahedral Elements
with Rotational Freedoms",
G. Skeie, 1993:17, ISBN 82-7119-472-0, ISSN 0802-3271.

"Høyfast betongs motstand mot piggdekkslitasje. Analyse av resultater fra prøving i Veisliter'n",
T. Tveter, 1993:62, ISBN 82-7119-522-0, ISSN 0802-3271.

"A Nonlinear Finite Element Based on Free Formulation Theory for Analysis of Sandwich Structures",
O. Aamlid, 1993:72, ISBN 82-7119-534-4, ISSN 0802-3271.

"The Effect of Curing Temperature and Silica Fume on Chloride Migration and Pore Structure of High Strength Concrete",
C. J. Hauck, 1993:90, ISBN 82-7119-553-0, ISSN 0802-3271.

"Failure of Concrete under Compressive Strain Gradients",
G. Markeset, 1993:110, ISBN 82-7119-575-1, ISSN 0802-3271.

"An experimental study of internal tidal amphidromes in Vestfjorden",
J. H. Nilsen, 1994:39, ISBN 82-7119-640-5, ISSN 0802-3271.

"Structural analysis of oil wells with emphasis on conductor design",
H. Larsen, 1994:46, ISBN 82-7119-648-0, ISSN 0802-3271.

"Adaptive methods for non-linear finite element analysis of shell structures",
K. M. Okstad, 1994:66, ISBN 82-7119-670-7, ISSN 0802-3271.

"On constitutive modelling in nonlinear analysis of concrete structures",
O. Fyrileiv, 1994:115, ISBN 82-7119-725-8, ISSN 0802-3271.

"Fluctuating wind load and response of a line-like engineering structure with emphasis on motion-induced wind forces",
J. Bogunovic Jakobsen, 1995:62, ISBN 82-7119-809-2, ISSN 0802-3271.

"An experimental study of beam-columns subjected to combined torsion, bending and axial actions",
A. Aalberg, 1995:66, ISBN 82-7119-813-0, ISSN 0802-3271.

"Scaling and cracking in unsealed freeze/thaw testing of Portland cement and silica fume concretes",
S. Jacobsen, 1995:101, ISBN 82-7119-851-3, ISSN 0802-3271.

"Damping of water waves by submerged vegetation. A case study of laminaria hyperborea",
A. M. Dubi, 1995:108, ISBN 82-7119-859-9, ISSN 0802-3271.

"The dynamics of a slope current in the Barents Sea",
Sheng Li, 1995:109, ISBN 82-7119-860-2, ISSN 0802-3271.

"Modellering av delmaterialenes betydning for betongens konsistens",
Ernst Mørtsell, 1996:12, ISBN 82-7119-894-7, ISSN 0802-3271.

"Bending of thin-walled aluminium extrusions",
Birgit Søvik Opheim, 1996:60, ISBN 82-7119-947-1, ISSN 0802-3271.

"Material modelling of aluminium for crashworthiness analysis",
Torodd Berstad, 1996:89, ISBN 82-7119-980-3, ISSN 0802-3271.

"Estimation of structural parameters from response measurements on submerged floating tunnels",
Rolf Magne Larssen, 1996:119, ISBN 82-471-0014-2, ISSN 0802-3271.

“Numerical modelling of plain and reinforced concrete by damage mechanics”,
Mario A. Polanco-Loria, 1997:20, ISBN 82-471-0049-5, ISSN 0802-3271.

“Nonlinear random vibrations - numerical analysis by path integration methods”,
Vibeke Moe, 1997:26, ISBN 82-471-0056-8, ISSN 0802-3271.

"Numerical prediction of vortex-induced vibration by the finite element method",
Joar Martin Dalheim, 1997:63, ISBN 82-471-0096-7, ISSN 0802-3271.

"Time domain calculations of buffeting response for wind sensitive structures",
Ketil Aas-Jakobsen, 1997:148, ISBN 82-471-0189-0, ISSN 0802-3271.

"A numerical study of flow about fixed and flexibly mounted circular cylinders",
Trond Stokka Meling, 1998:48, ISBN 82-471-0244-7, ISSN 0802-3271.

"Estimation of chloride penetration into concrete bridges in coastal areas",
Per Egil Steen, 1998:89, ISBN 82-471-0290-0, ISSN 0802-3271.

"Stress-resultant material models for reinforced concrete plates and shells",
Jan Arve Øverli, 1998:95, ISBN 82-471-0297-8, ISSN 0802-3271.

"Chloride binding in concrete. Effect of surrounding environment and concrete composition",
Claus Kenneth Larsen, 1998:101, ISBN 82-471-0337-0, ISSN 0802-3271.

"Rotational capacity of aluminium alloy beams",
Lars A. Moen, 1999:1, ISBN 82-471-0365-6, ISSN 0802-3271.

"Stretch Bending of Aluminium Extrusions",
Arild H. Clausen, 1999:29, ISBN 82-471-0396-6, ISSN 0802-3271.

"Aluminium and Steel Beams under Concentrated Loading",
Tore Tryland, 1999:30, ISBN 82-471-0397-4, ISSN 0802-3271.

"Engineering Models of Elastoplasticity and Fracture for Aluminium Alloys",
Odd-Geir Lademo, 1999:39, ISBN 82-471-0406-7, ISSN 0802-3271.

"Kapasitet og duktilitet av dybelforbindelser i trekonstruksjoner",
Jan Siem, 1999:46, ISBN 82-471-0414-8, ISSN 0802-3271.

"Etablering av distribuert ingeniørarbeid; Teknologiske og organisatoriske erfaringer fra en norsk ingeniørbedrift",
Lars Line, 1999:52, ISBN 82-471-0420-2, ISSN 0802-3271.

"Estimation of Earthquake-Induced Response",
Símon Ólafsson, 1999:73, ISBN 82-471-0443-1, ISSN 0802-3271.

"Coastal Concrete Bridges: Moisture State, Chloride Permeability and Aging Effects"
Ragnhild Holen Relling, 1999:74, ISBN 82-471-0445-8, ISSN 0802-3271.

"Capacity Assessment of Titanium Pipes Subjected to Bending and External Pressure",
Arve Bjørset, 1999:100, ISBN 82-471-0473-3, ISSN 0802-3271.

“Validation of Numerical Collapse Behaviour of Thin-Walled Corrugated Panels”,
Håvar Ilstad, 1999:101, ISBN 82-471-0474-1, ISSN 0802-3271.

“Strength and Ductility of Welded Structures in Aluminium Alloys”,
Miroslaw Matusiak, 1999:113, ISBN 82-471-0487-3, ISSN 0802-3271.

“Thermal Dilation and Autogenous Deformation as Driving Forces to Self-Induced Stresses in High Performance Concrete”,
Øyvind Bjøntegaard, 1999:121, ISBN 82-7984-002-8, ISSN 0802-3271.

“Some Aspects of Ski Base Sliding Friction and Ski Base Structure”,
Dag Anders Moldestad, 1999:137, ISBN 82-7984-019-2, ISSN 0802-3271.

"Electrode reactions and corrosion resistance for steel in mortar and concrete",
Roy Antonsen, 2000:10, ISBN 82-7984-030-3, ISSN 0802-3271.

"Hydro-Physical Conditions in Kelp Forests and the Effect on Wave Damping and Dune Erosion. A case study on Laminaria Hyperborea",
Stig Magnar Løvås, 2000:28, ISBN 82-7984-050-8, ISSN 0802-3271.

"Random Vibration and the Path Integral Method",
Christian Skaug, 2000:39, ISBN 82-7984-061-3, ISSN 0802-3271.

"Buckling and geometrical nonlinear beam-type analyses of timber structures",
Trond Even Eggen, 2000:56, ISBN 82-7984-081-8, ISSN 0802-3271.

”Structural Crashworthiness of Aluminium Foam-Based Components”,
Arve Grønsund Hanssen, 2000:76, ISBN 82-7984-102-4, ISSN 0809-103X.

“Measurements and simulations of the consolidation in first-year sea ice ridges, and some aspects of mechanical behaviour”,
Knut V. Høyland, 2000:94, ISBN 82-7984-121-0, ISSN 0809-103X.

”Kinematics in Regular and Irregular Waves based on a Lagrangian Formulation”,
Svein Helge Gjøsund, 2000-86, ISBN 82-7984-112-1, ISSN 0809-103X.

”Self-Induced Cracking Problems in Hardening Concrete Structures”,
Daniela Bosnjak, 2000-121, ISBN 82-7984-151-2, ISSN 0809-103X.

"Ballistic Penetration and Perforation of Steel Plates",
Tore Børvik, 2000:124, ISBN 82-7984-154-7, ISSN 0809-103X.

"Freeze-Thaw resistance of Concrete. Effect of: Curing Conditions, Moisture Exchange and Materials",
Terje Finnerup Rønning, 2001:14, ISBN 82-7984-165-2, ISSN 0809-103X

"Structural behaviour of post tensioned concrete structures. Flat slab. Slabs on ground",
Steinar Trygstad, 2001:52, ISBN 82-471-5314-9, ISSN 0809-103X.

"Slipforming of Vertical Concrete Structures. Friction between concrete and slipform panel",
Kjell Tore Fosså, 2001:61, ISBN 82-471-5325-4, ISSN 0809-103X.

"Some numerical methods for the simulation of laminar and turbulent incompressible flows",
Jens Holmen, 2002:6, ISBN 82-471-5396-3, ISSN 0809-103X.

“Improved Fatigue Performance of Threaded Drillstring Connections by Cold Rolling”,
Steinar Kristoffersen, 2002:11, ISBN: 82-421-5402-1, ISSN 0809-103X.

"Deformations in Concrete Cantilever Bridges: Observations and Theoretical Modelling",
Peter F. Takâcs, 2002:23, ISBN 82-471-5415-3, ISSN 0809-103X.

"Stiffened aluminium plates subjected to impact loading",
Hilde Giæver Hildrum, 2002:69, ISBN 82-471-5467-6, ISSN 0809-103X.

"Full- and model scale study of wind effects on a medium-rise building in a built up area",
Jónas Thór Snæbjørnsson, 2002:95, ISBN82-471-5495-1, ISSN 0809-103X.

“Evaluation of Concepts for Loading of Hydrocarbons in Ice-infested water”,
Arnor Jensen, 2002:114, ISBN 82-417-5506-0, ISSN 0809-103X.

”Numerical and Physical Modelling of Oil Spreading in Broken Ice”,
Janne K. Økland Gjøsteen, 2002:130, ISBN 82-471-5523-0, ISSN 0809-103X.

”Diagnosis and protection of corroding steel in concrete”,
Franz Pruckner, 20002:140, ISBN 82-471-5555-4, ISSN 0809-103X.

“Tensile and Compressive Creep of Young Concrete: Testing and Modelling”,
Dawood Atrushi, 2003:17, ISBN 82-471-5565-6, ISSN 0809-103X.

“Rheology of Particle Suspensions. Fresh Concrete, Mortar and Cement Paste with Various Types of Lignosulfonates”,
Jon Elvar Wallevik, 2003:18, ISBN 82-471-5566-4, ISSN 0809-103X.

“Oblique Loading of Aluminium Crash Components”,
Aase Reyes, 2003:15, ISBN 82-471-5562-1, ISSN 0809-103X.

“Utilization of Ethiopian Natural Pozzolans”,
Surafel Ketema Desta, 2003:26, ISSN 82-471-5574-5, ISSN:0809-103X.

“Behaviour and strength prediction of reinforced concrete structures with discontinuity regions”, Helge Brå, 2004:11, ISBN 82-471-6222-9, ISSN 1503-8181.

“High-strength steel plates subjected to projectile impact. An experimental and numerical study”, Sumita Dey, 2004:38, ISBN 82-471-6282-2 (printed version), ISBN 82-471-6281-4 (electronic version), ISSN 1503-8181.

“Alkali-reactive and inert fillers in concrete. Rheology of fresh mixtures and expansive reactions.”
Bård M. Pedersen, 2004:92, ISBN 82-471-6401-9 (printed version), ISBN 82-471-6400-0 (electronic version), ISSN 1503-8181.

“On the Shear Capacity of Steel Girders with Large Web Openings”.
Nils Christian Hagen, 2005:9 ISBN 82-471-6878-2 (printed version), ISBN 82-471-6877-4 (electronic version), ISSN 1503-8181.

”Behaviour of aluminium extrusions subjected to axial loading”.
Østen Jensen, 2005:7, ISBN 82-471-6873-1 (printed version), ISBN 82-471-6872-3 (electronic version), ISSN 1503-8181.

”Thermal Aspects of corrosion of Steel in Concrete”.
Jan-Magnus Østvik, 2005:5, ISBN 82-471-6869-3 (printed version), ISBN 82-471-6868 (electronic version), ISSN 1503-8181.

”Mechanical and adaptive behaviour of bone in relation to hip replacement.” A study of bone remodelling and bone grafting.
Sébastien Muller, 2005:34, ISBN 82-471-6933-9 (printed version), ISBN 82-471-6932-0 (electronic version), ISSN 1503-8181.

“Analysis of geometrical nonlinearities with applications to timber structures”.
Lars Wollebæk, 2005:74, ISBN 82-471-7050-5 (printed version), ISBN 82-471-7019-1 (electronic version), ISSN 1503-8181.

“Pedestrian induced lateral vibrations of slender footbridges”,
Anders Rönnquist, 2005:102, ISBN 82-471-7082-5 (printed version), ISBN 82-471-7081-7 (electronic version), ISSN 1503-8181.

“Initial Strength Development of Fly Ash and Limestone Blended Cements at Various Temperatures Predicted by Ultrasonic Pulse Velocity”,
Tom Ivar Fredvik, 2005:112, ISBN 82-471-7105-8 (printed version), ISBN 82-471-7103-1 (electronic version), ISSN 1503-8181.

“Behaviour and modelling of thin-walled cast components”,
Cato Dørum, 2005:128, ISBN 82-471-7140-6 (printed version), ISBN 82-471-7139-2 (electronic version), ISSN 1503-8181.

“Behaviour and modelling of selfpiercing riveted connections”,
Raffaele Porcaro, 2005:165, ISBN 82-471-7219-4 (printed version), ISBN 82-471-7218-6 (electronic version), ISSN 1503-8181.

”Behaviour and Modelling og Aluminium Plates subjected to Compressive Load”,
Lars Rønning, 2005:154, ISBN 82-471-7169-1 (printed version), ISBN 82-471-7195-3 (electronic version), ISSN 1503-8181.

”Bumper beam-longitudinal system subjected to offset impact loading”,
Satyanarayana Kokkula, 2005:193, ISBN 82-471-7280-1 (printed version), ISBN 82-471-7279-8 (electronic version), ISSN 1503-8181.

“Control of Chloride Penetration into Concrete Structures at Early Age”,
Guofei Liu, 2006:46, ISBN 82-471-7838-9 (printed version), ISBN 82-471-7837-0 (electronic version), ISSN 1503-8181.

“Modelling of Welded Thin-Walled Aluminium Structures”,
Ting Wang, 2006:78, ISBN 82-471-7907-5 (printed version), ISBN 82-471-7906-7 (electronic version), ISSN 1503-8181.

”Time-variant reliability of dynamic systems by importance sampling and probabilistic analysis of ice loads”,
Anna Ivanova Olsen, 2006:139, ISBN 82-471-8041-3 (printed version), ISBN 82-471-8040-5 (electronic version), ISSN 1503-8181.

“Fatigue life prediction of an aluminium alloy automotive component using finite element analysis of surface topography”.
Sigmund Kyrre Ås, 2006:25, ISBN 82-471-7791-9 (printed version), ISBN 82-471-7791-9 (electronic version), ISSN 1503-8181.

”Constitutive models of elastoplasticity and fracture for aluminium alloys under strain path change”,
Dasharatha Achani, 2006:76, ISBN 82-471-7903-2 (printed version), ISBN 82-471-7902-4 (electronic version), ISSN 1503-8181.

“Simulations of 2D dynamic brittle fracture by the Element-free Galerkin method and linear fracture mechanics”,
Tommy Karlsson, 2006:125, ISBN 82-471-8011-1 (printed version), ISBN 82-471-8010-3 (electronic version), ISSN 1503-8181.

“Penetration and Perforation of Granite Targets by Hard Projectiles”,
Chong Chiang Seah, 2006:188, ISBN 82-471-8150-9 (printed version), ISBN 82-471-8149-5 (electronic version), ISSN 1503-8181.

"Deformations, strain capacity and cracking of concrete in plastic and early hardening phases",
Tor Arne Hammer, 2007:234, ISBN 978-82-471-5191-4 (printed version), ISBN 978-82-471-5207-2 (electronic version), ISSN 1503-8181.

"Crashworthiness of dual-phase high-strength steel: Material and Component behaviour", Venkatapathi Tarigopula, 2007:230, ISBN 82-471-5076-4 (printed version), ISBN 82-471-5093-1 (electronic version), ISSN 1503-8181.

"Fibre reinforcement in load carrying concrete structures",
Åse Lyslo Døssland, 2008:50, ISBN 978-82-471-6910-0 (printed version), ISBN 978-82-471-6924-7 (electronic version), ISSN 1503-8181.

"Low-velocity penetration of aluminium plates",
Frode Grytten, 2008:46, ISBN 978-82-471-6826-4 (printed version), ISBN 978-82-471-6843-1 (electronic version), ISSN 1503-8181.

"Robustness studies of structures subjected to large deformations",
Ørjan Fyllingen, 2008:24, ISBN 978-82-471-6339-9 (printed version), ISBN 978-82-471-6342-9 (electronic version), ISSN 1503-8181.

"Constitutive modelling of morsellised bone",
Knut Birger Lunde, 2008:92, ISBN 978-82-471-7829-4 (printed version), ISBN 978-82-471-7832-4 (electronic version), ISSN 1503-8181.

"Experimental Investigations of Wind Loading on a Suspension Bridge Girder",
Bjørn Isaksen, 2008:131, ISBN 978-82-471-8656-5 (printed version), ISBN 978-82-471-8673-2 (electronic version), ISSN 1503-8181.

"Cracking Risk of Concrete Structures in The Hardening Phase",
Guomin Ji, 2008:198, ISBN 978-82-471-1079-9 (printed version), ISBN 978-82-471-1080-5 (electronic version), ISSN 1503-8181.

"Modelling and numerical analysis of the porcine and human mitral apparatus",
Victorien Emile Prot, 2008:249, ISBN 978-82-471-1192-5 (printed version), ISBN 978-82-471-1193-2 (electronic version), ISSN 1503-8181.

"Strength analysis of net structures",
Heidi Moe, 2009:48, ISBN 978-82-471-1468-1 (printed version), ISBN 978-82-471-1469-8 (electronic version), ISSN1503-8181.

"Numerical analysis of ductile fracture in surface cracked shells",
Espen Berg, 2009:80, ISBN 978-82-471-1537-4 (printed version), ISBN 978-82-471-1538-1 (electronic version), ISSN 1503-8181.

"Subject specific finite element analysis of bone – for evaluation of the healing of a leg lengthening and evaluation of femoral stem design",
Sune Hansborg Pettersen, 2009:99, ISBN 978-82-471-1579-4 (printed version), ISBN 978-82-471-1580-0 (electronic version), ISSN 1503-8181.

"Evaluation of fracture parameters for notched multi-layered structures",
Lingyun Shang, 2009:137, ISBN 978-82-471-1662-3 (printed version), ISBN 978-82-471-1663-0 (electronic version), ISSN 1503-8181.

"Modelling of Dynamic Material Behaviour and Fracture of Aluminium Alloys for Structural Applications"
Yan Chen, 2009:69, ISBN 978-82-471-1515-2 (printed version), ISBN 978-82 471-1516-9 (electronic version), ISSN 1503-8181.

"Nanomechanics of polymer and composite particles"
Jianying He 2009:213, ISBN 978-82-471-1828-3 (printed version), ISBN 978-82-471-1829-0 (electronic version), ISSN 1503-8181.

"Mechanical properties of clear wood from Norway spruce"
Kristian Berbom Dahl 2009:250, ISBN 978-82-471-1911-2 (printed version) ISBN 978-82-471-1912-9 (electronic version), ISSN 1503-8181.

"Modeling of the degradation of TiB_2 mechanical properties by residual stresses and liquid Al penetration along grain boundaries"
Micol Pezzotta 2009:254, ISBN 978-82-471-1923-5 (printed version) ISBN 978-82-471-1924-2 (electronic version) ISSN 1503-8181.

"Effect of welding residual stress on fracture"
Xiabo Ren 2010:77, ISBN 978-82-471-2115-3 (printed version) ISBN 978-82-471-2116-0 (electronic version), ISSN 1503-8181.

"Pan-based carbon fiber as anode material in cathodic protection system for concrete structures"
Mahdi Chini 2010:122, ISBN 978-82-471-2210-5 (printed version) ISBN 978-82-471-2213-6 (electronic version), ISSN 1503-8181.

"Structural Behaviour of deteriorated and retrofitted concrete structures"
Irina Vasililjeva Sæther 2010:171, ISBN 978-82-471-2315-7 (printed version) ISBN 978-82-471-2316-4 (electronic version) ISSN 1503-8181.

"Prediction of local snow loads on roofs"
Vivian Meløysund 2010:247, ISBN 978-82-471-2490-1 (printed version) ISBN 978-82-471-2491-8 (electronic version) ISSN 1503-8181.

"Behaviour and modelling of polymers for crash applications"
Virgile Delhaye 2010:251, ISBN 978-82-471-2501-4 (printed version) ISBN 978-82-471-2502-1 (electronic version) ISSN 1503-8181.

"Blended cement with reducted CO_2 emission – Utilizing the Fly Ash-Limestone Synergy",
Klaartje De Weerdt 2011:32, ISBN 978-82-471-2584-7 (printed version) ISBN 978-82-471-2584-4 (electronic version) ISSN 1503-8181.

"Chloride induced reinforcement corrosion in concrete" Concept of critical chloride content – methods and mechanisms.
Ueli Angst 2011:113, ISBN 978-82-471-2769-9 (printed version) ISBN 978-82-471-2763-6 (electronic version) ISSN 1503-8181.

"A thermo-electric-Mechanical study of the carbon anode and contact interface for Energy savings in the production of aluminium".
Dag Herman Andersen 2011:157, ISBN 978-82-471-2859-6 (printed version) ISBN 978-82-471-2860-2 (electronic version) ISSN 1503-8181.

"Structural Capacity of Anchorage Ties in Masonry Veneer Walls Subjected to Earthquake". The implications of Eurocode 8 and Eurocode 6 on a typical Norwegain veneer wall.
Ahmed Mohamed Yousry Hamed 2011:181, ISBN 978-82-471-2911-1 (printed version) ISBN 978-82-471-2912-8 (electronic ver.) ISSN 1503-8181.

"Work-hardening behaviour in age-hardenable Al-Zn-Mg(-Cu) alloys".
Ida Westermann , 2011:247, ISBN 978-82-471-3056-8 (printed ver.) ISBN 978-82-471-3057-5 (electronic ver.) ISSN 1503-8181.

"Behaviour and modelling of selfpiercing riveted connections using aluminium rivets".
Nguyen-Hieu Hoang, 2011:266, ISBN 978-82-471-3097-1 (printed ver.) ISBN 978-82-471-3099-5 (electronic ver.) ISSN 1503-8181.

"Fibre reinforced concrete".
Sindre Sandbakk, 2011:297, ISBN 978-82-471-3167-1 (printed ver.) ISBN 978-82-471-3168-8 (electronic ver) ISSN 1503:8181.

"Dynamic behaviour of cablesupported bridges subjected to strong natural wind".
Ole Andre Øiseth, 2011:315, ISBN 978-82-471-3209-8 (printed ver.) ISBN 978-82-471-3210-4 (electronic ver.) ISSN 1503-8181.

"Constitutive modeling of solargrade silicon materials"
Julien Cochard, 2011:307, ISBN 978-82-471-3189-3 (printed ver). ISBN 978-82-471-3190-9 (electronic ver.) ISSN 1503-8181.

"Constitutive behavior and fracture of shape memory alloys"
Jim Stian Olsen, 2012:57, ISBN 978-82-471-3382-8 (printed ver.) ISBN 978-82-471-3383-5 (electronic ver.) ISSN 1503-8181.

“Field measurements in mechanical testing using close-range photogrammetry and digital image analysis”
Egil Fagerholt, 2012:95, ISBN 978-82-471-3466-5 (printed ver.) ISBN 978-82-471-3467-2 (electronic ver.) ISSN 1503-8181.

“Towards a better under standing of the ultimate behaviour of lightweight aggregate concrete in compression and bending”,
Håvard Nedrelid, 2012:123, ISBN 978-82-471-3527-3 (printed ver.) ISBN 978-82-471-3528-0 (electronic ver.) ISSN 1503-8181.

“Numerical simulations of blood flow in the left side of the heart”
Sigrid Kaarstad Dahl, 2012:135, ISBN 978-82-471-3553-2 (printed ver.) ISBN 978-82-471-3555-6 (electronic ver.) ISSN 1503-8181.

“Moisture induced stresses in glulam”
Vanessa Angst-Nicollier, 2012:139, ISBN 978-82-471-3562-4 (printed ver.) ISBN 978-82-471-3563-1 (electronic ver.) ISSN 1503-8181.

“Biomechanical aspects of distraction osteogensis”
Valentina La Russa, 2012:250, ISBN 978-82-471-3807-6 (printed ver.) ISBN 978-82-471-3808-3 (electronic ver.) ISSN 1503-8181.

“Ductile fracture in dual-phase steel. Theoretical, experimental and numerical study”
Gaute Gruben, 2012:257, ISBN 978-82-471-3822-9 (printed ver.) ISBN 978-82-471-3823-6 (electronic ver.) ISSN 1503-8181.

“Damping in Timber Structures”
Nathalie Labonnote, 2012:263, ISBN 978-82-471-3836-6 (printed ver.) ISBN 978-82-471-3837-3 (electronic ver.) ISSN 1503-8181.

“Biomechanical modeling of fetal veins: The umbilical vein and ductus venosus bifurcation”
Paul Roger Leinan, 2012:299, ISBN 978-82-471-3915-8 (printed ver.) ISBN 978-82-471-3916-5 (electronic ver.) ISSN 1503-8181.

“Large-Deformation behaviour of thermoplastics at various stress states”
Anne Serine Ognedal, 2012:298, ISBN 978-82-471-3913-4 (printed ver.) ISBN 978-82-471-3914-1 (electronic ver.) ISSN 1503-8181.

“Hardening accelerator for fly ash blended cement”
Kien Dinh Hoang, 2012:366, ISBN 978-82-471-4063-5 (printed ver.) ISBN 978-82-471-4064-2 (electronic ver.) ISSN 1503-8181.

“From molecular structure to mechanical properties”
Jianyang Wu, 2013:186, ISBN 978-82-471-4485-5 (printed ver.) ISBN 978-82-471-4486-2 (electronic ver.) ISSN 1503-8181.

“Experimental and numerical study of hybrid concrete structures”
Linn Grepstad Nes, 2013:259, ISBN 978-82-471-4644-6 (printed ver.) ISBN 978-82-471-4645-3 (electronic ver.) ISSN 1503-8181.

“Mechanics of ultra-thin multi crystalline silicon wafers”
Saber Saffar, 2013:199, ISBN 978-82-471-4511-1 (printed ver.) ISBN 978-82-471-4513-5 (electronic ver). ISSN 1503-8181.

“Through process modelling of welded aluminium structures”
Anizahyati Alisibramulisi, 2013:325, ISBN 978-82-471-4788-7 (printed ver.) ISBN 978-82-471-4789-4 (electronic ver.) ISSN 1503-8181.

“Combined blast and fragment loading on steel plates”
Knut Gaarder Rakvåg, 2013:361, ISBN978-82-471-4872-3 (printed ver.) ISBN 978-82-4873-0 (electronic ver.). ISSN 1503-8181.

“Characterization and modelling of the anisotropic behaviour of high-strength aluminium alloy”
Marion Fourmeau, 2014:37, ISBN 978-82-326-0008-3 (printed ver.) ISBN 978-82-326-0009-0 (electronic ver.) ISSN 1503-8181.

“Behaviour of threated steel fasteners at elevated deformation rates”
Henning Fransplass, 2014:65, ISBN 978-82-326-0054-0 (printed ver.) ISBN 978-82-326-0055-7 (electronic ver.) ISSN 1503-8181.

“Sedimentation and Bleeding”
Ya Peng, 2014:89, ISBN 978-82-326-0102-8 (printed ver.) ISBN 978-82-326-0103-5 (electric ver.) ISSN 1503-8181.

“Impact against X65 offshore pipelines”
Martin Kristoffersen, 2014:362, ISBN 978-82-326-0636-8 (printed ver.) ISBN 978-82-326-0637-5 (electronic ver.) ISSN 1503-8181.

“Formability of aluminium alloy subjected to prestrain by rolling”
Dmitry Vysochinskiy, 2014:363,, ISBN 978-82-326-0638-2 (printed ver.) ISBN 978-82-326-0639-9 (electronic ver.) ISSN 1503-8181.

“Experimental and numerical study of Yielding, Work-Hardening and anisotropy in textured AA6xxx alloys using crystal plasticity models”
Mikhail Khadyko, 2015:28, ISBN 978-82-326-0724-2 (printed ver.) ISBN 978-82-326-0725-9 (electronic ver.) ISSN 1503-8181.

“Behaviour and Modelling of AA6xxx Aluminium Alloys Under a Wide Range of Temperatures and Strain Rates”
Vincent Vilamosa, 2015:63, ISBN 978-82-326-0786-0 (printed ver.) ISBN 978-82-326-0787-7 (electronic ver.) ISSN 1503-8181.

“A Probabilistic Approach in Failure Modelling of Aluminium High Pressure Die-Castings”
Octavian Knoll, 2015:137, ISBN 978-82-326-0930-7 (printed ver.) ISBN 978-82-326-0931-4 (electronic ver.) ISSN 1503-8181.

“Ice Abrasion on Marine Concrete Structures”
Egil Møen, 2015:189, ISBN 978-82-326-1034-1 (printed ver.) ISBN 978-82-326-1035-8 (electronic ver.) ISSN 1503-8181.

“Fibre Orientation in Steel-Fibre-Reinforced Concrete”
Giedrius Zirgulis, 2015:229, ISBN 978-82-326-1114-0 (printed ver.) ISBN 978-82-326-1115-7 (electronic ver.) ISSN 1503-8181.

“Effect of spatial variation and possible interference of localised corrosion on the residual capacity of a reinforced concrete beam”
Mohammad Mahdi Kioumarsi, 2015:282, ISBN 978-82-326-1220-8 (printed ver.) ISBN 978-82-1221-5 (electronic ver.) ISSN 1503-8181.

“The role of concrete resistivity in chloride-induced macro-cell corrosion”
Karla Horbostel, 2015:324, ISBN 978-82-326-1304-5 (printed ver.) ISBN 978-82-326-1305-2 (electonic ver.) ISSN 1503-8181.

“Flowable fibre-reinforced concrete for structural applications”
Elena Vidal Sarmiento, 2015-335, ISBN 978-82-326-1324-3 (printed ver.) ISBN 978-82-326-1325-0 (electronic ver.) ISSN 1503-8181.

“Development of chushed sand for concrete production with microproportioning”
Rolands Cepuritis, 2016:19, ISBN 978-82-326-1382-3 (printed ver.) ISBN 978-82-326-1383-0 (electronic ver.) ISSN 1503-8181.

“Withdrawal properties of threaded rods embedded in glued-laminated timer elements”
Haris Stamatopoulos, 2016:48, ISBN 978-82-326-1436-3 (printed ver.) ISBN 978-82-326-1437-0 (electronic ver.) ISSN 1503-8181.

“An Experimental and numerical study of thermoplastics at large deformation”
Marius Andersen, 2016:191, ISBN 978-82-326-1720-3 (printed ver.) ISBN 978-82-326-1721-0 (electronic ver.) ISSN 1503-8181.

“Modeling and Simulation of Ballistic Impact”
Jens Kristian Holmen, 2016:240, ISBN 978-82-326-1818-7 (printed ver). ISBN 978-82-326-1819-4 (electronic ver.) ISSN 1503-8181.

“Early age crack assessment of concrete structures”
Anja B. Estensen Klausen, 2016:256, ISBN 978-82-326-1850-7 (printed ver). ISBN 978-82-326-1851-4 (electronic ver.) ISSN 1503-8181.

“Uncertainty quantification and sensitivity analysis for cardiovascular models”
Vinzenz Gregor Eck, 2016:234, ISBN 978-82-326-1806-4 (printed ver.) ISBN 978-82-326-1807-1 (electronic ver.) ISSN 1503-8181.

“Dynamic behaviour of existing and new railway catenary systems under Norwegain conditions”
Petter Røe Nåvik, 2016:298, ISBN 978-82-326-1935-1 (printed ver.) ISBN 978-82-326-1934-4 (electronic ver.) ISSN 1503-8181.

“Mechanical behaviour of particle-filled elastomers at various temperatures”
Arne Ilseng, 2016-295, ISBN978-82-326-1928-3 (printed ver.) ISBN 978-82-326-1929-0 (electronic ver.) ISSN 1503-8181.

“Nanotechnology for Anti-Icing Application”
Zhiwei He, 2016:348, ISBN 978-82-326-2038-8 (printed ver.) ISBN 978-82-326-2019-5 (electronic ver.) ISSN 1503-8181.

“Conduction Mechanisms in Conductive Adhesives with Metal-Coated Polyer Spheres”
Sigurd Rolland Pettersen, 2016:349, ISBN 978-326-2040-1 (printed ver,) ISBN 978-82-326-2041-8 (electronic ver.) ISSN 1503-8181.

“The interaction between calcium lignosulfonate and cement”
Alessia Colombo, 2017:20, ISBN 978-82-326-2122-4 (printed ver.) ISBN 978-82-326-2123-1 (electronic ver.) ISSN 1503-8181.

“Behaviour and Modelling of Flexible Structures Subjected to Blast Loading”
Vegard Aune, 2017:101, ISBN 978-82-326-2274-0 (printed ver.) ISBN 978-82-326-2275-7 (electronic ver.) ISSN 1503-8181.

“Behaviour of steel connections under quasi-static and impact loading”
Erik Løhre Grimsmo, 2017:159, ISBN 978-82-326-2390-7 (printed ver.) ISBN 978-82-326-2391-4 (electronic ver.) ISSN 1503-8181.

“An experimental and numerical study of cortical bone at he macro and Nano-scale”
Masoud Ramenzanzadehkoldeh,, 2017:208, ISBN 978-82-326-2488-1 (printed ver.) ISBN 978-82-326-2489-8 (electronic ver.) ISSN 1503-8181.

“Optoelectrical Properties of a Novel Organic Semiconductor: 6,13-Dichloropentacene”
Mao Wang, 2017:130, ISBN 978-82-326-2332-7 (printed ver.) ISBN 978-82-326-2333-4) (electronic ver.) ISSN 1503-8181.

“Core-shell structured microgels and their behavior at oil and water interface”
Yi Gong, 2017:182, ISBN 978-82-326-2436-2 (printed. ver.) ISBN 978-82-326-2437-9 (electronic ver.) ISSN 1503-8181.